Volume 7, No. 6
April, 1961

THE SOVIET JOURNAL OF

ATOMIC ENERGY

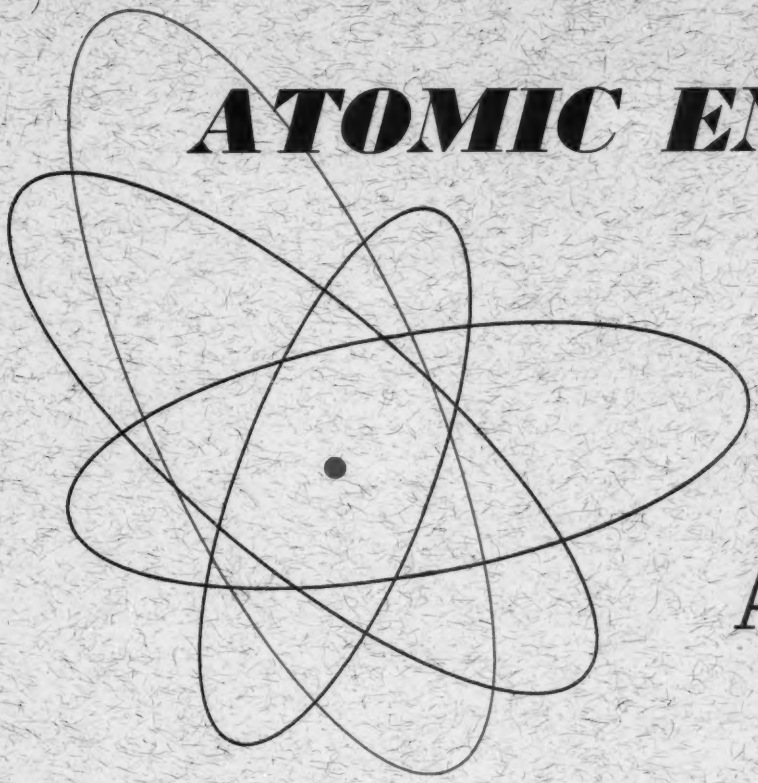

Атомная энергия

TRANSLATED FROM RUSSIAN

CONSULTANTS BUREAU

THE SOVIET JOURNAL OF

ATOMIC ENERGY

A translation of ATOMNAYA ÉNERGIYA,
a publication of the Academy of Sciences of the USSR

(Russian Original Dated December, 1959)

Vol. 7, No. 6 **April, 1961**

CONTENTS

Annual subscription	$ 75.00
Single issue	20.00
Single article	12.50

CONTENTS (continued)

NOTE

The Table of Contents lists all material that appears in Atomnaya Énergiya. Those items that originated in the English language are not included in the translation and are shown enclosed in brackets. Whenever possible, the English-language source containing the omitted reports will be given.

Consultants Bureau Enterprises, Inc.

DESIGN PRINCIPLES AND BASIC DATA OF BETATRON FACILITIES AT THE MOSCOW TRANSFORMER WORKS

B. B. Gel'perin

Translated from Atomnaya Énergiya, Vol. 7, No. 6, pp. 509-518
December, 1959
Original article submitted February 14, 1959

The present article gives the principles underlying the design of betatron accelerator facilities for nondestructive testing, medical, physical, and other research uses. The conditions under which azimuthal asymmetry of the betatron magnetic field may take shape, and methods for coping with it, are considered. The multiyoke electromagnet design for betatrons, developed at the Moscow Transformer Works (MTZ), is described; this design confers improved azimuthal homogeneity on the magnetic field. Data are also provided on specialized betatron designs of the following types at MTZ: a stationary 4-yoke model with accelerated-electron energies from 20 to 50 Mev, a rotating suspended-type betatron, 25 Mev, for medical purposes, a movable rotating 25 Mev model for nondestructive testing, and a 15 Mev pendulum-type tilting betatron, for medical purposes.

Introduction

Betatrons are being employed in an increasing number of applications for research in the physics of the atomic nucleus, in medicine (for therapy in malignant-tumor cases), and in industry (for nondestructive testing), etc.

The increasing use of betatrons in the national economy has thrown new light on the need to develop not only stationary installations, but also those facilities which can be moved or adjusted to a desired position: rotating and pendulum-type facilities, etc.

The principal requirement to be met by stationary betatrons is reliability of output parameters (energy and intensity of β- or γ-radiation). A necessary factor in the design of movable betatrons must, in addition, meet such requirements as minimized weight, size, and noise level. It is obvious that the donut chambers in movable betatrons must also be sealed off.

Basic Requirements for Betatron Electromagnets

To obtain maximum radiation intensity, a high degree of azimuthal homogeneity must characterize the magnetic field established in the air gap of the electromagnet. The magnetic field of the betatron always suffers from a certain azimuthal inhomogeneity in practice, since the orbital path of the accelerated electrons will not be a circle, because of distortions in the magnetic-field homogeneity, but some form of a closed curve.

It is a familiar fact from betatron theory* that the deviation of a perturbed orbit from the ideal orbit x_0 is expressed by the relation

$$\frac{x_0}{r_0} = \sum_{l=1}^{\infty} \frac{h_l}{l^2+n-1} \cos(l\theta + \alpha_l),$$

where r_0 is the radius of the ideal orbit; h_l is the relative magnitude of the l-th harmonic obtained by decomposing the magnetic field in a Fourier series; α_l is the phase of the l-th harmonic.

Let's consider in greater detail the reasons for the azimuthal inhomogeneity of the field and measures for coping with it. The field intensity H_1 at a point (θ_1, r_0) will differ from the intensity H_2 at a point (θ_2, r_0) both in amplitude and in phase. Let $H_1 = H_{01} \sin \omega t$, and $H_2 = H_{02} \sin(\omega t + \delta)$, where H_{01} and H_{02} are the amplitudes of the field intensities at points θ_1 and θ_2 and δ is the phase shift. Since δ is usually a small angle, we have

$$\frac{H_2 - H_1}{H_1} = \frac{\delta}{\tan \omega t} + \frac{H_{02} - H_{01}}{H_{01}} \left(1 + \frac{\delta}{\tan \omega t}\right).$$

The magnitude of $\frac{\delta}{\tan \omega t}$ may be neglected, compared to unity, since as a rule $\omega t_i \gg \delta$ at the time of injection. Then

$$\frac{H_2 - H_1}{H_1} = \frac{\delta}{\tan \omega t} + \frac{H_{02} - H_{01}}{H_{01}}.$$

Accordingly, the inhomogeneity of the magnetic field at two points may be broken down into two components: phase inhomogeneity $\gamma_p = \frac{\delta}{\tan \omega t}$ and amplitude inhomogeneity: $\gamma_a = \frac{H_{02} - H_{01}}{H_{01}}$.

The nature of these two components of field inhomogeneity is different. Phase inhomogeneity is due to the nonuniformity of active currents coupled to the tubes of force of the magnetic field at different azimuths, i.e., it is due to the nonuniformity of energy losses in the magnetic materials of the electromagnet.

* D. Bohm and L. Foldy, Phys. Rev. 70, 249 (1946).

The amplitude inhomogeneity, on the other hand, is due to the difference in the reluctance of the tubes. Since the reluctance of the tubes is determined principally by the reluctance of the air gaps and spacers between components, γ_a is due to the difference in dimensions of individual tubes of the field.

It is clear from Fig. 1 that γ_p is a vector perpendicular to the field intensity H_{01}, while γ_a is a vector coinciding with it.

At the initiation of the acceleration cycle, while ωt is still small, γ_p has a large value, since $\frac{\delta}{\tan \omega t}$ is practically 8-12% at the time of injection, whereas γ_a is about 2-3%. At the end of the acceleration cycle, γ_p will be insignificant, its value tending to zero. The time to combat field inhomogeneity is therefore primarily at the beginning of the acceleration cycle, when γ_p is large compared to the injection field. This problem is approached on the one hand by designing azimuthal symmetry into the electromagnet, to minimize "natural" inhomogeneity, and on the other hand by setting up a bank of coils to compensate for any "natural" inhomogeneity on the part of the field.

An example of symmetrical design in the magnetic circuit may be seen in the multiyoke design developed at MTZ (a 4-yoke design is shown in Fig. 2). The entire periphery of the pole piece is broken down into a large number (some 200-250) of segments, each of which is assembled from an identical number of steel laminations forming a portion of the pole piece and the yoke at the same time (Fig. 2a). The thicknesses of these segments azimuthally are so consigned that the pole is densely packed when all of the parts are assembled in place, while the segmental parts forming the yoke, also arranged radially, have a smaller stacking factor. The yoke portions of all of these segments are in turn broken down into m equal parts (4 parts in Fig. 2b), which are compressed to form m symmetrical yokes, identical in design. They are identical, magnetically speaking, except for the fringe segments (at the sides of the yokes), through which the fringing magnetic flux leaks. The shape of the curve for the azimuthal phase inhomogeneity distribution is found to be a consistent one with characteristic humps corresponding to the edges of the yokes. Figure 3 shows the approximate curve for the magnetic field distribution across the gap of a 4-yoke electromagnet. The fourth harmonic in the curve is the fundamental. However, its contribution to the distortion is limited, since its amplitude is divided by a factor less than the square of the harmonic number (at n = 0.7 by 15.7). In Table 1, we have the values for the harmonics of the curve, and their contribution to the distortion of the orbit. The "natural" azimuthal inhomogeneity of the magnetic field is thus held at a minimum in multiyoke-type magnets, because of symmetry in design.

We see a completely different pattern in the conventional two-yoke design for the magnetic path. It is clear from inspection of Fig. 4, for instance, that the pole piece is in this case assembled from a radial array of steel laminations, while the yokes and columns are assembled from parallel-stacked steel laminations. It

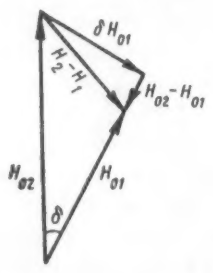

Fig. 1. Diagram of phase and amplitude inhomogeneities of the magnetic field.

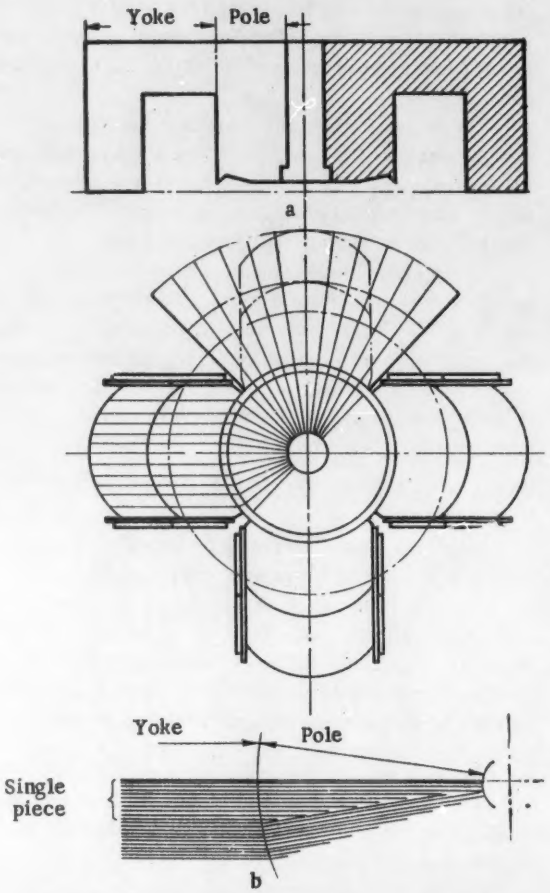

Fig. 2. Diagram of 4-yoke design of magnetic leads to betatron.

TABLE 1

Harmonic Analysis of the Curve in Fig. 3

Amplitude	Number of harmonics			
	1	2	3	4
h_l	0,29	0,517	0,14	0,995
$\frac{h_l}{l^2-n+1}$	0,435	0,141	0,0161	0,0635

TABLE 2

Harmonic Analysis of the Curve in Fig. 5

Amplitude	Number of harmonics			
	1	2	3	4
h_l	0,23	3,0	0,064	2,25
$\frac{h_l}{l^2+n-1}$	0,345	0,82	0,0074	0,144

is readily seen that the segments arranged closer to the center will saturate more strongly (see area abcd) than segments farther out (see area efgh). Specific energy losses in different segments of the yokes will not be the same, for that reason. It is evident that the curve for the azimuthal magnetic-field intensity distribution will in that case exhibit a clearly defined second harmonic (Fig. 5). Table 2 shows that the "natural" γ_p will be much larger in that case.

The compensation for γ_a is usually brought about by equalizing the gaps in the magnet (by inserting additional spacers, or reducing the thickness of existing ones).

The phase inhomogeneity is offset by means of coils, through which flows current shifted 90° in phase to the principal magnetizing current of the magnet. When these coils are properly positioned and connected up, the first and second harmonics of the azimuthal phase variation, of whatever magnitude, can be compensated for. Higher-order harmonics need not be cancelled out, as a rule, since their contribution to distortion of the orbit is negligible. The compensation circuit of the first harmonic in the four-yoke electromagnet design is shown in Fig. 6. In the two-yoke design, used in the betatron, the compensation coils are wound around segments of the yokes and columns (the medium and extreme segments), in corresponding manner. The ventilation ducts provided in the yoke columns are used for accomodating the compensation coils. The compensation system remains the same as described.

The advantage of this type of compensation system is that the compensation current may be controlled by the operator from a control console while the betatron is in operation, and the magnetic field of the facility is subject to control, to obtain peak γ-radiation intensity.

Design of Electromagnets in Stationary and Movable Betatrons

The considerations mentioned above provide grounds for the conclusion that a multiyoke design is in some ways superior to the two-yoke design in betatron applications. The stationary betatron facilities built at MTZ, and designed for 20 Mev energy and higher, are therefore based exclusively on the multiyoke design. When magnetic field intensities are equal throughout the air gap, the weight of multiyoke magnets shows little difference from that of two-yoke magnets.

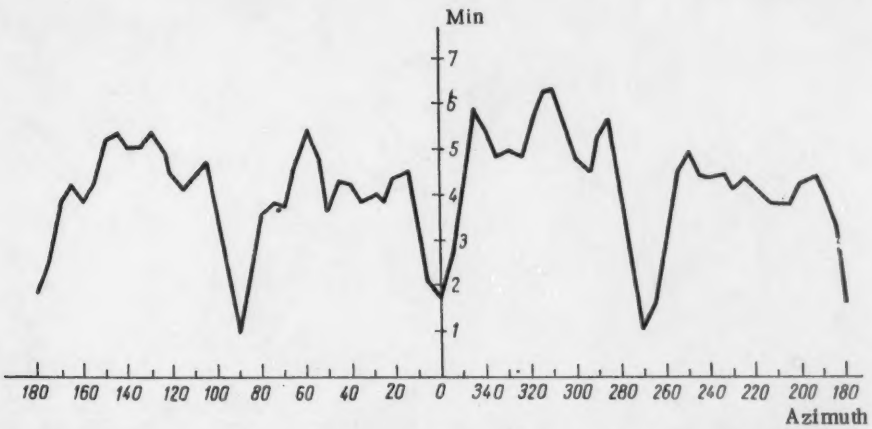

Fig. 3. Azimuthal phase variation of the magnetic field across the gap of a 4-yoke electromagnet.

Development work on movable betatrons demonstrated the need to reduce greatly the weight of the movable portion of the facility, i.e., the electromagnet. As we know, the weight of a betatron electromagnet is approximately proportional to the cube of the orbital radius. For some specified energy of accelerated electrons, the radius of the orbit may be reduced solely by increasing the magnetic field strength at the orbit. In addition to weight reduction, reduction in the radial dimensions of the electromagnet air gap may be achieved by reducing the radius of the orbit, since distortions of the orbit due to azimuthal field inhomogeneity are proportional to the radius of the orbit. The accelerator donut chamber is therefore made more compact and sturdier.

It was decided to employ cold-rolled steel in movable betatrons, to increase the magnetic field strength. The improved magnetic properties of this steel permit the field strength in the electromagnet air gap to be brought up to 5 kilo-oersteds, while only 3.3 kilo-oersteds are attained by the use of hot-rolled steel. The orbital radius may accordingly be reduced by 33%.

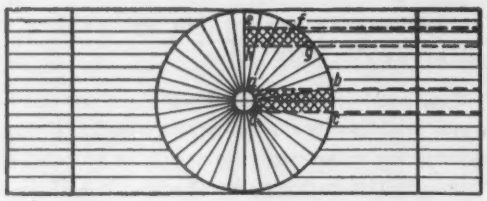

Fig. 4. Arrangement of steel laminations in a two-yoke electromagnet.

However, cold-rolled steel shows greater anisotropy in its magnetic properties. When the magnetic flux is directed along the rolling direction of the metal, the magnetic properties are excellent, but when the magnetic flux is directed at some angle, particularly 60° and 90°, magnetic properties deteriorate abruptly. Since the shape of the blank is punched from sheet steel to form the pole pieces and yoke simultaneously in multiyoke designs (Fig. 7), the magnetic flux will proceed partially along the rolling direction (sections 1 and 2), partially at right angles to the rolling direction (section 3), and partially off at different angles (sections 4 and 5). In that case, the improved magnetic properties of the cold-rolled steel will not be realized in practice.

In the two-yoke design, the magnet yoke and core may be assembled from metal cut only along the direction of rolling. The electromagnets used in movable betatrons are therefore made from the cold-rolled steel used in the two-yoke design.

Cooling Systems for Stationary and Movable Betatrons

The length of time a betatron may be operated depends on the field in which it is being used. In physics research and training demonstration applications stationary betatrons are generally employed, and the duty cycle is insignificant. Natural air cooling is used in such betatrons. In chemistry and biology, stationary betatrons are also used, but a certain dose of exposure is required here, so that the betatron duty cycle may take on significant proportions. Some approach to

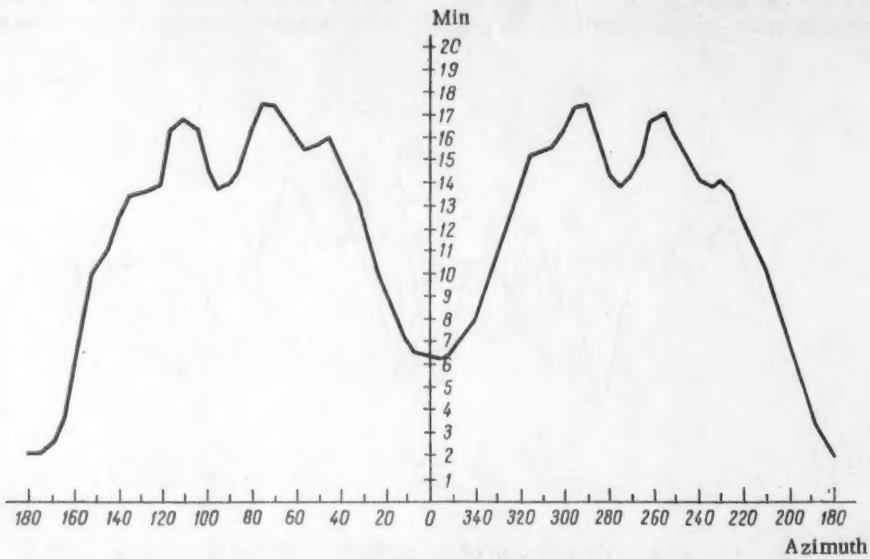

Fig. 5. Azimuthal phase variation of the magnetic field across the gap of a two-yoke electromagnet.

artificial cooling must be resorted to in these cases. Forced air cooling is employed as a rule.

Movable betatrons for medical applications and flaw detection have large duty cycles. In medical therapy, the duty factor is 60%, and in flaw detection, 100%. Forced-ventilation cooling arrangements are needed for movable betatrons.

The parts subject to greatest heating are exposed to the full force of the air blast: the inner bushing with its high magnetic saturation, and coils having comparatively high current density. In stationary betatrons, cooling air is drawn by suction from the betatron hall and driven through the electromagnet, to be discharged outside. This direction of air flow protects the rooms where people are working from contamination by radioactive air. Figure 8 shows the path of air flow through the electromagnet, which is used in stationary betatrons. The fan for the stationary betatron is usually installed in an underground room, to minimize fan noise in the betatron hall.

In movable betatrons, the fans are installed within the betatron enclosure. In this case, air from the betatron gains admittance to the room housing the betatron facility, thus putting a premium on good cross ventilation arrangements for the room. The speed of air flow in the ventilation ducts of the betatron varies 5-20 meters/sec.

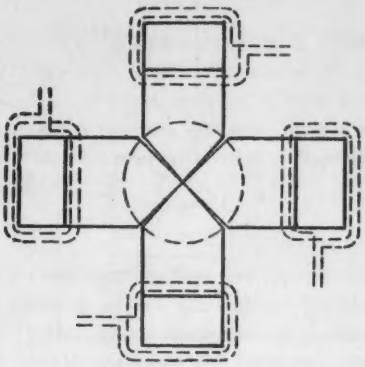

Fig. 6. Arrangement of compensation coils in a four-yoke electromagnet.

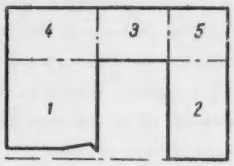

Fig. 7. Arrangment of segments in stock metal for a four-yoke electromagnet, prior to machining.

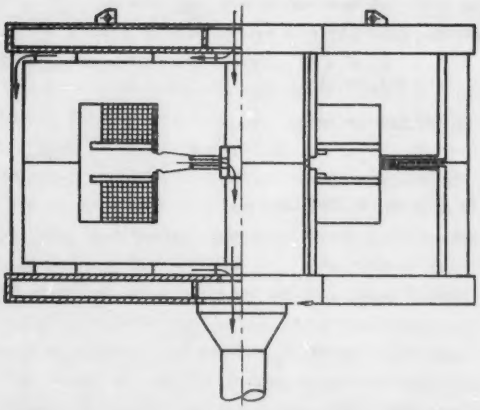

Fig. 8. Path of cooling air in electromagnet.

Choosing the Frequency for Betatron Current Supply

In choosing the frequency for the current supplied to the betatron, one must keep in mind that the com-

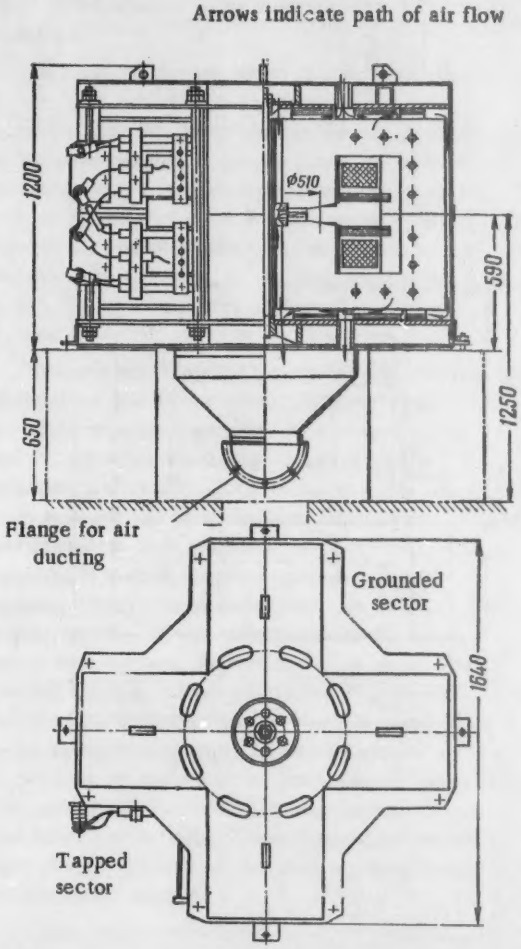

Fig. 9. Stationary 4-yoke betatron, 20 Mev.

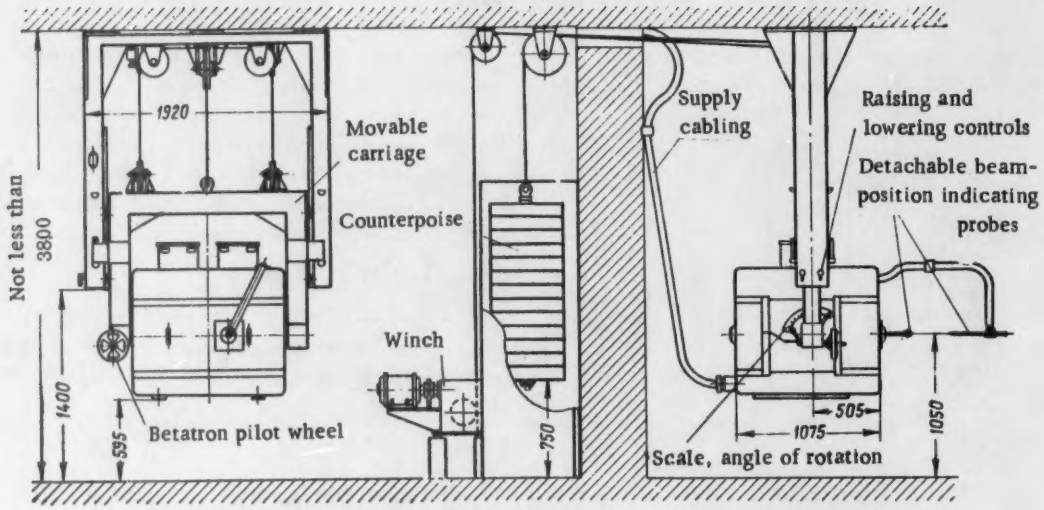

Fig. 10. Ceiling-suspended rotary betatron, 25 Mev, for medical applications.

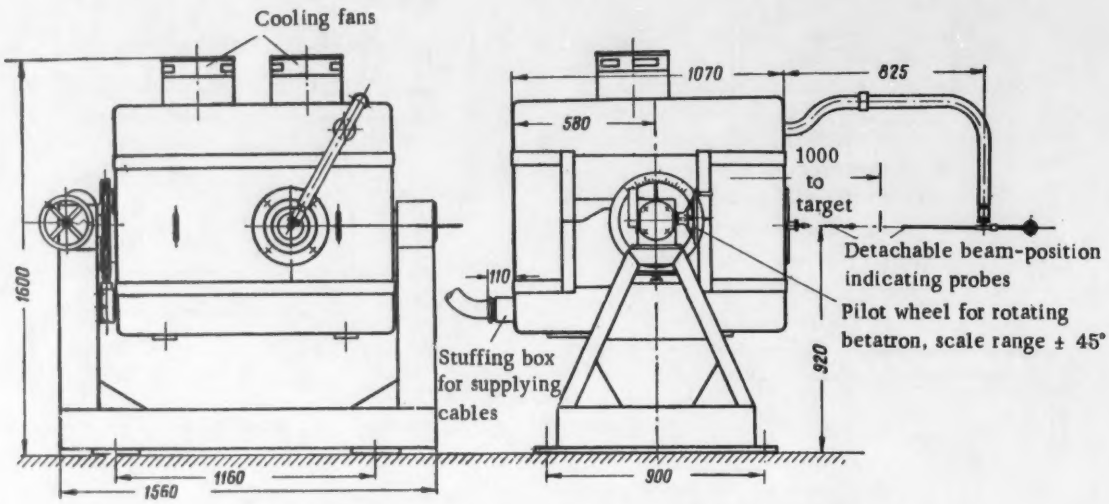

Fig. 11. Rotating 25 Mev betatron, for nondestructive testing.

plexity of the arrangement is increased as the frequency increases, with lessened reliability in performance and a pronounced weight penalty with respect to the electromagnet, since the allowable flux density in the steel decreases as the frequency is stepped up. On the other hand, the intensity of the betatron radiation increases as the frequency. Although a high radiation intensity is required in movable betatrons, industrial line frequency (50 cps) has been accepted for those applications, requiring less complex equipment; all the more so since the personnel who will be operating the facility will not be very highly skilled technically in this area (e.g., doctors, nurses). In the case of stationary facilities, where low weight is not such a prime consideration, the equipment used may be more complicated and higher weight may be tolerated, with an associated gain in radiation intensity. MTZ has devised a stationary betatron facility with supplied frequencies of 150, 300, and 600 cps. The high-frequency generator used is a vacuum-tube oscillator or a static frequency tripler.

Parameters of MTZ Betatrons

The following basic betatron designs have been evolved at MTZ:

1. The 20 Mev 4-yoke betatron (Fig. 9).
2. A ceiling-suspended rotating betatron for medical purposes, 25 Mev (Fig. 10). The suspension design makes it possible to position the magnet for both horizontal irradiation (with the target placed at 1050 cm from the floor) and vertical irradiation. The design provides for 600 mm displacement vertically and rotation of the electromagnet 120° about the horizontal

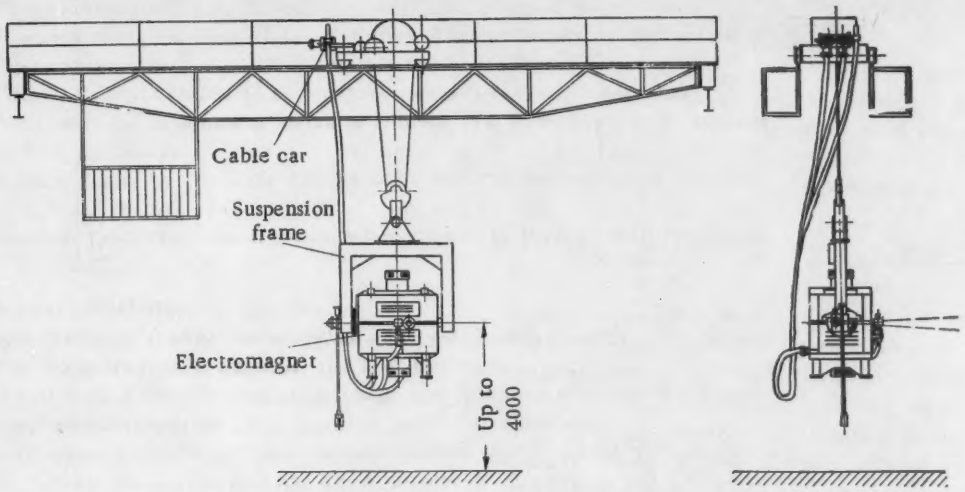

Fig. 12. Crane-suspended 25 Mev betatron, for nondestructive testing.

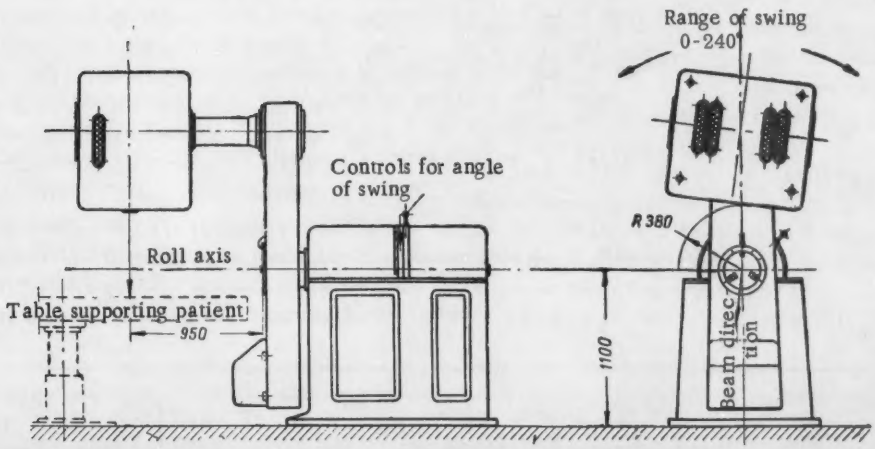

Fig. 13. Pendulum-type tiltable betatron, 15 Mev, for medical applications.

TABLE 3

Betatron Characteristics

Parameters	Betatron type					
	stationary, 4-yoke (Fig. 9)	suspension, rotating, medical (Fig. 10).	rotating platform, flaw detection (Fig. 11)	traveling-crane-suspension, flaw detection (Fig. 12)	pendulum-type, tiltable, medical (Fig. 13)	stationary, research
Energy of accelerated electrons, Mev	20	10-25	10-25	10-25	6-15	10-50
Weight of active steel, kg	4750	1625	1625	1625	420	15,000
Weight of electromagnet, kg	6600	2700	2700	2700	650	18,500
Weight of upper removable part, kg	3000	1200	1200	1200	300	9000
Cooling system	Forced air circulation	Forced air	Forced air	Forced air	Forced air	Forced air circulation
Fan capacity, meters^3/hr	3000	2 x 500	2 x 500	2 x 500	600	5000
Current supplies frequency, cps	150	50	50	50	50	50
Intensity of γ radiation, at 1 meter from target, r/min	100	30	30	30	4.5	200-250
Weight of lead shielding, kg	–	585	–	–	400	–
Donut chamber	Evacuated	Sealed-off	Sealed-off	Sealed-off	Sealed-off	Evacuated

axis, with the beam position variable over a range +90° to −30° from the vertical. All of the vertical displacements are controlled by a motor drive, and angular adjustments are controlled manually.

An array of diaphragms and equalizing filters allows for the following irradiation dose fields at a distance of 1 meter from the target: round 40 and 80 mm diameters and rectangular 100 x 150 mm, 80 x 100 mm, 60 x 80 mm, and 50 x 180 mm (the dose field over the ranges can be stabilized to within 10%).

The betatron is lead-shielded on the patient's side. The thickness of the lead shielding is based on the dose rate of unused γ radiation, not exceeding 0.5% of the dose rate at the beam axis (with a filter in use).

3. A 25 Mev betatron for nondestructive testing; one model on a rotating platform, another crane-suspended. The rotating betatron (Fig. 11) can vary its beam axis to 30° off horizontal. The crane-suspended betatron (Fig. 12) can be moved to a distance of 20 meters from the location of the controls, and the beam axis can be lowered to 90° below or raised to 30° above the horizontal.

4. A pendulum-type tiltable betatron, 15 Mev, for medical applications. (Fig. 13). The betatron electromagnet may be swung through any angle to 210°. This provides a maximum dose of exposure at the center of the tilt excursion (at the tumor), with a much smaller dose rate at the surface of the healthy skin (at the points where the beam enters and leaves the body).

The distance from the center of the swing excursion to the target is 800 mm. The betatron is equipped with the same array of diaphragms and filters as is the 25 Mev medical betatron, with the further addition of one 70 x 30 mm diaphragm. The lead shielding cuts the dose rate of unused γ radiation down to 0.5% of the dose rate at the beam axis (with filter in use). The motion of the betatron is controlled by two remote-control facilities (from a control desk) and also directly from the room where the betatron is installed.

5. The 50 Mev research betatron. This betatron is of the 2-yoke design, made of cold-rolled steel, and is in the production stage at the present time.

The basic characteristics of the betatron types described herein are presented in Table 3.

SIMULATION OF CONTROL AND TEMPERATURE VARIATION OF WATER DENSITY IN INTERMEDIATE-NEUTRON URANIUM-WATER REACTORS

V. B. Klimentov and V. M. Gryazev

Translated from Atomnaya Énergiya, Vol 7, No. 6, pp 519-523
December, 1959
Original article submitted March 12, 1959

This article deals with the results of experiments on the physical simulation of control and of the temperature effect due to changes in water density in intermediate-neutron uranium-water reactors. The values of control rods of different types were determined, and the dependence of the critical size of uranium-water reactors on the density of the water filling the reactor core was found.

Introduction

The physical simulation of various processes in nuclear reactors may be achieved by simulation procedures carried out on critical facilities. This makes available much information needed in the design and construction of nuclear reactors, and is a much cheaper variant than carrying out criticality experiments during the reactor start-up. Physical simulation makes it possible to arrive at a highly accurate estimate of the optimum reactor loading at peak power operation, better than that obtainable from theoretical calculations.

Specially heightened interest is focused in studies of the temperature effect due to variation in water density, and problems connected with the control of intermediate-neutron uranium-water reactors. The authors of the present article have performed investigations of these problems on the critical assembly of a uranium-water multiplying system. The design of the facility and several of the experiments performed on it are described in detail in a report submitted to the Second Geneva Conference on the Peaceful Uses of Atomic Energy [1].

The possiblity of altering the configuration and composition of the core and reflector, and arrangment of control rods, was provided for in the design of the critical assembly.

The working components of the critical assembly were plates 250 x 70 x 2.7 mm, compacted from a mixture of uranium dioxide and trioxide (90% U^{235}) plus polyethylene. The plates were assembled, 5-8 units each in a stainless steel cell. The cells were mounted on a scale-model table forming a core of the required size and shape. The volume of a single casing was 0.62 liter. The ratio of the number of hydrogen nuclei to number of U^{235} nuclei (ρ_H/ρ_{235}) varied from 17 to 50. Two hollow cadmium automatic-control rods and two scram rods were positioned near the core. The critical facility was lowered into an aluminum tank 3 meters across and 1.6 meters high. The tank was instrumented for controlled loading of water and rapid discharge. The water level was indicated by a water gauge. The critical facility was fully instrumented for reliable control and monitoring of the process during all phases of its performance. While experiments were in progress, particular attention was devoted to radiation hygiene problems.

1. Control Rod Value Studies

Empirical determinations of control rod worth are not difficult and may be carried out with ease on a critical assembly of the type described at a power level no higher than 1 w. A solid boron rod (B_4C) measuring 60 mm in diameter and a hollow cadmium rod of the same diameter, wall thickness 1 mm, were studied. The

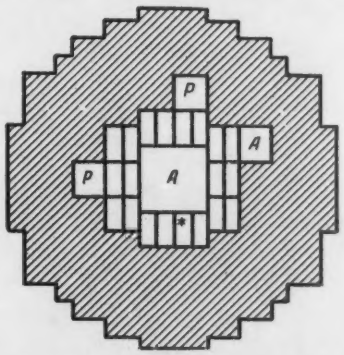

Fig. 1. Diagram of annular uranium-water system, with graphite lateral reflector ($\rho_H/\rho_{235} = 31$): The blank rectangles are working cells, while the hatched area is the graphite; P are control rods; A are scram rods; * indicates a movable cell.

length of the rods was 400 mm, with the height of the core of the multiplying system equal to 250 mm. Measurements were carried out for systems with water reflector and graphite lateral reflector 210 mm thick and 400 mm high. Rods placed at distances of 35, 70, and 140 mm from the reactor core were studied. Water was used in all instances as the upper and lower reflector. The measurements were performed on a ring multiplying system, with an interior cavity, 140 × 140 mm, for water. A diagram of this system, illustrating the case with a side reflector, of graphite, is seen in Fig. 1. The scram rods could be relied upon to shut down the facility at any given position of the control rods or test rods. Neutron spectrum energy was determined from the ratio ρ_H/ρ_{235} = = 31. According to the paper mentioned earlier [1], the fraction of fissions of U^{235} due to neutrons of energies above 0.4 ev is about 30% for this type of arrangement.

The procedure employed in the measurements included prior calibration of the control rods P, by using a removable working cell. A special setup with a lead screw was used to move the cell. The worth of the cadmium and boron rods, and that of the working cell, was determined by this means. The experiment was as follows. An automatic controller was started and the test cell was removed from the core. Control rods P were automatically raised. The worth of the extracted portion of the control rods was tentatively estimated from the reactor doubling time. Similar operations were repeated until the test cell had been completely withdrawn from the core. Control rod displacement was shown by a synchro position indicator.

The effectiveness or worth $\Delta\rho$ of a single working cell in the mutiplying system of 25 cells, with a water reflector, was 0.015, and was found to be 0.021 for the system of 20 cells with graphite side reflector. The calibration curve for two cadmium rods inserted together and placed in the graphite side reflector flush to the core is seen in Fig. 2.

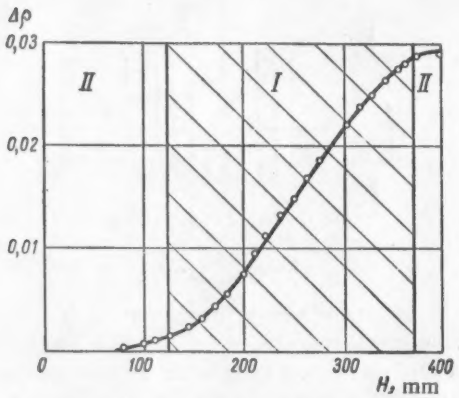

Fig. 2. Calibration of control rods: I) core; II) top and bottom water reflectors.

The worth of the boron and hollow cadmium rods was found to be virtually the same. Their relationship to the arrangement of rods about the core was determined from the distribution of thermal neutrons in the reflector, as shown in Fig. 3.

Liquid absorbers may prove useful in the control of pressurized uranium-water reactors. Controllers with liquid absorbers have no moving parts, which entails an appreciable simplification of the reactor design.

An estimate of the effectiveness of a mercury absorber placed at the center of the core of a uranium-water system with water reflector was obtained by experimental means. A diagram of this system appears in Fig. 4.

The energy spectrum of the neutrons in the multiplying system was determined from the ratio ρ_H/ρ_{235} = = 25. The number of fissions caused by neutrons of energies higher than 0.4 ev amounted to not less than 50% [1]. The mercury absorber consisted of 12 copper tubes filled with mercury (2.7 kg of Hg). It replaced two withdrawn test cells. The outer and inner diameters of the tubing were 10 and 8 mm, respectively, and the height 400 mm. The tubes were placed along the perimeter of a square of sides 53 mm. Corrosive attack by the mercury on the copper presented no hazard, since the rods were not used for any period in excess of a few days. Gradual withdrawal of the mercury absorber was effected as part of the reactor automatic controls, the variation in reactivity being compensated by introducing control rods and withdrawing peripheral cells. For a rod filled with mercury, $\Delta\rho' = 0.088$, and without mercury $\Delta\rho^* = 0.023$. Accordingly, the effectiveness of 2.7 kg of mercury for the given rod design in the system is $\Delta\rho' - \Delta\rho^* = 0.065$.

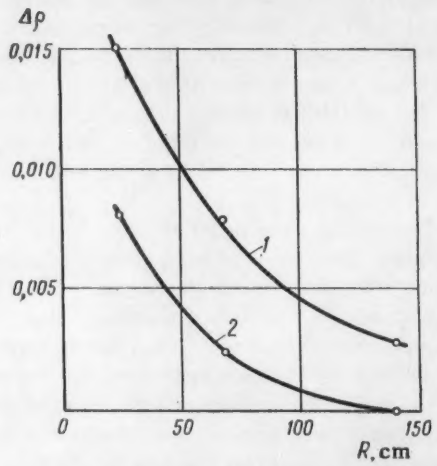

Fig. 3. Effectiveness of absorber rods as a function of their position around the core: 1) reflector (210 mm, graphite); 2) reflector (water).

2. Physical Simulation of Temperature Variation of Water Density

Temperature-induced changes in water density result in increased neutron migration length and greatly modify the physical characteristics of uranium-water reactors. Variation in water density in the core of a nuclear reaction was simulated by introducing special layers into the space between working plates. These layers were made from a thin resin film on a copper base and were filled with air. The volumes of air and layering material were determined by the volume of water displaced by them. The distance between working plates was small compared to the neutron diffusion length in water, and remained within 3-4 mm, while the thickness of the air-containing layers was about 2 mm. Experiments aimed at calculating the degree of heterogeneity of uranium-water systems with plate-type fuel elements such as described in [1] showed that such systems may be viewed as homogeneous systems at $\rho_H/\rho_{235} < 40$. In the case $\rho_H/\rho_{235} = 50$, the effect of the size of clearances between working plates in a cell on the critical dimensions of the systems did not exceed 4%. The uranium-water systems investigated were found to be quasi-homogeneous. Introduction of the special air-containing layers was therefore deemed to correspond to reduced pressure on the part of water filling the core. The mean water density in the core was calculated by taking into account the air found in the layers and the polyethylene contained in the working plates. Polyethylene is very similar in its slowing-down and diffusion properties to ordinary water. Its density is 0.9 g/cm^3. The density of the water filling the working cells was 1 g/cm^3 at the operating temperature of about 5°C. Water density within the reflector remained constant.

The effect of variation in the mean water density of the core on the critical size of multiplying systems was investigated for different ratios of moderator nuclei to fuel nuclei, ρ_H/ρ_{235}. The effect of the material used in the layers on the critical size of the systems was estimated by performing control experiments.

The usual procedure followed in these experiments was to admit water into the previously assembled core. The shape of the core was made as close as possible to a cylindrical configuration. The degree of subcriticality of the system was determined from the dependence of $1/n$ on the water level in the tank, where n is here the number of counts recorded by the triggering arrangement used to monitor the density of neutron flux near the core. A Po–Be neutron source was kept at all times in the vicinity of the core. The number of cells N at which the system was supercritical, and the number N–1 at which it was subcritical were also determined.

The error ΔV in critical size was thus ±0.31 liter. The mean water density was estimated to an accuracy within $\Delta\gamma = \pm 0.005$ g/cm^3. The results of experiments taking into account the material of the layering, are shown in Fig. 5, where the relationship between the critical volume of uranium-water systems and ρ_H/ρ_{235} ratios is shown.

In a system having a mean core water density γ = = 1.0 g/cm^3, γ = 0.9 g/cm^3, and γ = 0.8 g/cm^3, this relationship is represented by corresponding isodensity lines. Figure 5 shows the straight lines of constant U^{235} concentration in the systems studied plotted for three experimental cycles. Each cycle was carried through with the same number of working plates per cell (8, 6, and 5) and with a different number of air layers. The dependence of the critical volumes of uranium-water systems on the ratio of moderator to fuel densities over the range $\rho_H/\rho_{235} = 45-20$ was close to a linear one. The experiments performed made it possible to obtain

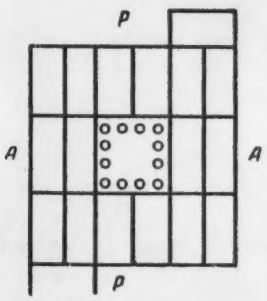

Fig. 4. Diagram of uranium-water system with mercury absorber ($\rho_H/\rho_{235} = 25$): P) control rods; A) scram rods. The mercury absorber was placed in the center of the system.

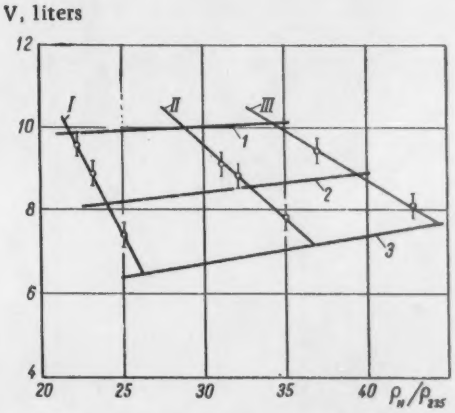

Fig. 5. Dependence of critical dimensions of uranium-water system on ratio ρ_H/ρ_{235} for different water densities: 1, 2, 3) water density γ equal to 0.8, 0.9, 1.0 g/cm^3, resp.; I, II, III) U^{235} concentrations equal to 836, 627, 523 g/liter, resp.

a quantitative estimate by varying the critical dimensions of the uranium-water multiplying systems based on intermediate neutrons as the density of the water filling the core was varied. It was found that at U^{235} isotope concentations of 836, 627, and 523 g/liter, a reduction in water density in the core of 0.1 g/cm^3 was accompanied by increased critical volume $\Delta V =$ $= (1.6 \pm 0.4)$ liters, $\Delta V = (1.4 \pm 0.4)$ liters, and $\Delta V =$ $= 1.2 \pm 0.4)$ liters, respectively. On the basis of experiments involving control of multiplying systems of this type, an estimate was made of the corresponding change in reactivity $\Delta\rho/\Delta\gamma$. These changes, for all three cases considered where the density of core water was varied by 0.1 g/cm^3, were 0.039, 0.034, and 0.029.

The compostion of the working plates included polyethylene witha density different from that of water. The values adduced in [1] for the critical dimensions of uranium-water systems with intermediate-spectrum neutrons should therefore be raised slightly. From Fig. 5, we may estimate the correction for different water and polyethylene densities over the interval $\rho_H/\rho_{235} =$ 45–20. The results obtained are close to those reported in [2].

The authors were unfortunately unable to carry out direct experiments on determination of the effect of polyethylene on the critical dimensions of the systems studied, which would be particularly important at low values of the ρ_H/ρ_{235} ratio.

In the previous work [1], the effect of various structural materials on the critical size of uranium-water water systems was evaluated. It was shown that the introduction of aluminum into the core at values of ρ_H/ρ_{235} in the range 30–17 sharply increased the critical size of the system.

The effect of aluminum and air layers on the critical dimensions of such systems at $\rho_H/\rho_{235} < 30$ was found to be the same in our experiments as in the previous ones [1]. When 190 g aluminum were introduced into the core in a volume of 70 cm^3 with U^{235} at a concentration of 836 g/liter, the critical volume of the system increased by (3.2 ± 0.3) liters. Experiments carried out with air layers showed that a reduction in mean density corresponding to a displacement of 70 cm^3 of water brought about the same change in the critical dimensions of the system as the addition of 190 g of aluminum to the core.

In conclusion, the authors would like to take this opportunity to express their heartfelt gratitude to S. M. Feinberg who was responsible for the general supervision of the work, to V. A. Tsykanov for his participation in discussion of the work, and to A. D. Merkulov, N. N. Kolpakov, B. A. Pryadekhin, and other workers who took part in the experimental work.

LITERATURE CITED

1. S. M. Feinberg, E. D. Vorob'ev, V. M. Gryazev, V. B. Klimentov, V. A. Tsykanov, and N. Ya. Lyashchenko, Paper 2142, presented at the Second International Conference for the Peaceful Uses of Atomic Energy (Geneva, 1958).
2. D. Callihan, Nucleonics 14, 7 (1956).

UTILIZATION OF NATURAL URANIUM IN A HOMOGENEOUS REACTOR

Vatslov Bartoshek

Translated from Atomnaya Énergiya, Vol. 7, No. 6, pp. 524-530, December, 1959
Original article submitted June 4, 1959

One of the main advantages of homogeneous reactors over heterogeneous reactors is the absence of stability problems with heat-emitting elements. Therefore, the permissible degree of uranium utilization, and consequently, the economic characteristics of a homogeneous reactor can be significantly improved.

This paper indicates the magnitude of uranium utilization with respect to the initial system parameters and establishes conditions for the probability of capture by U^{238} of slowed neutrons, the occurrence of which permits maximum utilization in a reactor using regenerated uranium.

Introduction

A homogeneous reactor operating with natural uranium and heavy water, and using as an enriching fuel the plutonium reproduced in the same reactor, operates during a major portion of its operating period in a so-called stationary cycle, in which a constant quantity of fissioning isotopes (U^{235}, Pu^{239}, Pu^{241}) is established [1]. The economic characteristics of such a reactor depend to a significant degree on the utilization of the introduced natural uranium as attained in this cycle. Since this is determined primarily by the reactivity of the system in the case of a homogeneous reactor, we shall try to determine from this viewpoint the conditions which permit one to attain maximum utilization

Neutron Balance Equation

In order to describe the isotopic concentration change while the reactor is operating, we shall select as an independent variable the exposure s, whose relation to the average neutron flux Φ and to the duration of reactor operation t is given by the expression

$$s = 10^{-21} \int_0^t \Phi(t')\, dt'$$

in such a way that the exposure s = 1 corresponds to the irradiation for one year with a flux $\Phi = 3.17 \cdot 10^{13}$ neutrons/cm^2 · sec. Furthermore, we shall introduce the following notation: N_n is the number of nuclei of the n-th isotope in one cm^3; N_n^0 is the number of nuclei of the n-th isotope in one cm^3 when the reactor is started up; $\rho_n = N_n/N_5^0$; $\rho_n^0 = N_n^0/N_5^0$; $\beta = N_M/N_5^0$; $v^0 = N_8^0/N_5^0$; σ_n is the capture cross section of the n-th isotope; I_n is the resonant-capture integral for the n-th isotope, φ_n is the probability of avoiding resonant capture by the n-th isotope; ν_i is the number of fast neutrons produced in fission of the i-th isotope; $\nu_i' = \nu_i \frac{\sigma_i^f}{\sigma_i}$; D is the diffusion coefficient; B^2 is the Laplacian of the system; ξ is the logarithmic energy loss of the neutron in a single collision; τ is the neutron multiplication. The meaning of the superscript indices is as follows: c signifies radiative capture; f signifies fission; s signifies scattering; st signifies contamination and poisoning; M signifies moderator. The subscript indices 5, 6, 8, 9, 0, 1, and 2 correspond to the isotopes U^{235}, U^{236}, U^{238}, Pu^{239}, Pu^{240}, Pu^{241}, and Pu^{242}.

The fuel to regenerated uranium balance in the reactor can be expressed as

$$\frac{d\varrho_5}{ds} \equiv \varrho_5' = -\varrho_5\left(\sigma_5 + \frac{1}{S}\right) + \frac{\varrho_5^d}{S}; \qquad (1a)$$

$$\varrho_6' = \varrho_5\sigma_5^c - \varrho_6\left(\sigma_6 + \frac{1}{S}\right); \qquad (1b)$$

$$\varrho_8' = -\varrho_8\left(\sigma_8 + \frac{1}{S}\right) - (1-\varphi_8)\, e^{-B^2\tau} f + \frac{\varrho_8^d}{S}; \qquad (1c)$$

$$\varrho_9' = \varrho_8\sigma_8 + (1-\varphi_8)\, e^{-B^2\tau} f - \varrho_9\sigma_9, \qquad (1d)$$

$$\varrho_0' = \varrho_9\sigma_9^c - \varrho_0\left(\sigma_0 + \frac{I_0}{\xi\sigma_M^s}\frac{\varphi_8 e^{-B^2\tau}}{\beta} f\right); \qquad (1e)$$

$$\varrho_1' = \varrho_0\left(\sigma_0 + \frac{I_0}{\xi\sigma_M^s}\frac{\varphi_8 e^{-B^2\tau}}{\beta} f\right) - \varrho_1\sigma_1; \qquad (1f)$$

$$\varrho_2' = \varrho_1\sigma_1^c - \varrho_2\left(\sigma_2 + \frac{J_2}{\xi\sigma_M^s}\frac{\varphi_s e^{-B^2\tau}}{\beta} f\right), \qquad (1g)$$

where the relative number of fast neutrons is designated by

$$f = \nu_5'\varrho_5\sigma_5 + \nu_9'\varrho_9\sigma_9 + \nu_1'\varrho_1\sigma_1, \qquad (2)$$

and terms with the quantity S express the influence of regenerated uranium: ρ^d_5/S determines the relative number of U^{235} nuclei introduced into the system during the course of unit irradiation; ρ_5/S is the relative number of U^{235} nuclei withdrawn from the system during the same period. The terms in S in Equations (1b) and (1c) have analogous significance. Equations (1a)-(1g) do not take into account the influence of neptunium, which is considered insignificant; also, resonant capture in Pu^{240} is expressed in a simplified manner.

The system of differential Equations (1a)-(1g) is nonlinear, and is usually solved numerically. In the steady state (index = ∞) for isotopes U^{235} – Pu^{241}, $\rho'_n = 0$ and $f = f^{\infty} = \text{const}$. With the help of designations

$$\gamma_8 = \sigma_8 + \frac{(1-\varphi_8)\,e^{-B^2\tau}}{\varrho_8} f \qquad (3a)$$

and

$$\gamma_h = \sigma_k + \frac{J_k}{\xi\sigma_M^s}\frac{\varphi_8 e^{-B^2\tau}}{\beta} f \qquad (k = 0 \text{ or } 2) \qquad (3b)$$

the solution of the system in the steady state may be written as follows:

$$\varrho_5^{\infty} = \frac{\varrho_5^d}{1+\sigma_5 S}; \qquad (4a)$$

$$\varrho_6^{\infty} = \frac{\sigma^c S}{1+\sigma_6 S}\varrho_5^{\infty}; \qquad (4b)$$

$$\varrho_8^{\infty} = \frac{\sigma_8^d}{1+\gamma_8^{\infty} S}; \qquad (4c)$$

$$\varrho_9^{\infty} = \frac{\gamma_8^{\infty}\varrho_8^{\infty}}{\sigma_9}; \qquad (4d)$$

$$\varrho_0^{\infty} = \frac{\gamma_8^{\infty}\varrho_8^{\infty}}{\gamma_0^{\infty}}\frac{\sigma_9^c}{\sigma_9}; \qquad (4e)$$

$$\varrho_1^{\infty} = \frac{\gamma_8^{\infty}\varrho_8^{\infty}}{\sigma_1}\frac{\sigma_9^c}{\sigma_9}. \qquad (4f)$$

It follows from the numerical solution of Equations (1a)-(1g) that because of the relatively small value of σ_2 the concentration of Pu^{242} reaches equilibrium very slowly, and therefore this concentration can be considered insignificant at the beginning of the steady state. From this it follows that the behavior of $\rho_2(s)$ can be satisfactorily found by solving Equations (1a)-(1g) using constant coefficients $\gamma_8'^{\infty}$, γ_0^{∞}, and γ_2^{∞}. From such a solution it follows that for irradiation $s \simeq 50$ the concentration of Pu^{242} assumes an equilibrium value

$$\varrho_2^{\infty} = \frac{\gamma_8^{\infty}\varrho_8^{\infty}}{\gamma_2^{\infty}}\frac{\sigma_9^c}{\sigma_9}\frac{\sigma_1^c}{\sigma_1}, \qquad (5a)$$

while in the interval s = 10 to 50

$$\varrho_2(s) \simeq \varrho_2^{\infty} 0{,}02s. \qquad (5b)$$

It follows from Equations (4a)-(4f) and (5) that the equilibrium concentrations of plutonium isotope nuclei depend on the breeding of Pu^{239} from U^{238}, which can be expressed by the relation

$$\varrho_8^{\infty}\gamma_8^{\infty} = \varrho_8^{\infty}\sigma_8 + (1-\varphi_8)\,e^{-B^2\tau}\nu_5'\varrho_5^{\infty}\sigma_5 + \\ + \varrho_8^{\infty}\gamma_8^{\infty}(1-\varphi_8)\,e^{-B^2\tau}\left(\nu_9' + \nu_1'\frac{\sigma_9^c}{\sigma_9}\right);$$

consequently, the Pu^{239} breeding coefficient in the stationary state is

$$R_9^{\infty} \equiv \frac{\varrho_8^{\infty}\gamma_8^{\infty}}{\varrho_5^{\infty}\sigma_5} = \frac{\vartheta^{\infty}\frac{\sigma_8}{\sigma_5} + (1-\varphi_8)\,e^{-B^2\tau}\nu_5'}{1-(1-\varphi_8)\,e^{-B^2\tau}\nu_{Pu}}, \qquad (6)$$

where we designate

$$\nu_{Pu} = \nu_9' + \frac{\sigma_9^c}{\sigma_9}\nu_1'; \quad \vartheta^{\infty} = \frac{\varrho_8^{\infty}}{\varrho_5^{\infty}}. \qquad (7)$$

Neutron Excess

In order to be able to use the solutions of the fuel-balance equations, we shall state the criticality equation

$$\frac{e^{-B^2\tau}\varphi_8\varphi_0\varphi_2 f}{(1+L^2B^2)\left(\sum_i \varrho_i\sigma_i + \sum_j \varrho_j\sigma_j + \sum_l \varrho_l\sigma_l\right)} = 1 + \Delta k, \qquad (8)$$

in which we have apportioned the capture of thermal neutrons into the categories of a) capture by fissioning isotopes (index i), b) capture by isotopes which then become fissioning isotopes (j = 8.0), and c) unproductive capture (index l), in the following manner:

$$\Delta k\left(\sum_n \varrho_n\sigma_n + \frac{DB^2}{N_5^0}\right) = e^{-B^2\tau}f - \\ - \sum_i \varrho_i\sigma_i - \varrho_8\sigma_8 - (1-\varphi_8)\,e^{-B^2\tau}f - \\ - \varrho_0\sigma_0 - (1-\varphi_0)\,\varphi_8\varphi_2 e^{-B^2\tau}f - \varrho_2\sigma_2 - \\ - (1-\varphi_2)\,\varphi_8 e^{-B^2\tau}f - \varrho_6\sigma_6 - \beta\sigma_M - \frac{DB^2}{N_5^0}.$$

We shall define the neutron excess δ as the quantity of surplus thermal neutrons (over that needed

to maintain the chain reaction) relative to each neutron captured by a fissioning isotope. Using the same approximations as for Equations (1a)-(1g), i.e., with

$$(1-\varphi_0)\simeq \varrho_0\frac{I_0}{\beta\xi\sigma_M^s};\quad (1-\varphi_2)\simeq \varrho_2\frac{I_2}{\beta\xi\sigma_M^s},$$

and neglecting second-order quantities [$(1-\varphi_0)(1-\varphi_2)\simeq \simeq 0$], we obtained the following expression for the neutron excess:

$$\delta=\frac{\Delta k\left(\sum_n \varrho_n\sigma_n+\frac{DB^2}{N_8^0}\right)}{\sum_i \varrho_i\sigma_i}= =\frac{e^{-B^2\tau}f}{\sum_i \varrho_i\sigma_i}-1-\frac{\sum_j \varrho_j\gamma_j}{\sum_i \varrho_i\sigma_i}- -\frac{\varrho_2\gamma_2+\varrho_6\sigma_6+\beta\sigma_M+\frac{DB^2}{N_8^0}}{\sum_i \varrho_i\sigma_i}. \tag{9}$$

The neutron excess serves as a measure of the system reactivity; the reaction becomes critical for $\delta = 0$ and has a positive reactivity for $\delta > 0$.

The first term on the right-hand side of Equation (9) (we shall call it η) gives the number of thermalized neutrons remaining in the system relative to each fissioning isotope nucleus. The expression

$$R=\frac{\sum_j \varrho_i\gamma_i}{\sum_i \varrho_i\sigma_i}=\frac{\varrho_8\gamma_8+\varrho_0\gamma_0}{\sum_i \varrho_i\sigma_i} \tag{10}$$

appears as the breeding coefficient of the fissioning isotopes in the system (i.e., it gives the number of fissionable nuclei produced for each nucleus disappearing by fission). The next term on the right side (we shall call it Z) gives the relative unproductive neutron capture by non-fissioning isotopes of plutonium and uranium, the relative losses in the moderator, and the escape of thermal neutrons.

For the initial state of the homogeneous system with uranium (index 0) we obtain

$$\eta^0=e^{-B^2\tau}\nu_5'; \tag{11a}$$

$$R^0\equiv\frac{\vartheta^0\gamma_8^0}{\sigma_5}=\vartheta^0\frac{\sigma_8}{\sigma_5}+(1-\varphi_8)e^{-B^2\tau}\nu_5'; \tag{11b}$$

$$Z^0\equiv\frac{\beta\sigma_M+\frac{DB^2}{N_8^0}}{\sigma_5}=(1+L_M^2B^2)\vartheta^0\frac{\sigma_8}{\sigma_5}\frac{N_M}{N_8}\frac{\sigma_M}{\sigma_8}$$

(assuming that $D = D_M$).

Neutron Excess in the Stationary State

Solving the fuel balance equations permits us to calculate the neutron excess in the stationary state. The relative number of the thermalized neutrons remaining in the system is

$$\eta^\infty=\nu_5'e^{-B^2\tau}+\frac{a_{Pu}R_9^\infty}{1+a_{Pu}R_9^\infty}e^{-B^2\tau}(\nu_{Pu}'-\nu_5'), \tag{12}$$

where

$$a_{Pu}=1+\frac{\sigma_9^c}{\sigma_9};\quad \nu_{Pu}'=\frac{\nu_{Pu}}{a_{Pu}}$$

and R_9^∞ is the breeding coefficient of Pu^{239}, determined by the relation (6).

The breeding coefficient (10) is

$$R^\infty=\frac{a_{Pu}R_9^\infty}{1+a_{Pu}R_9^\infty}. \tag{13}$$

It follows from expressions (12) and (13) that the difference between the number of fast neutrons formed in the capture of one neutron by fissioning plutonium isotopes and the number of fast neutrons formed in the capture by U^{235} is reflected in the neutron excess, with a value equal to the breeding coefficient of the system.

In an equilibrium system, thermal neutrons are lost primarily through capture by non-fissioning isotopes of uranium and plutonium, i.e., in U^{236} and Pu^{242}. The losses in U^{236} are

$$Z_6=\frac{\sigma_6 S}{1+\sigma_6 S}\frac{\sigma_5^c}{\sigma_5}\frac{1}{1+a_{Pu}R_9^\infty}; \tag{14}$$

the losses in Pu^{242} in the range s = 10 to 50 depends on s:

$$Z_2=\frac{R_9^\infty}{1+a_{Pu}R_9^\infty}\frac{\sigma_9^c}{\sigma_9}\frac{\sigma_1^c}{\sigma_1}0{,}02s, \tag{15}$$

while for s = 50, the losses assume an equilibrium (i.e., maximum) value. The losses due to capture by the moderator and due to escape are

$$Z^\infty=\frac{\beta\sigma_M+\frac{DB^2}{N_8^0}}{\varrho_5^\infty\sigma_5(1+a_{Pu}R_9^\infty)}. \tag{16}$$

Losses occur likewise in a stationary cycle due to neutron capture by the contaminating fission fragments. If the relative capture in the contaminants, which are produced by the fission, of U^{235}, Pu^{239}, and Pu^{241}, is designated by $\sum_k \varrho_k\sigma_k$, then the losses in fission fragments are

$$Z_{sl}=\frac{\sum_k \varrho_k\sigma_k}{\varrho_5^\infty\sigma_5(1+a_{Pu}R_9^\infty)}. \tag{17a}$$

s	$\varphi_s=0{,}766$ $R_{crit}=182$ cm		$\varphi_s=0{,}788$ $R_{crit}=172$ cm		$\varphi_s=0{,}813$ $R_{crit}=166$ cm		$\varphi_s=0{,}827$ $R_{crit}=166$ cm		$\varphi_s=0{,}855$ $R_{crit}=173$ cm		$\varphi_s=0{,}869$ $R_{crit}=181$ cm	
	ρ_5^∞	E, milliwatt-days/ton	ρ_5^∞	E, milliwatt-days/ton	ρ_5^∞	E, milliwatt-days/ton	ρ_5^∞	E, milliwatt-days/ton	ρ_5^∞	E, milliwatt-days/ton	ρ_5^∞	E, milliwatt-days/ton
10	0,453	9671	0,464	8026	0,476	6660	0,468	6320	0,495	5060	0,503	4603
20	0,499	7557	0,501	6546	0,506	5625	0,493	5520	0,517	4457	0,523	4092
30	0,548	5534	0,540	5122	0,537	4624	0,518	4750	0,539	3868	0,543	3594
40	0,602	3571	0,582	3740	0,570	3649	0,545	4003	0,561	3292	0,563	3107
50	0,659	1641	0,627	2385	0,604	2696	0,572	3278	0,585	2728	0,584	2628

For individual fission fragments which comprise the overwhelming majority, proper clearing produces the equation

$$\frac{dQ_k}{ds} = w_{5k}Q_5\sigma_5' + w_{9k}Q_9\sigma_9' + \\ + w_{1k}Q_1\sigma_1' - Q_k\sigma_k\left(1 + \frac{\lambda_k}{\Phi\sigma_k} + \frac{1}{S_k\sigma_k}\right),$$

where w_{1k} is the yield of the k-th fission fragment on fission of the i-th isotope; λ_k is the disintegration constant of the k-th fission fragment; S_k (in analogy to the case of uranium breeding) designates the operating time during which the equilibrium quantity of the k-th fission fragment is produced in the reactor. The losses due to individual fission fragments in the stationary state are equal to

$$Z_{st} = \frac{W_5 + R_9^\infty W_9}{1 + a_{Pu}R_9^\infty}, \qquad (17b)$$

where

$$W_5 = \sum_k \frac{w_{5k}\frac{\sigma_5'}{\sigma_5}}{1 + \frac{\lambda_k}{\Phi\sigma_k} + \frac{1}{S_k\sigma_k}} \qquad (18)$$

and

$$W_9 = \sum_k \frac{w_{9k}\frac{\sigma_9'}{\sigma_9} + w_{1k}\frac{\sigma_1'}{\sigma_1}\frac{\sigma_9^c}{\sigma_9}}{1 + \frac{\lambda_k}{\Phi\sigma_k} + \frac{1}{S_k\sigma_k}}. \qquad (19)$$

Utilization of Uranium

In its initial state the system has a neutron excess expressed by Equations (9), (11a), and (11b). If the breeding of uranium in the reactor occurs in such a way that the quantity of U^{238} nuclei per cm^3 remains constant ($N_8^\infty = N_8^0$), then it can be shown that the relative volume change of the moderator is

$$\frac{\Delta V_M}{V_M} \leqslant 0{,}1\%.$$

This means that the moderation and diffusion characteristics of the system are practically invariant, and therefore one can write

$$(N_M\sigma_M + DB^2)^0 = (N_M\sigma_M + DB^2)^\infty; \qquad (20)$$

$$\left.\begin{aligned} \varphi_s^0 &= \varphi_s^\infty = \varphi_s; \\ (B^2\tau)^0 &= (B^2\tau)^\infty. \end{aligned}\right\} \qquad (21)$$

In such an equilibrium system the neutron excess is determined by the expression

$$\delta^\infty = \nu_5' e^{-B^2\tau} - 1 - R^\infty\left[1 + e^{-B^2\tau}(\nu_5' - \nu_{Pu}') +\right.$$

$$+\frac{\sigma_9^c}{\sigma_9}\frac{\sigma_1^c}{\sigma_1}\frac{0{,}02s}{a_{Pu}}+\frac{W_9}{a_{Pu}}\Big]-$$

$$-\frac{1}{1+a_{Pu}R_9^\infty}\left(\frac{Z^0}{\varrho_5^\infty}+W_5+\frac{\sigma_5^c}{\sigma_5}\frac{\sigma_6 S}{1+\sigma_6 S}\right). \quad (22)$$

If the neutron excess in the system is initially equal to δ^0, we can convert expression (22) into the expression

$$\bar{\delta}^\infty \equiv \delta^\infty(1+a_{Pu}R_9^\infty) =$$

$$=\eta^0-1-\overline{W}_5-K\frac{\psi_8\eta^0}{1-\psi_8 e^{-B^2\tau}\nu_{Pu}}-$$

$$-\frac{1}{\varrho_5^\infty}\left(\eta^0-1-\delta^0-\vartheta^0\frac{\sigma_8}{\sigma_5}-\psi_8\eta^0+\right.$$

$$\left.+K\frac{\vartheta^0\frac{\sigma_8}{\sigma_5}}{1-\psi_8 e^{-B^2\tau}\nu_{Pu}}\right), \quad (23)$$

where we define

$$\overline{W}_5=W_5+\frac{\sigma_6 S}{1+\sigma_6 S}\frac{\sigma_5^c}{\sigma_5}; \quad (24a)$$

$$K(s)=a_{Pu}(2-e^{-B^2\tau}\nu'_{Pu})+0{,}02s\frac{\sigma_9^c}{\sigma_9}\frac{\sigma_1^c}{\sigma_1}+W_9; \quad (24b)$$

$$\psi_8=1-\varphi_8 \quad (24c)$$

and have used expressions (6), (7), and (11b).

If the reactor was initially critical ($\delta^0 = 0$), and remained critical after a given operating time in an equilibrium state ($\bar{\delta}^\infty = 0$), then under these conditions Equation (23) was satisfied, and consequently, it was possible to utilize the introduced uranium ρ_5^∞. We have employed in our computations the fact that W_5 can be considered independent of s because of the small value of σ_6.

The operating period S (which we define to be that operating period in which we have total renewal of the uranium in the reactor) is linked to the concentrations of the introduced uranium $\rho_5^d = N_5^d/N_5^0$ and of the utilized uranium, in accord with expression (4a), by the relation

$$S=\frac{1}{\sigma_5}\left(\frac{\varrho_5^d}{\varrho_5^\infty}-1\right). \quad (25)$$

In the course of an equilibrium-state operation with one ton of introduced natural uranium, we obtain the energy

$$E=\left(1-\frac{\varrho_5^\infty}{\varrho_5^d}\right)\left[\frac{\sigma_5^f}{\sigma_5}+\right.$$

$$\left.R_9^\infty\left(\frac{\sigma_9^f}{\sigma_9}+\frac{\sigma_1^f}{\sigma_1}\frac{\sigma_9^c}{\sigma_9}\right)\right] \text{ 6450 millwatt-days/ton.} \quad (26)$$

If we substitute ρ_5^∞ and R_9^∞ into expression (26), we shall obtain the corresponding energy yield. It can be seen from this formula that in general E increases with decreasing ρ_5^∞ and with increasing R_9^∞, but the values of these quantities are related to each other by the limiting criticality conditions, which by expression (22) demand that $\bar{\delta}^\infty = 0$.

The table shows several values of U^{235} equilibrium concentrations (ρ_5^∞) and the corresponding energy release (E) per ton of introduced natural uranium in relation to the over-all operating time S since beginning of reactor operation, using several critical assembly dimensions [2]. The table wes compiled using the following parameter values:

$$\vartheta^0=97{,}8;$$

$$\varrho_5^d=0{,}712;\ \vartheta^0\frac{\sigma_8}{\sigma_5}=0{,}4086;\ T=500^\circ\text{K};\ \nu'_5=2{,}08;$$

$$\nu_{Pu}=2{,}64;\ \nu'_{Pu}=1{,}97;\ a_{Pu}=1{,}34;\ \frac{\sigma_9^c}{\sigma_9}\frac{\sigma_1^f}{\sigma_1}=0{,}106;$$

$$\frac{\sigma_9^f}{\sigma_9}+\frac{\sigma_1^f}{\sigma_1}\frac{\sigma_9^c}{\sigma_9}=0{,}994;\ W_{Pu}=0{,}0210;\ \overline{W}_5=0{,}0216;$$

$$\nu_0=1{,}91,\ \nu'_1=2{,}14.$$

The figure shows the attainable utilization E per ton of introduced natural uranium, with respect to S. It can be seen from the figure that for identical reactor dimensions and short operating periods it is possible to attain higher utilization with high uranium concentrations, while for long operating periods a higher utilization is attained with low uranium concentrations. One can therefore expect that for given

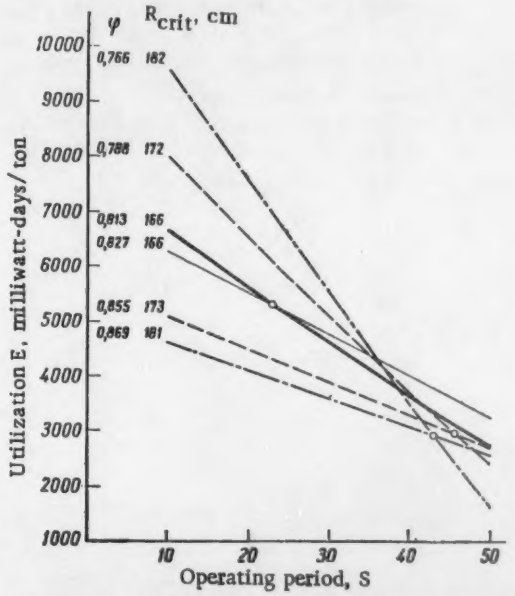

Utilization of natural uranium in a homogeneous reactor

reactor dimensions and corresponding to each operating period S there exists a certain optimum uranium concentration (optimum φ_s) which permits attaining a minimum ρ_s^{∞} and consequently, maximum utilization.

Optimum Cycle in an Equilibrium State

For a reactor of fixed dimensions the conditions

$$\delta^0 \equiv \eta^0 (1 - \psi_s) - $$
$$- 1 - \vartheta^0 \frac{\sigma_s}{\sigma_5} \left[1 + \frac{N_M \sigma_M}{N_s \sigma_s} (1 + L_M^2 B^2) \right] = 0$$

determine the reciprocal relation between ϑ^0 and ψ_s. The requirement $\bar{\delta}^{\infty} = 0$ (23) specifies the attainable equilibrium concentration ρ_s^{∞} as a function of the values of ϑ^0 and ψ_s. It can be seen from expression (23) that for $\bar{\delta}^{\infty} = 0$, the quantity ρ_s^{∞} decreases monotonically with increasing ϑ^0; on the other hand, it can increase or decrease as a function of ψ_s, and for $\partial \rho_5^{\infty} / \partial \psi_s = 0$ it can assume a locally extreme value, leading to the result

$$(1 - \psi_s e^{-B^2 \tau} \nu_{Pu})^2 = K \left(\varrho_s^{\infty} + \frac{\nu_{Pu}}{\nu_5'} \frac{\sigma_s}{\sigma_5} \vartheta^0 \right), \quad (27a)$$

or

$$\psi_s = \frac{1}{e^{-B^2 \tau} \nu_{Pu}} \left[1 \pm \sqrt{K \left(\varrho_s^{\infty} + \frac{\nu_{Pu}}{\nu_5'} \frac{\sigma_s}{\sigma_5} \vartheta^0 \right)} \right]. \quad (27b)$$

A more detailed analysis shows that a local minimum of ρ_5^{∞} corresponds to the negative sign in Equation (27b), and that this value appears to be physically realizable in contrast to the value which corresponds to the positive sign in Equation (27b).

It is possible to eliminate ρ_5^{∞} from Equations (27) and (23) and to find a relation between ψ_s and ϑ^0 for which ρ_5^{∞} appears as a minimum:

$$\vartheta^0 \frac{\sigma_s}{\sigma_5} = $$
$$= \frac{1 - K - (\eta^0 - 1 - \bar{W}_5) \frac{\nu_{Pu}}{\nu_5'}}{\eta^0 - 1 - \frac{\eta^0 - 1 - \bar{W}_5}{K} (1 - \psi_s e^{-B^2 \tau} \nu_{Pu})^2 - \psi_s^2 \eta^0 e^{-B^2 \tau} \nu_{Pu}}. \quad (28)$$

In order to have the reactor initially critical, we must satisfy

$$\vartheta^0 \frac{\sigma_s}{\sigma_5} = \frac{\eta^0 (1 - \psi_s)}{1 + \frac{N_M}{N_s} \frac{\sigma_M}{\sigma_s} (1 + L_M^2 B^2)}, \quad (29)$$

in such a way that Equations (28) and (29) determine the parameters for which the reactor is initially critical and at the same time has a value of ψ_s (optimum uranium concentrations) such that for S it has a minimum attainable concentration ρ_s^{∞} as determined by Equation (27). By calculating the values of $\psi_{s\,opt}$ corresponding to various values of $\underline{s}$ in the interval $s = 10$ to 50, we shall obtain the function $\psi_{s\,opt}(s)$ and the corresponding concentration of uranium in heavy water for which one can always attain the maximum uranium utilization.

Smaller $\underline{s}$ means we get smaller values of $\varphi_{s\,opt}$ (i.e., the concentration of uranium in the moderator will be large), while for increased $\underline{s}$ the values of $\varphi_{s\,opt}$ will also grow (i.e., the uranium concentration will decrease). This means that the optimum cycle in the equilibrium state occurs not for a constant uranium concentration, but rather for a gradually decreasing concentration; this reminds one of the dilution cycle proposed in [1] as a means of extending the period of use of an equilibrium-state reactor which had stopped being critical.

It is necessary to note once more that the analysis we have conducted concerning an optimum cycle is based on the assumptions that $\bar{W}_s$ and W_9 do not depend on the utilization and appear to be constant; i.e., removal of fission fragments from the reactor is carried out at a constant rate and is independent of the operating cycle, and neutron capture in U^{236} is small. However, even in the case where fission fragment removal from the reactor is carried out simultaneously with uranium renewal ($S_k = S$), the above analysis remains qualitatively valid.

LITERATURE CITED

1. V. M. Byakov and B. L. Ioffe, Transactions of the Second International Conference on Peaceful Uses of Atomic Energy [Russian translation], (Geneva, 1958) 2; Nuclear Reactors and Nuclear Power [in Russian] (Atomizdat, Moscow, 1959), p. 398.
2. I. Rochek, Calculations on the Critical Dimensions of Homogeneous Reactors [Russian translation], Trudy In-ta yadernoi fiz. (Prague, 1958), No. 325.

DETERMINATION OF THE SOLUBILITY OF METALS IN LITHIUM

Yu. F. Bychkov, A. N. Rozanov, and V. B. Yakovleva

Translated from Atomnaya Énergiya, Vol. 7, No. 6, pp. 531-536
December, 1959
Original article submitted March 9, 1959

The solubility of uranium, zirconium, iron, nickel, titanium, molybdenum, niobium and beryllium in lithium at temperatures of 700-1000°C was determined to assess the stability of metals in lithium and establish the mechanism of corrosion. It was found that nickel and beryllium have a high solubility (of the order of 1%), iron, zirconium, titanium and uranium are slightly soluble (from hundredths to thousands of one percent) and niobium and molybdenum have a very low solubility (less than 10^{-4}%). Crucibles of the lithium to be tested were filled in a special still with distilled lithium and hermetically sealed in a container in a medium of argon. The solubility of the metal to be tested was determined by chemical analysis of rapidly cooled lithium fusions after they had been kept for 50-100 hours in the container at a predetermined temperature. The presence of isothermal transfer of aluminum, beryllium, zirconium and silicon via lithium to steel and iron was discovered. Under these conditions maximum solubility of the metal in lithium was reached far more slowly than in the absence of transfer. Lithium can be purified by getters – uranium and zirconium – slightly soluble in lithium.

The thermophysical properties of lithium are superior to the properties of other metallic heat carriers and it is, therefore, of great interest to find materials which are stable in lithium at high temperatures.

To assess the stability of metals in lithium and determine the mechanism of corrosion, it is necessary to know the solubility of various metals in it at different temperatures, i.e., the lines of the liquidus of the phase diagrams of the metals with lithium. There is little data in literature on the solubility of high melting point metals in lithium which could provide a basis for selecting alloys stable in lithium. It is known that after a residence time of 100 hours at 480° C in vibrating zirconium crucibles, the lithium contained 0.01% zirconium, and after tests at 760°C – about 1% zirconium [1]. It is also known that chrome steels, iron, niobium, molybdenum and tantalum have a high stability in lithium at temperatures up to 800°C, whereas chrome-nickel steels are stable only up to 500°C [2].

Lithium forms alloys with magnesium, aluminum, silicon, silver, platinum, copper and gold at comparatively low temperatures [3]. Leaching of nickel to a depth of 0.02 mm was detected metallographically in type YaO chrome-nickel stainless steel after a residence time of 40 hours in lithium at 1000°C; this converted the γ phase in the surface layers of the crucible to the α phase [4].

The change in the mechanical properties, structure and composition of carbon, chrome and chrome-nickel steels after 230 hours corrosion testing in lithium at 800°C was investigated in [5]. The tests were carried out in Armco iron crucibles. Under these conditions chrome-nickel steels and also chrome steels with 2% nickel were intensely corroded while chrome steels were more stable. 1Kh12MV4B steel was the most stable. The resistance of stainless steels, iron, beryllium and thorium to corrosion in lithium at 300 and 600°C under static conditions was investigated in [6] by the metallographic method and the change in weight. According to the data of this work, thorium and low-carbon high-chrome steel containing 14-18% chromium had the maximum resistance. The resistance of pure iron and chrome-nickel steel of type 18-8 alloyed with niobium was almost as high; ordinary 18-8 steel and high-chrome steel with 0.6-0.7% carbon underwent severe corrosion; nickel and Inconel were still more markedly corroded.

Investigation Procedure and Apparatus. Crucibles of the metals to be tested were used to determine the solubility in lithium. The inner surface of the crucible was ground, after which it was electrolytically polished or etched. These crucibles were filled in a special still with freshly distilled lithium (Fig. 1). Electrolytic lithium 10 was placed in a stainless-steel evaporator 8, welded to the lower flange of a vacuum chamber 1. The crucible was heated by furnace 9 to a temperature of about 800°C. The vaporizing lithium heated the stainless-steel condenser 2 (of thickness 1 mm) to 250°C; this condenser was in the form of a trihedral pyramid with guides welded to the sides. The lithium deposited on the condenser flowed down the three guides into three crucibles 6, installed on the sole

and filled them, while the elements more volatile than lithium condensed in the cold parts of the chamber. Difficultly volatile elements remained in the evaporator. During the distillation the pressure in the chamber was kept at 10^{-4}-10^{-3} mm Hg. After the process had been completed the still was filled with pure argon; the content of impurities in the lithium after distillation was reduced: sodium to 0.02-0.06%, potassium to 0.015%, iron to $1\text{-}4 \cdot 10^{-4}$%, magnesium to 0.002% and less; silicon, nickel and chromium were not detected.

The crucibles filled with lithium were placed in Ya1-T stainless steel containers, to which the covers were slowly welded in an arc furnace in an atmosphere of argon. The containers were then placed in the furnace for isothermal treatment. Crucibles of metals which react at the temperature of the test with stainless steel were isolated from the steel by sheet molybdenum, with which they were fixed in the containers.

Since the content of lithium-dissolved metal depended markedly on the rate of cooling from the temperature of isothermal treatment, after the treatment was finished the containers were cooled in water. As was shown by direct measurements, this ensured cooling of the lithium fusions to the solidification point in less than 50 sec.

The content of the elements dissolved in lithium was determined calorimetrically. The initial materials for the investigation were zirconium iodide of 99.9% purity, titanium of grade TG-O smelted into rods of diameter 30-40 mm in a MIFI SM-3 arc furnace, baked briquets of molybdenum and niobium powder, Armco iron smelted and cast under vacuum, distilled beryllium, uranium and nickel crucibles cast or obtained from sheet by pressing.

The mechanical properties of molybdenum, niobium and zirconium before and after reaction with lithium were determined on a micromachine for specimens of diameter 1.2 mm. The properties of the other metals were investigated on specimens of diameter 3 mm with a working length of 20 mm.

Isothermal Transfer of Metals via Lithium. Crucibles of Armco iron, Ya1 chrome-nickel steel and Zh1 chrome steel, in which lithium and the samples of the metal to be tested were placed, were used in the ini-

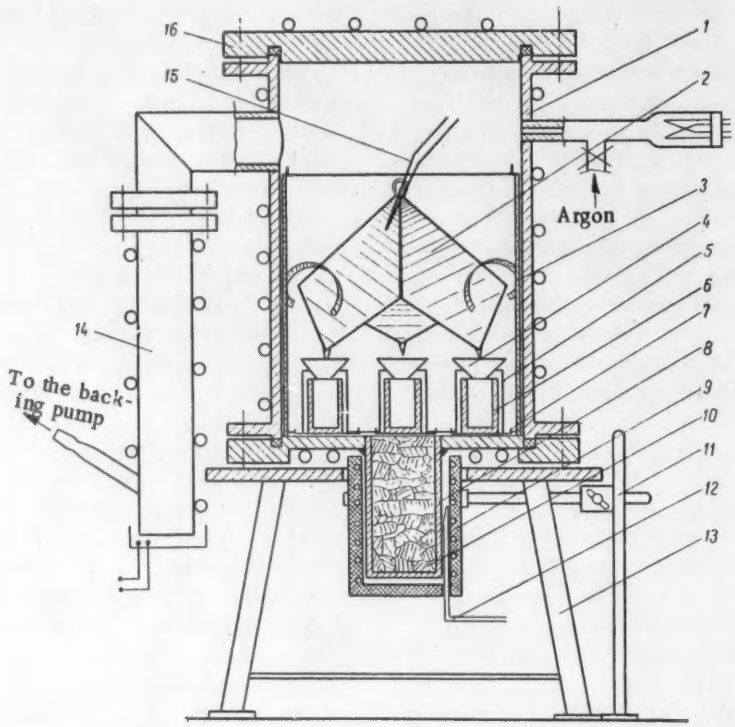

Fig. 1. Diagram of the apparatus for filling crucibles with distilled lithium: 3) screen on which sodium and potassium condense; 4) funnel; 5) screen; 7) backing; 11) support; 12) thermocouple; 13) brace; 14) diffusion pump; 15) thermocouple; 16) cover (remainder of the legend given in the text).

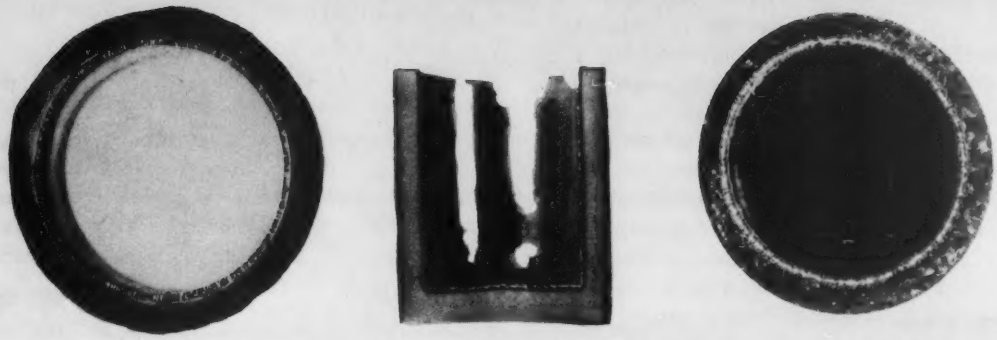

a b c

Fig. 2. Macrostructure (× 2) of the crucible walls after isothermal transfer via lithium at 1000°C: a) silicon on iron after 40 hours; b) aluminum on iron after 50 hours; c) beryllium on Yal-T after 400 hours.

tial experiments. After they had been kept at the temperature of the test, the welded sealed containers containing the crucibles with lithium and the samples were cooled in water.

It was found that if the material of the crucible differs from the material of the sample, precipitation of the metals from the lithium fusion may occur on the walls of the crucible. The precipitation of large crystals of silicon on iron (Fig. 2a), aluminum on iron (Fig. 2b) and beryllium on steel (Fig. 2c) can be detected very clearly by visual means. The transfer and precipitation of metals from the fused system can also be judged by the variation in the microhardness of the surface of these crucibles (Fig. 3).

The transfer and precipitation of metals during isothermal treatment is only possible if the chemical affinity of the dissolved metal for the material of the crucible is greater than the affinity for lithium. Whereas silicon and aluminum, which have a high affinity for iron, were precipitated from lithium, lithium-dissolved magnesium was not precipitated on iron.

The transfer and precipitation of zirconium were investigated by means of the radioactive isotope Zr^{95}. After Zr^{95} powder wrapped in tantalum foil and placed in a Yal-T stainless-steel crucible had been kept in lithium for 100 hours at 900°C it was found that the tantalum foil had not become active, whereas the crucible, with which the zirconium was not in direct contact, had a γ activity corresponding to $4 \cdot 10^{-3}$ g of zirconium. At 800°C about 10^{-4} g of zirconium was transferred in 10 hours from a plate of radioactive zirconium to a Yal steel crucible. This shows that at temperatures of 800-900°C the chemical affinity of zirconium for tantalum is slight, whereas that of iron for nickel, included in the composition of stainless steel, is high. By reacting with zirconium dissolved in lithium, stainless steel disturbs the equilibrium, which leads to further dissolution of zirconium and its transfer on to the crucible walls. Naturally, in the presence of transfer the rate of dissolution of the metals increases.

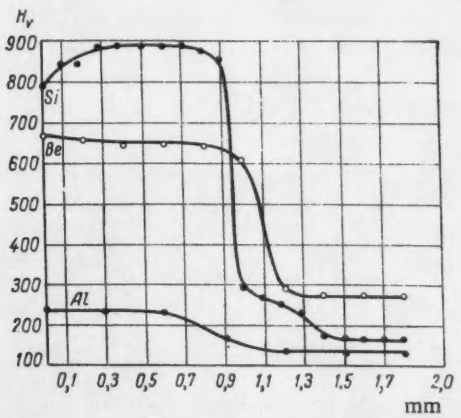

Fig. 3. Microhardness of the surface of the crucibles: O) stainless steel crucible ; ●) iron crucible.

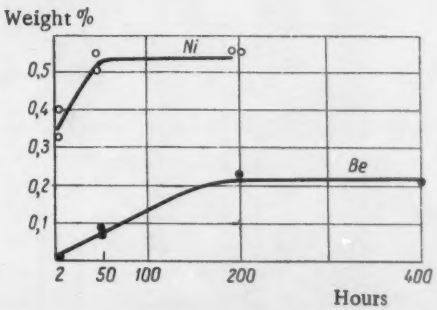

Fig. 4. Kinetics of the dissolution of nickel in lithium at 750°C and beryllium at 1000°C.

The concentration of zirconium in lithium under conditions of transfer was determined by comparing the γ activity of Zr^{95} in a given sample of lithium and the radioactivity of a known sample of the initial Zr^{95}. The uniformity of the distribution of zirconium was checked by measuring the radioactivity of different lithium samples. After 100 hours in stainless-steel crucibles the zirconium content in lithium determined by means of Zr^{95} at 900°C was $1\text{-}1.4 \cdot 10^{-2}$%. This value was of the same order as the solubility of zirconium in lithium determined chemically. From these experiments it follows that, in particular, tantalum crucibles can be used for the determination of the solubility of zirconium in lithium. In [5] carburization of chrome-nickel steel to 0.6-0.7% carbon and chrome steel to 1% carbon as a result of isothermal transfer at 800°C of carbon from an iron crucible via lithium was observed.

Solubility of Metals in Lithium. The attainment of the limiting (equilibrium) solubility of metals in lithium is a fairly long process. The limiting solubility is reached only after several hours. For example, at 750°C after 2 hours the nickel content in lithium was 0.33-0.4%; after 50 and 200 hours the nickel content was 0.5-0.55%, i.e., the maximum solubility, equal to 0.5%, was reached after several hours. Similar behavior was also shown by other metals. The beryllium content in lithium at 1000°C increased when the residence time was more than 50 hours.

The values of the maximum solubility from the exit of the curves on the plateau were taken as the limiting solubility (Fig. 4). The limiting solubility of beryllium is reached far more slowly than that of nickel, as a result of which isothermal transfer of beryllium onto steel, reducing the beryllium content in lithium, takes place in the first case. Moreover, the rate of dissolution of beryllium was probably somewhat less because the surface of the beryllium sample was less reactive than the nickel surface.

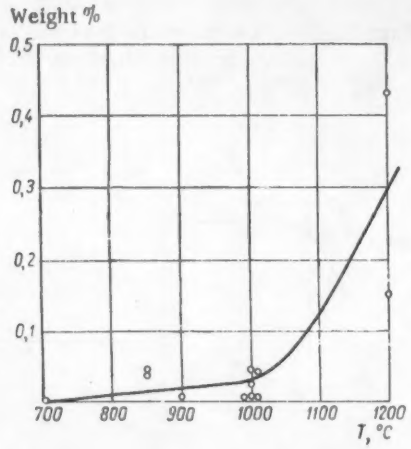

Fig. 5. Solubility of zirconium in lithium at 700-1000°C.

TABLE 1

Solubility of High-Melting Point Metals in Lithium

Metal	Temp., °C	Solubility, weight %
Iron	900	0.01
"	1000	0.02—0.1
"	1200	0.35
Nickel	700	0.15
"	750	0.5
"	850	1.36
"	950	3.2
Titanium	900	0.014
Molybdenum	1000	$<10^{-4}$
"	1200	0.03—0.1
Niobium	1000	$<10^{-4}$
Beryllium	1000	0.25

When the experiments on the determination of the solubility of the metal were carried out the metals were in contact with lithium at the temperature of the test for more than 50 hours (usually 100 hours), i.e., longer than required to attain equilibrium. The results of the determination of the solubility of several metals in lithium are given in Figs. 4-6 and Table 1.

The investigation of the solubility of uranium and zirconium (Figs. 5, 6) in lithium made it possible to assess the use of these metals as getters for the purification of lithium from chemically active impurities. It was found that distilled lithium in which uranium was kept at 800°C for 50 hours (zirconium crucible) had a shiny silver surface after the container was opened; the color of this surface did not change for more than 4 hours, whereas in other similar cases the lithium darkened in a few minutes. The cause of this behavior of lithium was that in this case uranium was a getter and purified the lithium from a number of impurities (probably oxygen and nitrogen), and lithium purified by a getter is more resistant to corrosion in air than distilled lithium. A golden-brown film of zirconium nitride is

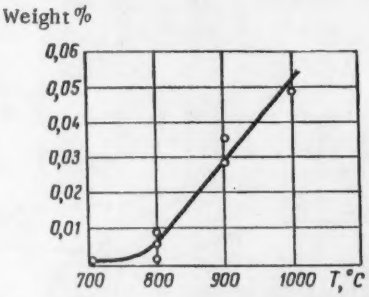

Fig. 6. Solubility of uranium in lithium at 700-1000°C. Part of the determinations were carried out in molybdenum crucibles.

TABLE 2

Alteration in the Mechanical Properties of Metals and Alloys After Keeping in Lithium

Metal	Crucible material	Temperature, °C	Residence time, hours	After keeping in argon without lithium			After keeping in lithium		
				Tensile strength, kg/mm²	Relative elongation, %	Relative contraction %	Tensile strength, kg/mm²	Relative elongation, %	Relative contraction %
Molybdenum	Molybdenum	900	220	40	21	40	41	16,4	26
Molybdenum*	Yal-T steel	950	40	35	13	22	42	1	0,6
Niobium	Niobium	900	220	19,3	18,1	47	37	10	16,5
Zirconium	Zirconium	900	220	30,5	—	35	30	11	—
Iron	Iron	900	220	27,7	33,2	80	26,2	42,7	93
Yal-T steel	Yal-T steel	900	220	58	54	78	52	61	81,5
Zh1 steel	Zh1 steel	900	220	86	14	70	78,3	15	71,5
Zh1 steel	Yal-T steel	950	40	—	—	—	36,5	20	61

*Technical lithium was used.

formed on the surface of zirconium kept in distilled lithium; this indicates that zirconium can also be used for purifying lithium. But at ordinary temperatures, zirconium, titanium and their alloys purify lithium to a somewhat lesser extent than uranium, so that uranium must be considered as another getter as a result of its low solubility in lithium. Zirconium and uranium can be used as getters for the purification of lithium because their solubility in lithium is low.

From an analysis of the data of Table 1 and Figs. 5 and 6 the investigated metals can be divided into the following groups:

1. metals with a high solubility (of the order of 0.1%) – nickel and beryllium;

2. metals with a slight solubility (from hundredths to thousandths of one percent) – iron, zirconium, titanium and uranium;

3. metals with a very low solubility (less than 10^{-4}%) – niobium and molybdenum.

It can be assumed that metals of the first group and alloys based on them are unstable in lithium. Metals of the second group and their alloys can be used in lithium at moderate temperatures. Metals of the third group are probably suitable for use in a medium of liquid lithium at high temperatures. Data on the solubility, characterizing the resistance of metals, are complemented by the results of mechanical tests on them after retention in lithium and without lithium, under identical conditions (Table 2). After retention in lithium, molybdenum and niobium exhibited somewhat reduced plastic behavior, particularly niobium, whose rigidity markedly increased.

Zirconium became less plastic after being stored in lithium but zirconium ribbon kept for 40 hours at 950°C had a high plasticity: it withstood 115 distortions by twisting. Iron kept in lithium became very plastic as a result of its purification of certain impurities by the lithium.

In experiments where the metal of the crucible differed from the metal of the samples a considerable alteration in the mechanical properties was observed as a result of the occurrence of transfer. Molybdenum tested in a Yal-T steel crucible became far less plastic; samples of Zh1 steel kept in lithium at 950°C in a Yal-T steel crucible were reduced in strength to 36.5 kg/mm² and the relative elongation was increased to 20%.

After Zh1 chrome steel and Yal-T chrome-nickel steel had been kept at 900°C for 220 hours the variations in their properties were roughly the same: the tensile strength was somewhat reduced and the plasticity was increased. Changes in the microstructure of Yal-T steel after keeping in lithium were not observed. From the results of the tests of samples of diameter 3 mm it follows that chrome-nickel steel containing an element – nickel – readily soluble in lithium does not corrode more than chrome steel, which is free from nickel, during tests of short duration in lithium up to 900°C.

After Yal-T chrome-nickel steel (8% nickel) had been kept in lithium at 900°C for 220 hours, the content of the main components of the alloy, iron, in the lithium was 0.01%, i.e., it was equal to its solubility in lithium at 900°C, whereas the nickel content was less than 10^{-3}%, i.e., it was less than 10% of the amount of iron present in the lithium. After lithium had been kept for 5 hours at 1200°C in a crucible of the same type of steel the lithium contained 0.34% iron, 0.19% chromium; there was less than 10^{-3}% nickel. The rate of dissolution from steel of the markedly soluble component, nickel, was several times less than the rate of dissolution of pure nickel (for equal surfaces of the tested samples). After retention for 220 hours at 900°C equilibrium was not reached, the lithium remained unsaturated with nickel,

which continued to be slowly leached from the steel. This leaching of nickel was detected by the metallographic method after retention for 240 hours at 1000°C.

LITERATURE CITED

1. B. Lustman and F. Kerze, Metallurgy of Zirconium (New York - Toronto - London, MoGraw-Hill, New York, 1955).
2. Documents of AEC USA. Nuclear Reactors: The Technique of Nuclear Reactors [Russian translation] (IL, Moscow, 1957) Vol. II, p. 236.
3. F. I. Shamrai, Lithium and its Alloys [in Russian] (Izd. AN SSSR, Moscow, 1952).
4. A. Brasunas, Corrosion 3, 78 (1953).
5. V. S. Lyashenko, V. V. Zotov, V. E. Andreev, M. D. Abramovich, and V. A. Ivanov, Report No. 2194, presented to the Second International Conference on the Peaceful Uses of Atomic Energy (Geneva, 1958).
6. W. Wilkinson and F. Yaggee, Attack on Metals by Lithium, US AEC Report ANL-4990 (Oak Ridge, 1950).

IDENTIFICATION TABLES FOR USE IN THE ANALYSIS OF α AND β ACTIVITIES

A. A. Lbov, and L. I. Sel'chenkov

Translated from Atomnaya Énergiya, Vol. 7, No. 6, pp. 537-538
December, 1959
Original article submitted February 18, 1959

In order to facilitate the identification of activities being subjected to analysis, tables are compiled according to data published prior to 1958 containing the distribution of all known β- and α-radioactive isotopes as a function of their $T_{\frac{1}{2}}$, end-point energies of their β-spectra, and α-particle energies. The tables make it possible to establish a group of isotopes with a previously established $T_{\frac{1}{2}}$ and energies of radioactive emission. In a number of cases, the use of a scheme involving the radioactive decay chain may also prove expedient in the identification of activities.

At the present time, radioactive isotopes permeate the various fields of science and engineering to a greater and greater extent. The measurement of specific activities is continually involved with their use. However, these measurements are frequently complicated by the presence of interfering activities. The latter, for example in connection with an activation analysis, can be caused by foreign and frequently unknown impurities. Chemical methods of separation of elements of interest to us sometimes considerably facilitate the measurements; however, in these cases the influence of the contaminating activities may turn out to be substantial (especially in measurements of weak activities when the degree of chemical purification is not high enough).

The identification of the activities under investigation and especially of the contaminating activities frequently presents serious difficulty. The tables presented in the present article, based upon the latest (published) data [1], can facilitate such identification considerably. In addition, the tables may help considerably in the choice of radioactive isotopes with previously given half-lives ($T_{\frac{1}{2}}$) and energies (E_β, E_α).

Tables 1-3 (β-active isotopes). In Tables 1-3 all the known β-active isotopes are listed, giving their $T_{\frac{1}{2}}$, E_β, and signs of particles emitted.

Similar tables for β emitters were published in 1955 [2]. It included only isotopes with $T_{\frac{1}{2}} > 6$ hr although, as is well known, practical application is also made of isotopes with smaller $T_{\frac{1}{2}}$. The sign of the charge of the emitted particles was not given in data [2]; it was also necessary to take additional data on radioactive isotopes published in 1958 into account.

The tables include all β-active isotopes with $T_{\frac{1}{2}}$ from 1 sec and less to 100 years and more, and end-point energies of β spectra (E_β) from 0 to 17 Mev; the signs of the charges of the emitted particles are also indicated.

In using the present tables it is necessary to know $T_{\frac{1}{2}}$ of the β activities being identified (they are determined from the decay curves), the end-point energies of the corresponding β spectra (these are determined approximately by the absorption method, and more exactly by the method of β spectroscopy), and also the signs of the charges of the emitted β particles (determined, for example, by the simplest magnetic analyzer). In most cases it is sufficient to determine only $T_{\frac{1}{2}}$ and E_β.

Isotopes which emit β^+ particles are distinguished by boldface type in the tables. In those cases in which the decay is accompanied by the emission of both β^- and β^+ particles, the isotope is indicated twice (for example, Cu^{64}, Cu^{64}). If $T_{\frac{1}{2}}$ or E_β of any of the isotopes is at the end of the interval corresponding to its row or column, it is placed in the following row or column. If several simple β spectra belong to one isotope, that isotope is indicated in the several appropriate columns. If the contribution of the simple β spectrum is not over 5%, nothing is put in the corresponding column; if the contribution is unknown, all values of E_β are taken into account. Isotopes whose decay is not accompanied by the emission of α- and β-particles are placed in the last columns of the tables. This pertains to the cases of K-capture and an isomeric transition, for example. Those isotopes for which the form of emission was not indicated in data [1] are put in these same columns.

Table 4 (α-active isotopes). All known α-active isotopes, together with their $T_{\frac{1}{2}}$ and energies of emitted α particles (E_α), are located in Table 4.

TABLE 1

Beta-Active Isotopes (Half-life up to 1 hr)

$T_{\frac{1}{2}}$	E_β, Mev											
	0—0,1	0,1—0,3	0,3—0,5	0,5—0,7	0,7—0,9	0,9—1,1	1,1—1,3	1,3—1,5	1,5—1,7	1,7—1,9	1,9—2,3	2,3—2,7
<1 sec												
1-5 sec												
5-15 sec												
15-30 sec											C^{10}, Ne^{19}, Tc^{100}, Ag^{110}	Na^{21}, Ag^{110}
30-60 sec											Au^{203}, Ac^{230}	Br^{87}, Rh^{104}, Rh^{106}
1-3 min							Re^{180}	Te^{123}	Pa^{234m}	O^{15}, F^{17}, O^{14}, Ag^{108}, Re^{190}	Ag^{113m}, In^{114}, Tl^{209}, Tl^{210}	V^{53}, Mn^{57}, Zn^{71}, Mo^{91m}, Te^{123}, Pa^{234m}
3-5 min					Zr^{89m}		Ne^{24}	Tl^{207}	In^{118}, Gd^{161}, Tl^{206}	Tl^{208}	Ne^{24}, Tc^{102}, Ce^{145}, Pr^{140}	V^{52}, Br^{85}, Cs^{129} Zr^{89m}
5-15 min				Sn^{125}	n', Co^{62}, Ce^{146}, Np^{240}, Br^{84}	Ca^{49}, Tc^{101}, Ta^{178}	N^{13}, Ga^{74}, Sn^{125}, Np^{240}	Al^{29}, Tc^{101}, Nb^{94m}	Mg^{27}, S^{37}, Ti^{51}, Co^{60m}, Cu^{66}, Ir^{197}, Np^{240}	Mg^{27}, Re, Hg^{205}	Ca^{49}, Ti^{51}, Ga^{74}, Mo^{101}, Sn^{125}, La^{136}, Nd^{151}, Ta^{186}, Br^{84}, Os^{185}, Np^{240}	Al^{29}, K^{41}, Fe^{53}, Cu^{66}, Ga^{74}, As^{79}, Br^{78}, Rh^{96}, Sm^{143}
15-30 min			Ag^{106}, Pb^{214}, Bi^{214}	In^{112}, Ta^{182m}, Pb^{214}	Ga^{65}, Br^{80}, Pb^{214}	C^{11}, Bi^{214}	Rh^{107}, Fr^{223}, Th^{233}, U^{239}	Ga^{63}, Se^{81}, Br^{80}, Ag^{106}, Te^{131}, Ho^{160}, Pa^{235}, Am^{246}	K^{44}, Ga^{70}, Se^{83}, In^{112}, Sn^{109}, Te^{131}, I^{126}, Au^{201}, Bi^{214}, Am^{244}, Am^{246}	Sb^{120}, Sm^{155}, Bi^{214}	Cu^{60}, Ga^{65}, Br^{80}, Pd^{99}, Pd^{111}, Ag^{106}, Te^{131}, Am^{246} I^{128},	Mn^{52m}, Rb^{88}, Sb^{116}, Xe^{138}, Pr^{135}, Pr^{146}, Nd^{136}, Pm^{141}, Eu^{164}
30-60 min		Ta^{185}	Cs^{130}	In^{116m}, Au^{200}, Pb^{211}	Cr^{49}, Zn^{69}, In^{113m}, Pt^{199}	In^{116m}, Ho^{164}, Bi^{213}	Cl^{38}, Sn^{123}, Pt^{199}	Cl^{34m}, Cr^{49}, Zn^{63}, As^{70}, Rb^{81m}, Pt^{199}, Pb^{211}, Bi^{213}, Ra^{227}	Cr^{49}, $Cd^{105, 134}$, Sn^{111}, La^{131}	V^{47}, Se^{73}, Br^{84}, Ta^{185}, Pt^{199}	Cl^{39}, Sc^{49}, Mn^{51}, In^{107}, Cs^{125} Cs^{130}, Au^{200}	Cl^{34m}, Zn^{63}, As^{70}, Br^{86}, Te^{94}, In^{108m}, I^{126}

TABLE 1 (Continued)
Beta-Active Isotopes (Half-life up to 1 hr)

$T_{\frac{1}{2}}$	E_β, Mev							β-active isotopes with unknown E_β	Isotopes whose decay is not accompanied by the emission of α- and β-particles
	2,7—3,1	3,1—3,7	3,7—4,3	4,3—5	5—7,5	7,5—10	10—17		
< 1 sec	Li^8	He^6	Na^{20}	Sc^{41}, Sc^{42}	Li^8, Na^{24m}, V^{48}, Mn^{50}	Li^9, Cl^{32}, Sc^{40}, Co^{54}	Li^8, B^8, B^{12}, N^{12}, P^{28}	B^{13}, Ca^{36}, K^{38}	Be^6, Mg^{22}, Al^{32}, Ti^{43}, Ti, Cr^{47}, Mn^{49}, Cu^{57}, Ge^{73m}, $Br^{79,81m}$, As^{86}, Y^m, Zr^{90m}, Zr^m, Cd, Sn^m, Ho^{163m}, Yb^m, Ta^m, Ta, W^{180m}, Hg^{194}, Tl^{197m}, $Tl^{203,204m}$, Tl, Pb^{207m}, Pb^m, Pa^{227m}
		Ne^{18}	N^{17}, Si^{27}, P^{29}, S^{31}, Cl^{33}	C^{15}, Cl^{34}, A^{35}	K^{37}, Ca^{39}	C^{15}, Al^{24}, Cu^{58}		Br^{89}, Kr^{92}, Kr^{93}, Kr^{94}, Kr^{97}, I^{139}, Xe^{141}, Xe^{143}	Si^{26}, Cl^{36}, Cr^{46}, Br^{90}, In^m, Er^{167m}, Hf^{178m}, $Au^{191,193}$, Tl^{195m}, Au^{193m}
5-15 sec	Mg^{23}	N^{16}, Al^{25}, Al^{26m}, P^{34}, Kr^{91}, In^{116}		N^{16}, Tc^{102}, Ag^{114}, In^{116}	F^{20}, P^{34}		N^{16}	I^{138}	F^{21}, $Br^{79,80m}$, Kr^{81m}, Tb^{150m}, Yb^m, W^{183m}, Ir^{191m}, Au^{197m}, Pb^{203m}
15-30 sec	O^{19}, Tc^{100}	Tc^{100}		O^{19}, Rh^{108}				$Se^{86,87}$, Br^{88}, Ag^{115m}, ^{137}, Xe^{140}, Ba^{143}, $Au^{202,204}$	Sc^{46m}, Se^{77m}, Y^{89m}, Nb^{98m}, Pd^{107m}, Hf^{179m}
30-60 sec	Cu^{68}, Ge^{77m}	V^{54}, Kr^{90}, Rh^{106}, Ir^{198}	Ne^{23}, Pm^{142}	Ne^{23}		Br^{87}		Se^{85}, Sr^{95}, Zr^{99}, Ru^{93}, Pd^{115}, In^{120}, $Sb^{134,135}$, Xe^{139}	Ge^{75m}, Kr^{79m}, As^{80}, Rh^{105m}, Ag^{107m}, Ag^{109m}, Xe^{125m}, Ce^{139m}, Yb^m, Au^{195m}
1-3 min	Na^{25}, Al^{28}, Ga^{64}, Mo^{91m}	P^{30}, Cl^{40}, Sc^{50}, Se^{83}, Rb^{82}, Sb^{124m}	Na^{25}, Mo^{91m}, Cu^{59}, I^{136}, Cs^{126}	Zn^{61}, Rb^{91}	Ga^{64}, Rb^{90}, Ag^{116}, I^{136}	Cl^{40}		Mn^{54m}, Co^{62}, Zn^{60}, Rb^{92}, Sr^{94}, Mo^{105}, Tc^{107}, Pd^{113}, Pd^{114}, Ag^{114}, Ag^{117}, Cd^{119}, Sn^{130}, Sn^{132}, Sb^{132}, Te^{135}, Te, Cs^{140}, Cs^{142}	Rb^{86m}, Nb^{97m}, Tc^{103}, Ag^{111m}, In^{109m}, In^{119}, Xe^{127m}, Ba^{137m}, Dy^{165m}, W^{185m}, Ir^{192m}, Pb^{201m}
3-5 min	Cr^{55}, Cs^{128}	Se^{71}, Nb^{99}, Sb^{118m}, I^{122}, Xe^{137}	Kr^{89}, Tc^{92}, Ru^{107}					Sc^{84}, Ru^{106}, Cd, Sn^{131}, Sb^{133}	$Br^{<74}$, Se^{79m}, Rh^{104m}, Pd^{109m}, Sb^{122m}, Au^{188}
5-15 min	Co^{62}, Cu^{62}, Rb^{91}, Sb^{128}, La^{131}	Br^{84}		S^{37}				Fe^{61}, Cu^{58}, Sr^{93}, Y^{98}, Mo^{103}, Tc^{105}, Cd^{119}, In, Sb^{130}, Cs^{133}, Cs^{139}, Ba^{127}, Ba^{142}, Bi^{215}, Pa^{237}	Co^{64} As^{83}, Br^{78m}, Nb^{94m}, Sn^{108}, Sb, I^{118}, $Tb^{162,163}$, Dy^{149}, W^{179}, Os^{180m}, Pb^{190m}, Np^{228}
15-30 min	Cu^{60}, Ge^{67}, As^{69}, Rb^{89}, Tc^{104}, Ag^{115}, In^{119}, Ba^{141}, Pr^{144}, Ag^{104}	Rb^{88}, Mo^{91}, Pd^{111}, Re^{178}, Bi^{214}	Cu^{60}, Rb^{89}, I^{119}, Pr^{148}	K^{44}	Rb^{88}, Y^{94}			Rb^{79}, Sr^{81}, Nb^{98}, Sb^{126}, Sb^{131}, Te, La^{143}, Re^{177}	Rb^{84m}, Pd^{98}, Ag^{102}, In^{113m}, Sb^{124m_2}, Xe^{135m}, Eu^{159}, Ho^{162}, Yb^{167}, Tu^{171}, $Lu^{176,179}$, Re^{180}, Re^{188m}, Os^{181}, Au^{186}, Hg^{189}, Pb^{195}, Pb^{198}, At^{206}, U^{235m}
30-60 min	Cl^{38}	Cl^{39}, Br^{86}, In^{108}, Cs^{136}	Ce^{131}	Cl^{34m}, Cl^{38}, Br^{84}				Se^{70}, Br^{74}, Nb^{89m}, Rh^{97}, Rh^{109}, Cd^{117}, Cd^{118}, In, Sn^{126}, Sn^{128}, Sb^{130}, Te^{134}, Xe^{131}	K^{43}, As^{78}, Se^{81m}, Y^{91m}, Tc^{98m}, Tc^{96m}, Ru^{94}, Rh^{103m}, Cd^{104}, Cd^{111m}, Sb, Ho^{159}, W^{179}, Au^{189}, Hg^{191}, Hg^{193m}, Pb^{196}, Pb^{197m}, Bi^{200}, Po^{203}, Mv^{256}

TABLE 2

Beta-Active Isotopes (Half-life from 1 hr to 30 days)

$T_{\frac{1}{2}}$	E_β, Mev									
	0—0,1	0,1—0,3	0,3—0,5	0,5—0,7	0,7—0,9	0,9—1,1	1,1—1,3	1,3—1,5	1,5—1,7	1,7—1,9
1-3 hr		Te^{129}	Br^{75}, Dy^{165}	F^{18}, Mn^{56}, Ni^{65}, Ge^{75}, Br^{75}, Kr^{88}, Sr^{92}	Br^{75}, Kr^{77}, Te^{93}, Rh^{106}, In^{117}, Sb^{115}, Ba^{139}, Nd^{141}, Dy^{165}, Np^{240}	Mn^{56}, Ni^{65}, Ge^{78}, Br^{83}, Kr^{88}, Te^{129}, I^{132}, Nd^{149}, Ta^{178}, Am^{245}, Cm^{249}	S^{38}, A^{41}, Co^{61}, Ge^{75}, Nb^{97}, Ru^{95}, Sb^{115}, I^{121}, I^{125}, Nd^{140}, Dy^{165}, Ra^{230}	Si^{31}, As^{78}, Kr^{87}, Ag^{103}, Sb^{116}, Te^{129}, Pr^{138}, Yb^{177}, Hf^{183}, Ir^{195}	Kr^{77}, Sr^{93}, In^{117m}, I^{132}, Ba^{139}, Nd^{140}	Ga^{68}, Br^{75}, Kr^{77}, In^{117m}, Xe^{122}, Pr^{137}
3-6 hr		Tb^{156m}, Ho^{167}	Rb^{81}, Pu^{243}, In^{109}	Cu^{61}, Cs^{134m}, Pb^{209}, Pu^{243}, Rb^{81}	Sc^{43}, Kr^{85m}, Rh^{99}, In^{109}, In^{115m}, Sb^{116}	Ti^{45}, Cu^{61}, Rb^{81}, Ag^{112}, La^{141}, Pr^{139}, Ho^{167}, Bk^{250}	Sc^{42}, Cu^{61}, Mo^{99}, Ru^{105}, La^{133}, Er^{161}, Lu^{173}, Lu^{176m}, Hg^{192}	Sc^{46}, Ga^{72}, Y^{92}	$Zn^{71\,n}$	Sb^{129}, Pr^{145}
6-12 hr		Ta^{184}, Pa^{234}	Cd^{107}, Hg^{193m}, Pb^{212}, Ac^{228}, Pa^{234}	Zn^{63}, Sr^{91}, Pd^{101}, I^{135}, Cs^{127}, Eu^{152}, Ta^{180m}, Pb^{201}, Pb^{212}, Ac^{228}, Pa^{234}	Fe^{52}, Ga^{66}, Ge^{77}, Se^{73}, Rb^{82m}, Te^{127}, Eu^{152}, Ta^{180m}	Sr^{91}, Sb^{126}, I^{135}, Xe^{135}, Sm^{156}, Er^{171}	Ta^{184}, Hg^{193m}, Ac^{228}, Pa^{234}	Ge^{77}, Se^{73}, Sr^{91}, I^{135}, Ce^{133}, Er^{171}		Eu^{152}, Ac^{226}
12-24 hr		K^{43}, Pd^{112}	Mg^{28}, K^{43}, Nb^{96}, I^{133}, Ir^{194}, Np^{236}, U^{240}	Cu^{64}, Cu^{64}, Ga^{72}, Br^{76}, I^{130}, Pr^{142}, Gd^{159}, Pt^{197}, Np^{236}, Am^{242m}, Bk^{248}	K^{43}, Br^{76}, Nb^{96}, Ce^{135}, Bi^{203}	Co^{55}, Ga^{72}, Pd^{109}, I^{130}, Eu^{150}, Eu^{157}, Gd^{159}, Ir^{194}	K^{43}, Br^{76}, Y^{86}, Rh^{100}	Na^{24}, I^{132}, Bi^{203}	Co^{55}, Ga^{72}, Nb^{90}, Tb^{154},	Br^{76}, Y^{86}, Eu^{157}
1-3 days	Th^{231}	Ni^{66}, Ce^{143}, Sm^{153}, Th^{231}, Pa^{232}, Np^{238}, Au^{198}	Cu^{67}, Zn^{72}, Br^{77}, Br^{82}, Kr^{79}, Mo^{99}, Sn^{121}, La^{140}, Ho^{166}, W^{187}, Pa^{232}, Np^{239}, Te^{131m}	Sc^{48}, Cu^{67}, Ge^{69}, As^{72}, As^{77}, Kr^{79}, Rh^{105}, Cd^{115}, Co^{143}, Sm^{153}, W^{187}, Os^{193}, Pa^{232}, Np^{239}, Te^{131m}	Ni^{57}, As^{71}, La^{140}, Ce^{143}, Sm^{153}, Ho^{166}, Os^{193}, Np^{239}	Pm^{149}, Os^{193}, Au^{198}, Tl^{200}, E^{254}	Ge^{69}, Sr^{83}, Mo^{99}, Cd^{115}, La^{140}, Ce^{143}, Pm^{151}, Os^{193}, Au^{194}, Ac^{226}, Pa^{232}, Np^{238}	Sb^{122}, La^{140}, Ce^{143}, W^{187}, Tl^{200}	Zn^{72}, La^{140}, Tu^{172}, Au^{194}	As^{72}, As^{76}, Ho^{166}
3-5 days	Yb^{175}	Te^{132}, Dy^{166}, Au^{199}	Sc^{47}, Yb^{175}, Au^{199}	Ca^{47}, Sc^{47}	Y^{87}, Sb^{127}, I^{124}, Np^{234}	Zr^{89}, Re^{186}	Sb^{127}		Sb^{127}, I^{124}	
5-10 days	Ir^{196}	Tb^{156}, Lu^{177}, Au^{196}, U^{237}	Sn^{125}, I^{131}, Xe^{133}, Tb^{161}, Er^{169}, Lu^{177}	Mn^{52}, Ag^{111}, I^{131}, Tb^{156}, Tb^{161}, Ta^{183}	Ag^{111}	Mn^{57}, Ag^{111}	Bi^{210}			
10-15 days		Nd^{147}, Pu^{246}	I^{126}, Cs^{136}, Ba^{140}, Nd^{147}, Ra^{225}, Pu^{246}	Cs^{136}	I^{126}, Nd^{147}	Ba^{140}, Pr^{143}, Bi^{205}	I^{126}			P^{32}
15-20 days		Os^{191}, Cf^{253}	Pm^{145}, Eu^{156}, Pa^{230}	V^{48}	As^{74}, Rb^{86}	As^{74}		As^{74}	As^{74}	Rb^{86}
20-30 days		P^{32}, Th^{234}, Pa^{233}		Pa^{233}						

TABLE 2 (Continued)

Beta-Active Isotopes(Half-life from 1 hr to 30 days)

$T_{\frac{1}{2}}$	E_β, MeV					β-active isotopes with unknown E_β	Isotopes whose decay is not accompanied by the emission of α- and β-particles
	1,9–2,3	2,3–2,7	2,7–3,1	3,1–3,7	3,7–4,3		
1-3 hr	Ni^{65}, Zr^{87}, In^{110}, I^{132}, Ba^{139}, Pr^{136}, Pm^{160}, W^{176}, Ir^{195}, Bi^{212}	Ba^{139}, Eu^{158}, Yb^{167}, Hf^{170}	S^{38}, Mn^{56}, Kr^{88}, Nb^{89}, Pm^{150}, Pb^{195}	Kr^{87}	As^{78}, Kr^{87}	Ge^{66}, Ag^{104}, Sn^{127}, Sb^{117}, Te, Te^{133m}, La^{142}, Sm^{142}, Ac^{229}	Kr^{83m}, Sr^{85m}, Sr^{87m}, Y^{82}, Cd^{117m}, In^{113m}, Sb^{117}, Te, I^{130}, I^{132}, Ba^{126}, Ho^{166}, Ho^{161}, Ho^{162}, Ho^{169}, Er^{163}, W^{177}, Re^{m}, Pt^{188}, Pt^{197m}, $Hg<^{191}$, Tl^{195}, Tl^{196}, Tl^{197}, Tl^{198m}, Pb^{198}, Pb^{199}, Pb^{204m}, Bi^{202}, At^{206}, Am^{228}, Cm^{229}, Cf^{247}, Bi^{201}
	Y^{84}, Ag^{112}, Ir^{190}, Au^{192}, Bk^{250}	La^{141}	Y^{92}, Ag^{112}	Y^{92}, Ag^{112}, Nd^{139}	Ag^{112}, La^{132}	Ce^{132}, Pd^{111m}	Br^{80m}, Y^{83}, Y^{85}, In^{110m}, Sn^{119}, Sb, Ho^{160m}, Hf^{180m}, Os^{189m}, Au^{191}, $Hg<^{191}$, Tl^{198}, Pb^{202m}
6-12 hr	Ge^{77}, Pd^{101}, Tu^{166}, Hg^{193m}, Ac^{228}	Sr^{91}, Pb^{201}	Y^{93}		Ga^{66}	Sb^{128}, Pt^{200}, Pu^{245}	Co^{58m}, Kr^{76}, Mo^{93m}, Tc^{99m}, Te, Ce^{137}, Tb, Dy^{155}, Dy^{157}, Tb^{149}, Er^{165}, Ta^{176}, Os^{183m}, Pt^{189}, Hg^{193}, Hg^{195}, Tl^{199}, Pb^{201}, Bi^{204}, At^{205}, E^{250}
12-24 hr	K^{42}, Zr^{97}, Rh^{100}, Pr^{142}, Re^{190}, Re^{188}, Ir^{194}	Ga^{72}, Rh^{100}, Tb	Tb^{154}	K^{42}, Ga^{72}, Br^{76}, Tb		Pm	Cr^{48}, Zn^{69m}, Y^{87m}, Zr^{86}, Nb^{92m}_{1}, I^{128}, Xe^{129}, Xe^{125}, La^{135}, Tb^{164}, Hf^{171}, Hf^{175}, Re^{181}, Re^{182}, Os^{182}, Os^{183}, Ir^{185}, Ir^{186}, Ir^{187}, Au^{198}, Au^{200}, Pb^{200}, Tc^{95}, Tb^{154}, Os^{191m}
1-3 days	Y^{90}, Sb^{122}, La^{140}, Ir^{188}	As^{72}, As^{76}	As^{76}	As^{72}		Er^{172}	Sc^{44m}, Ru^{97}, In^{111}, Sb^{119}, $Xe^{133}n$, Cs^{129}, Ba^{128}, $Ba^{133}n$, Ba^{135m}, Ce^{137m}, Eu^{146}, Gd^{147}, Tb^{153}, Er^{160}, Tu^{165}, Yb^{166}, Lu^{169}, Lu^{170}, Ta^{177}, Re^{182}, Re^{186}, Os^{187m}, Ir^{188}, Hg^{195m}, Hg^{197m}, Hg^{197}, Tl^{200}, Pb^{203}, Am^{240}, Bk^{246}
3-5 days	Ca^{47}, I^{124}						Tc^{96}, Rh^{101}, Pd^{100}, Te^{119}, Ce^{134}, Nd^{140}, Pt^{191}, Pt^{193m}, Pt^{195m}, Tl^{201}, Np^{234}, Ga^{67}, Nb^{95m}
5-10 days		Sn^{125}, Pm^{148}				Sb	Ni^{56}, Se^{72}, $Rb\leqslant^{80}$, Ag^{106}, Sb^{120}, Te^{118}, $Xe^{130}n$, Cs^{131}, Cs^{132}, Eu^{145}, Tb^{158}, Tu^{167}, Lu^{171}, Lu^{172}, Bi^{206}
10-15 days							Ge^{71}, Ge, Sr^{89m}, Nb^{92}, $Sn^{117}n$, $Xe^{131}m$, Ba^{131}, Ir^{189}, Ir^{190}, $Ir^{192}n$, Pt^{188}, Tl^{202}, Bi^{205}
15-20 days		Eu^{156}				Rh^{99}	Pd^{103}, Te^{121}
	Sb^{126}					E^{255}	Cr^{51}, Sr^{82}, W^{178}, Os

TABLE 3

Beta-Active Isotopes (Half-lives more than 30 days)

$T_{\frac{1}{2}}$	E_β, Mev						
	0—0,1	0,1—0,3	0,3—0,5	0,5—0,7	0,7—0,9	0,9—1,1	1,1—1,3
30-50 days		Fe^{59}, Nb^{95}, Ru^{103}, Hg^{203}	Fe^{59}, Ce^{141}, Hf^{181}	Ce^{141}, Pm^{148}	Rb^{84}		
50-100 days		S^{35}, Sb^{124}	Sc^{46}, Co^{58}, Y^{91}, Zr^{95}, Tc^{95m}, Tb^{160}, W^{185}	Tc^{95m}, Sb^{124}, Tb^{160}, Ir^{192}	Tb^{160}	Sb^{124}	
100-200 days		Ca^{45}, Re^{139}	Ta^{182}	Lu^{17} , Ta^{182}, Y^{88}	Tu^{170}	Tu^{170}	
200-365 days	Ag^{110m}	Ce^{144}, Bk^{249}	Zn^{65}, Ce^{144}	Ag^{110m}	Rh^{102}		Rh^{102}, Rh^{102}
1-3 years	Ru^{106}, Tu^{171}	Sb^{125}, Pm^{147}, Eu^{155}	Sn^{121m}, Cs^{134}	Na^{22}, Sb^{125}, Cs^{134}	Pm^{148}		
3-5 years					Tl^{204}		
5-10 years	Ra^{228}		Co^{60}	Cd^{113m}	Re		
10-30 years	H^3, Pb^{210}, Ac^{227}, Pu^{241}	Eu^{152}, Eu^{154}	Sr^{90}, Eu^{152}	Kr^{85}, Cs^{137}, Eu^{152}, Eu^{154}	Eu^{154}	Eu^{152}	Cs^{137}
30-100 years	Sm^{151}	Ho^{166}					Ho^{166}
> 100 years	Ni^{63}, Zr^{93}, Pd^{107}, Re^{187}	C^{14}, Si^{32}, Se^{79}, Rb^{87}, Tc^{99}, I^{129}, Cs^{135}, La^{138}	Tc^{98}, Lu^{176}	Be^{10}, A^{39}, Nb^{94}, In^{115}, Am^{242}	Cl^{36}		Al^{26}

TABLE 3 (Continued)

Beta-Active Isotopes (Half-lives more than 30 days)

$T_{\frac{1}{2}}$	E_β, Mev					β-active isotopes with unknown E_β	Isotopes whose decay is not accompanied by the emission of α- and β-particles
	1,3–1,5	1,5–1,7	1,7–1,9	1,9–2,3	2,3–2,7		
30-50 days		Rb^{84}, Cd^{115m}, Te^{129m}			Pm^{148}		A^{37}, Ag^{105}, Te^{129m}, Xe^{127}, Yb^{169}
50-100 days	Sr^{89}	Co^{56}, Y^{91}, Sb^{124}			Sb^{124}	W^{188}	Be^{7}, As^{73}, Rb^{83}, Sr^{85}, Zr^{88}, Nb^{91m}, Tc^{97m}, In^{114n}, Te^{125m}, I^{125}, Eu^{148}, Gd, Tu^{168}, Hf^{175}, Re^{183}, Re^{184}, Os^{185}
100-200 days	Sn^{123}					Te^{127m}	Se^{75}, Y^{88}, Sn^{113}, Te^{121m}, Te^{123m}, Ce^{139}, Eu^{149}, Gd^{154}, Dy^{159}, W^{181}, Au^{195}, Hg^{194}
200-365 days							V^{49}, Mn^{54}, Co^{57} Ge^{68}, Sn^{119m}, Pm^{143}, Pm^{144}, Sm^{145}, Gd^{153}
1-3 years						Os^{194}	Fe^{55}, Mo^{93}, Cd^{109}, Lu^{171}, Lu^{172}, Ta^{179}
3-5 years						A^{42}	Hf^{172}
5-10 years							Rh^{101}, Ba^{133}, Bi^{207}
10-30 years	Eu^{152}		Eu^{154}				Nb^{93m}, Pm^{145}
30-100 years							
>100 years	K^{40}					Fe^{60}	Ca^{41}, Ti^{44}, Mn^{53}, Ni^{59}, Kr^{81}, Tc^{97}, La^{137}, Pb^{202}, Pb^{205}, Bi^{208}

TABLE 4

Alpha-Active Isotopes

$T_{1/2}$	α, Mev								
	<4	4—4,25	4,25—4,5	4,50—4,75	4,75—5	5—5,25	5,25—5,50	5,50—5,75	5,75—6
< 1 min								$Hg^{<195}$	
1-20 min		$Dy^{<153}$, Ho?				$Au^{183-187}$	Bi^{214}	Bi^{211}, Po^{201}	Po^{200}, Bi^{198}, Po^{199}, Po^{198}, At^{205}, Po^{218}
20-60 min							Fr^{222}, Bi^{199}	Np^{233}, Po^{202}	Pu^{235}, Bi^{212}, Am^{205}
1-24 hr	Dy^{154}, Tb^{151}, Dy^{153}, Dy^{152}, Tb^{149}				Bi^{208}	Po^{207}, Bi^{201}, Po^{205}	At^{210}, Bi^{212}, Po^{201}	At^{210}, Rn^{211}, B^{12}, At^{208}, At^{209}	At^{207}, Bi^{218}, Am^{239}, Rn^{211}, Pa^{228}, At^{211}
1-30 days	Eu^{147}, Gd^{149}					Po^{206}	Ra^{223}, Ra^{224}, U^{231}, Rn^{222}	U^{230}, Ra^{226}, T^{27}, Pa^{230}, Ra^{225}, A^{125}	Ac^{226}, Ra^{223}, U^{230}, Bk^{245}, Th^{227}
1-12 months						Bk^{249}	Po^{210}, Pu^{237}, Bk^{249}	Pu^{237}	Cm^{241}, Cm^{242}
1-100 years					Pu^{241}, Ac^{227}	Po^{208}, Np^{235}, U^{232}, Th^{228}, Pu^{238}	U^{232}, Th^{226}, Pu^{236}	Cm^{244}, Pu^{236}, C^{243}	Cm^{243}, Pu^{236}, Cm^{244}, Cf^{250}
10^3-10^5 years	Gd^{148}			Th^{230}, Pa^{231}	Ra^{226}, Th^{229}, Po^{209}, Pa^{231}, Pu^{239}	Pa^{231}, Th^{229}, Pu^{239}, Pu^{240}, Am^{243}	Am^{243}, Bk^{247}, Cm^{245}, Cm^{246}, Am^{241}	Am^{241}, Cf^{249}, Bl^{147}	Cf^{249}
> 10^5 years	Ce^{142}, Nd^{144}, Sm^{147}, Sm^{146}, Pt^{192}, Gd^{150}, Bi^{209}, Pt^{190}	Th^{232}, U^{235}, U^{238}	U^{235}, U^{233}, U^{236}	U^{235}, Np^{237}, U^{233}, U^{234}	U^{234}, Np^{237}, U^{233}, Pu^{242}, Bi^{210}	Cm^{246}			
α-active isotopes with unknown $T_{\frac{1}{2}}$	W								

TABLE 4 (Continued)
Alpha-Active Isotopes

$T_{\frac{1}{2}}$	6–6,25	6,25–6,50	6,50–6,75	6 75–7	7–8	8–9	>9	α-active isotopes with unknown E_α
< 1 min		At^{219}, Rn^{220}, Rn^{219}	$At^{<202}$, Po^{217}, Rn^{219}, Ra^{222}, Po^{211}, At^{218}, Fr^{220}, Ra^{221}	Po^{216}, Rn^{219}, Po^{211}, Ac^{222}	At^{217}, Th^{224}, Rn^{218}, Po^{211m}, Fr^{219}, Po^{215}, Po^{211}, Ra^{220}, Th^{223}, Po^{214}, Rn^{217}, At^{216}, Fr^{218}	At^{215}, Ra^{219}, Rn^{216}, Po^{213}, Rn^{215}, Po^{211n}, Po^{212}, At^{214}, Po^{214}	Po^{212}, Po^{214}	Pa^{225}, $Fm^{248, 249}$, 102^{254}
1-20 min	Po^{197}, At^{203}, Rn^{207}, Po^{196}, $Bi^{<196}$, Fr^{221}	Rn^{206}, Bi^{211}, Rn^{204}, Fr^{221}, $At^{<203}$, Fr^{213}, U^{229}	Th^{225}, Bi^{211}, Ac^{223}, U^{228}	U^{227}, Pa^{226}, Ra^{213}	E^{246}			
20-60 min	Rn^{221}, Th^{226}, Rn^{209}, Rn^{208}	Rn^{212}, Np^{231}, Pu^{233}, Th^{226}, U^{229}, Pa^{227}	Pu^{232}	E^{248}	Cf^{245}, Cf^{244}, Fm^{250}			
1-24 hr	Am^{237}, Rn^{210}, Bi^{212}, Pa^{228}, Ac^{224}, Pu^{234}	Bk^{243}	Cm^{238}, Bk^{242}, Bk^{244}	E^{249}, Fm^{251}	Fm^{252}, Fm^{255}, Fm^{254}			
1-30 days	Th^{227}, Bk^{245}, E^{253}, Cm^{240}	Cm^{240}, Bk^{245}, E^{251}, E^{253}	E^{253}, Cf^{246}	Fm^{253}, Cf^{246}				
1-12 months	Cm^{242}	Cf^{248}	E^{252}					
1-100 years	Cf^{250}, Cm^{243}, Cf^{252}	E^{254}						
10^2-10^5 years	Cf^{249}							Cf^{251}
$>10^5$ years								Pu^{244}, Cm^{247}
α-active isotopes with unknown $T_{\frac{1}{2}}$					Ac^{221}	Fr^{217}	At^{213}	

To determine E_α one can use, for example, ionization or magnetic α spectrometers. It should be noted that when several groups of α particles with different energies belong to the same isotope, all of the E_α are taken into account, and the given isotope is appropriately indicated in the various columns of the table.

If $T_{\frac{1}{2}}$ or E_α of any isotope is exactly at the end of the interval corresponding to a particular row or column, that isotope is placed in the following row or column.

Tables 1-4 herein presented enable one to indicate a group of appropriate isotopes for an indicated interval of $T_{\frac{1}{2}}$ and $E\beta$ (or E_α). To make the latter more precise, it is convenient to use the detailed table of isotopes [1], and the use of a radioactive decay chain scheme may be of additional assistance in a number of cases in identifying the activities.

We consider it our duty to express our gratitude to Yu. A. Zysin for a discussion and his advice.

LITERATURE CITED

1. D. Strominger, J. Hollander, and G. S. Seaborg, Rev. Mod. Phys. 30, 585 (1958).
2. N. Hallden, Nucleonics 13, 78 (1955).

MORPHOLOGICAL TYPES OF INDUSTRIAL URANIUM DEPOSITS AND METHODS FOR THEIR PROSPECTING

D. Ya. Surazhskii

Translated from Atomnaya Énergiya, Vol. 7, No. 6, pp. 539-543
December, 1959
Original article submitted May 30, 1959

The grouping of uranium deposits according to the combination of their morphological features is proposed. Five groups of deposits are distinguished, for each of which the following are examined: the prospecting system, the most efficient ratio between mining and drilling operations, the density of the prospecting network and the conditions for the classification of reserves.

General Remarks

As with other mineral ore deposits, the prospecting of uranium deposits is carried out either by drilling or mining operations or a combination of both. The choice of the prospecting system, the most effective ratio between mining and drilling operations, the density of the prospecting network and the conditions for the classification of the reserves are determined mainly by the shape of the ore bodies, their dimensions, the degree of variability with respect to the metal content (generally expressed by the coefficient of variation) and the degree of discontinuity of the mineralization (expressed by the coefficient of ore bearing, i.e., the ratio between the area occupied by the conditioning ores and the total area of the ore-bearing bed or ore-containing fissure). From the combination of these morphological features, known uranium deposits can be divided into five groups: 1) mineralized beds; 2) large bed-like deposits; 3) bed-like, pillar-like and vein-like deposits; 4) lenticular and pocket-like deposits; 5) systems of thin veins.

Prospecting of Mineralized Beds (First Group of Deposits)

This group includes continuous beds of uranium-bearing sedimentary rocks developed in areas measuring tens of square kilometers. They are characterized by uniformly poor mineralization distributed without interruption along the strike, to the dip and with respect to the thickness of the productive levels. The boundaries of the mineralization coincide with the lithological boundaries and can be determined visually. The coefficient of ore bearing is close to unity and the coefficient of variation with respect to the metal content in the ore does not exceed 20-30%.

The most characteristic deposits of this type are uranium-bearing marine shales, uranium-containing phosphorites and analogous sedimentary syngenetic deposits in which appreciable distribution of the metal deposited simultaneously with the adjoining rocks is not found.

The prospecting of such deposits consists mainly in the drilling of the ore bed according to an isometric network. Mining operations (small shafts, prospecting pits and crosscuts driven from them) are carried out on a small scale, solely to check the data of borehole samples. Reserves of all industrial categories (A, B, and C) may be revealed during prospecting. In this connection the network of boreholes must not be less than 100 x 100, 200 x 100 and 400 x 200 m, respectively. In deposits which are prepared for exploitation, the reserves between mine workings at a distance of up to 200 m from each other can be included in group A_2, and reserves between workings at a distance of 400 m from each other in group B.

Prospecting of Large Bed-Like Deposits (Second Group of Deposits)

Deposits of this group consist of large bed-like bodies with nonuniform distribution of the metal, correlated with specific stratigraphic levels. In contrast to deposits of the first group, not all of the bed thickness, but only part of it, is industrially valuable; the continuity of the mineralization may be interrupted by instances of narrowing. Instead of a single ore body, in practice it is, therefore, necessary to deal with several more or less isolated ore bodies, each of which occupies an area sometimes measuring several square kilometers.

The contours of the ore bodies are determined solely from test data on samples. The coefficient of ore bearing varies from 1.0 to 0.8, and the coefficient of variation with respect to metal content reaches 100%.

This group includes the largest of the known epigenetic uranium deposits in sandstones, conglomerates and other sedimentary rocks of primarily continental facies. A combined mining-drilling system with a

marked predominance of core drilling is usually employed for the prospecting of these deposits. The main task of drilling operations is the mapping of the ore bodies in contour, while that of the mining operations is to record the boundaries of the industrial mineralization with respect to the thickness of the ore-containing formations, and also obtain data for the complete characteristics of the chemical and mineralogical composition of the ores, their physicotechnical properties, etc.

In the case of isometric forms of the ore bodies drilling is carried out according to a square network, in all other cases by lines perpendicular to the plane of maximum variability of mineralization.

If there is sufficient evidence to assume that the ore lenses are located in several layers and pass beyond the limits of the main ore bed, part of the boreholes (up to 10-15% of the total) is sunk to a depth ensuring the intersection of all the ore-bearing measures and the recording of ore bodies below the main ore-bearing level.

As usual, mining operations consist in driving roadways and rises at intervals of 80-120 m in one of the ore districts, principally to check drilling data and obtain material for technological samples. If prospecting is carried out by roadways and the thickness of the ore body exceeds the width of the roadway, crosscuts are also driven, generally at intervals of 40-60 m.

In contrast to deposits of the first group, reserves exposed by boreholes of the 200 x 100 m network are not placed higher than category C_1. Reserves of category B are considered to be those within the limits of enclosures found by drilling on the 100 x 100 m network; mine workings which confirm the drilling data being present in one of the districts where the deposit is located.

Prospecting of Bed-Like, Pillar-Like and Vein-Like Deposits (Third Group of Deposits)

The difference between these deposits and those described above is that the form of their ore bodies and their location in the area are determined not only by the lithological composition of the adjoining rocks but also (in some cases, chiefly) by folded and ruptural deformations. Many of the ore bodies are characterized by a relatively high thickness (reaching several tens of meters in places) and also by marked variations in the shape, dimensions, conditions of occurrence and the area of the transverse section at comparatively small intervals along the strike and to the dip. The mineralization is generally uninterrupted but the shape of the ore bodies is complicated by the presence of isolated blocks of waste rock. The boundaries of the industrial mineralization are determined solely from test data. The coefficient of ore bearing varies between 0.8-0.5; the coefficient of variation sometimes reaches 150%. The area of such deposits (in the dip plane) does not exceed several hundreds of thousands of square meters. Such deposits generally consist of one or more (two-four) ore bodies.

This group includes many bed-like bodies in sedimentary rocks of continental facies, metasomatic deposits on the flanks of steep folds, vein-like deposits within major faults, stockworks in crushing zones associated with the faults, pillar-like bodies at the intersections of two tectonic zones, etc. The main role in the prospecting system is played by mine workings, a series of crosscuts intersecting the ore body along the short axis at distances depending on the configuration and cross-sectional area of the deposit at the given level. In some cases the crosscuts may be partially replaced by chamber-diamond drilling boreholes. The alternation of cross cuts and chamber-diamond boreholes is fairly common in practice. Staples and rises, which serve to confirm the continuity of the mineralization along the vertical, between the levels of the roadways, are also important.

Deep drilling on a very close network (generally 50 x 50 m) makes it possible to assess the reserves not higher than category C_1. As a result of the complexity of the shape and the markedly nonuniform distribution of the metal in the ore, reserves of category B are considered only within the limits of sublevels completely prepared for extraction operations. Reserves of category A_2 are generally not revealed at the normal density employed for the prospecting network.

Prospecting of Lenticular and Pocket-Like Like Deposits (Fourth Group of Deposits)

The ore bodies are sometimes localized in specific stratigraphic levels or are associated with ruptural deformations (for example, in the contact zone of granites and sedimentary-metamorphic rocks), but in general the lithologic and structural control of the mineralization is less clearly expressed here than in deposits of the other groups. The outlines of the industrial mineralization are determined solely from the data of tests. In many cases the zones of distribution of the lenses are in the form of narrow (up to 300-500 m) bands of considerable extent. The dimensions of the ore bodies in the dip plane do not exceed several tens of square meters. The coefficient of ore bearing within the individual lenses does not exceed 0.50-0.25; the coefficient of variation of the metal content within the individual lenses often reaches 200%.

The group described above includes small lenses of hydrothermal ores in zones of tectonic contacts, bedded and anticlinal veins, and domal structures of higher orders, and also a number of deposits, the predominant role in which is occupied either by purely infiltration processes or processes of the metamorphism

Grouping of Uranium Deposits According to the Main Morphological Features

Group	Characteristics	Maximum areas of the ore bodies	Coefficient of variation (maximum), %	Coefficient of ore bearing
1	Continuous seams of uranium-bearing sedimentary rocks with uniform mineralization, recorded uninterruptedly over large areas. In general, the boundaries of the mineralization coincide with the lithologic boundaries and are established visually.	Tens of square kilometers	30	1
2	Large bed-like deposits with nonuniform distribution of the metal, correlated with specific stratigraphic levels. The boundaries of the mineralization are established only by the results of tests or γ measurements.	Square kilometers	100	1.0-0.8
3	Bed-like, pillar-like and vein-like deposits controlled by folded and ruptural deformations. The boundaries of the mineralization are established only by the results of tests or γ measurements.	Hundreds of thousands of square meters	150	0.8-0.5
4	Lenticular and pocket-like deposits with markedly nonuniform distribution of the metal. In general, lithologic and structural control is not clearly expressed. The boundaries of the mineralization are established only from the results of tests or γ measurements.	Tens of thousands of square meters	200	0.5-0.25
5	Thin veins in rupture and shear fractures. The mineralization is very nonuniform, in the form of small lenses, the combination of which forms ore pillars. The boundaries of the mineralization are established visually.	Tens of thousands of square meters	200	0.25-0.02

of rocks having an increased content of radioactive elements in comparison with the clarke.

A combined mining-drilling system is used for prospecting these deposits.

Core drilling on a network of 50-70 x 30-40 m by lines at right angles to the general direction of the ore bands makes it possible to determine the width and extent of the mineralized zones, assess approximately the value of the area coefficient of ore bearing and map the individual largest lenses roughly. The mine workings, a system of adits, roadways and are plotted to determine the outlines of the individual ore lenses.

With the normal density of the prospecting network, the reserves of these deposits cannot be included in categories A_2 and B. Reserves of category C_1 are revealed mainly by mine workings on a 40-60 x 40-60 m network. They are sometimes also considered by interpolation between the mine workings and boreholes.

Prospecting of Thin Veins (Fifth Group of Deposits)

This group includes hydrothermal deposits formed by the filling of fissures. In general, they are characterized by extremely nonuniform distribution of the metal. The ore accumulations are generally in the form of flat lenses localized in thin rupture and shear fractures resting on larger dislocations. A combination of such lenses sometimes forms ore pillars inclined at different angles to the level; such pillars alternate with oreless or poorly productive districts of vein fissures, the ratio of the total area of the ore lenses to the area of the whole ore-containing fissure being frequently more than 0.10 and generally equal to 0.04-0.03.

The prospecting of these deposits is carried out almost exclusively by means of mine workings. Since the deposits in the majority of cases are represented by tens or even hundreds of parallel veins, not by one vein,

crosscuts play a very important part in the system of mining operations. The length of the crosscuts and the optimum distance between them are determined in each individual case on the basis of the average extent of the ore bodies and the established or proposed boundaries of the distribution of rocks lithologically favorable for mineralization.

The underground prospecting of individual veins revealed by crosscuts is carried out by continuous tracing in each prospecting-extraction level or by the complete excision of blocks of size 30 x 40 to 40 x 50 m. According to existing standards of mining development work, such distances between the boundary working are minimal but even they cannot ensure the provision of reliable data on the reserves and quality of the ores within the limits of individual extraction blocks.

A comparison of the calculation of the reserves with the results of extraction indicates that the actual reserves of metal in the individual blocks are in a number of cases several times less or more than the reserves calculated from prospecting data. But as a result of the mutual compensation of high and low errors, the error in the determination of a combination of blocks (10-12 blocks) does not exceed the limits permissible for category C_1.

During the prospecting of the above-described deposits an important role is played by small crosscuts or long boreholes in the walls of the workings. The necessity for such boring operations and drilling is caused by the generally increased tendency of the productive fissures to ramification, with the concentration in the ore apophyses of considerable reserves of metal sometimes exceeding the reserves in the main vein.

The importance of the different types of workings depends on the position of the ore pillars. In the case of steep inclination of the latter the assessment of the veins is carried out mainly from the data obtained as a result of roadway drivage. When the ore pillars are gently inclined, the data for the assessment of the veins can be obtained mainly by driving vertical workings, i.e., raises and staples.

The low coefficient of ore bearing and the slight thickness of the ore veins, which are often in the form of thin tectonic joints, exclude the possibility of a reliable assessment of the reserves of these deposits by means of boreholes. Under such conditions drilling is used only for an approximate solution of the problem of the possible depth of the industrial mineralization.

It was established, for example, that when the ore veins lie in a gneiss-shale stratum the lower boundary of the uranium deposits frequently coincides with the surface of the granite massifs forming the basement of the surrounding rocks. The topography of this surface can be established by drilling so-called structural boreholes. Small drillings from the mine workings sometimes give a considerable effect both during prospecting and the geological servicing of existing mines; they successfully replace small crosscuts during the prospecting of parallel veins, ore apophyses and displaced parts of the ore-containing fissures.

SUMMARY

The above-given morphological characteristics of the present known uranium deposits can be jointly summarized, as shown in the table, as follows.

Deposits of the first group prospected by drilling; deposits of the second, third and fourth group – by a combination of mine workings and boreholes with a different density of the prospecting network; deposits of the fifth group – by mine working only.

The groups of uranium deposits indicated in the table also differ from each other according to the conditions of classification of the reserves. During the process of geological-prospecting operations, the reserves of all three industrial categories (A_2, B and C_1) can be revealed only in deposits belonging to the first group. In deposits of the second and third groups the reserves do not have a higher classification than B; in deposits of the fourth and fifth groups the extraction must be based mainly on reserves of category C_1.

EXTERNAL γ-RADIATION DOSAGE DUE TO FALLOUT OF SEVERAL FISSION PRODUCTS

V. P. Shvedov, G. V. Yakovleva, M. I. Zhilkina, and T. P. Makarova

Translated from Atomnaya Énergiya, Vol. 7, No. 6, pp. 544-545
December, 1959
Original article submitted July 18, 1959

A flask, 1 m^2 area, was used to make a monthly collection of radioactive fallout during 1958 in the city of Zelenogorsk. After having been dessicated and incinerated, the contents of the flask were analyzed, using a single-channel scintillation γ spectrometer with a large CsI crystal.

γ-lines whose energies were approximately 150, 500, and 750 kev, and whose intensities dropped off in periods of about 30, 40, and 70 days, were discovered in the spectra of the fallout samples. These could be unambiguously attributed to the γ lines of Ce^{141}, Ru^{103}, and $(Zr+Nb)^{95}$. With the aid of a 4π counter, a calibration of the γ spectrometer was made in order to make the conversion from the area of the photopeak to the absolute β activity of each isotope. The isotopes being identified were radiochemically separated from the series of samples, and a subsequent measurement made of their β activity with calibrated end-window β-counters. A comparison of the spectrometer method and the radiochemical method showed that the error in the determination of the absolute activity of the γ emitters by the use of the spectrometer technique was at most 10%. The absolute activity of the Cs^{137} contained in the fallout samples was determined by the radiochemical method.

The absolute activity in the monthly fallout per 1 m^2 of the earth's surface of an arbitrary isotope (A_{tot}) can be represented in the form of a geometrical progression

$$A_{tot} = A_0 + A_0 e^{-\lambda} + A_0 e^{-2\lambda} + \ldots + A_0 e^{-t\lambda},$$

where A_0 is the average activity of the daily fallout per 1 m^2 of the isotope; λ is the decay constant of the isotope ($days^{-1}$); t is the sampling period in days. Or

$$A_{tot} = \frac{A_0 (1 - e^{-\lambda t})}{1 - e^{-\lambda}}.$$

It is possible to determine from this the average activity of the isotope (A_0), and therefore the number of active atoms of this isotope in the daily fallout. The knowledge of the number of active atoms (which is equal to the number of future decays of the isotope) enables one to calculate the γ radiation dosage from this isotope for the future.

The γ-radiation dosage of radioactive fallout was calculated for a point 100 cm from the earth's surface neglecting the shielding of the γ radiation. The calculation of the dosage was made by integrating the γ radiation over an infinite plane surface [1], using the Hirschfelder formula [2, 3] to calculate the secondary rays.

The results of the dosage calculations are shown in the Table. The 30-year dosage rate from Zr^{95}, Ru^{103}, and Ce^{141} is equal to the dosage rate for the year.

Thus, for a dosage rate in the year from the γ radiation of Cs^{137} equal to ~1 mr/year, the dosage rate from Zr^{95}, Ru^{103}, and Ce^{141} amounts to 7.5 mr; i.e., as a result of the continued tests of atomic weapons, the short-lived isotopes make a considerable contribution to the dosage from the external radiation. The dosage rate from radioactive fallout in 1958 already amounts to ~1/3 of the world-wide average dosage rate due to cosmic radiation (28 mr). The value calculated previously [4] by us for the 30-year dosage due to radioactive fallout for the years 1954-1956, inclusively, was 16 mr, and for the year 1957 a value of 18 mr was obtained. The sharp increase in the dosage attests to the growing danger from the testing of nuclear weapons.

30-Year Dosage Due to Radioactive Fallout in 1958

Isotope	Dosage, mr
$(Zr+Nb)^{95}$	6,5
Ru^{103}	0,9
Ce^{141}	0,1
Cs^{137}	32,6
Total	40,1

LITERATURE CITED

1. G. V. Gorshkov, Gamma Radiation of Radioactive Substances [in Russian] (LGU, Leningrad, 1956).
2. J. Hirschfelder and E. Adams, Phys. Rev. 73, 863 (1948).
3. J. Hirschfelder, J. Magee, and M. Hall, Phys. Rev. 73, 853 (1948).
4. L. I. Gedeonov, V. P. Shvedov, and G. V. Yakovleva, Atomnaya Énergiya 7, 545 (1959).*

*Original Russian pagination. See C. B. translation.

* * *

CALCULATION OF THE EXTERNAL γ-RADIATION DOSAGE DUE TO FALLOUT OF RADIOACTIVE FISSION PRODUCTS

L. I. Gedeonov, V. P. Shvedov, and G. V. Yakovleva

Translated from Atomnaya Énergiya, Vol. 7, No. 6, pp. 545-547, December, 1959
Original article submitted May 20, 1957

In connection with the performance of atomic weapons tests and the fallout of radioactive fission products over the whole earth's surface, an estimate based on continuous observation of radioactive fallout is made for the external γ-radiation dosage. It is not possible to make a direct measurement of the γ-radiation dosage due to radioactive fallout at great distances from the explosion site, since the natural γ background is much larger than the γ radiation of the fallout of fission products. A calculation appears to be the only possible method of determining the dosage.

In the present paper, an estimate is made of the dosage of the γ radiation due to fallout of fission products in the territory of the Leningrad region from the beginning of the atomic weapons tests up until January 1, 1957.

The dosage was calculated for a point located 100 cm above the earth. It was assumed in the calculation that all of the fallout of active substances remains in an infinitely wide and thin upper layer of the earth's surface. Such factors (which would tend to cause a decrease in the activity) as washing out of the soil, the action of the wind, the shielding due to surface irregularities, and others, were not considered; only the natural decay of the radioactive substances in the fallout was taken into account. The γ-radiation dosage was calculated from the time of the fallout to the complete decay of the fragments (till $t = \infty$). Only such a calculation enables one to tell what the upper limit of the dosage will be.

The calculation was made according to the formula

$$D = kQ,$$

where D is the dose (in roentgens), i.e., the amount of energy evolved in 1 cm^3 of air by the γ radiation; Q is the total number of future β decays of the fission fragments which have been deposited on 1 cm^2 of soil during the whole preceding time starting from the moment of fallout; k is a coefficient which characterizes the value of the dose at a height of 100 cm above the the earth due to 1 decay per 1 cm^2 on soil.

The number of future decays of the fragment activity for an age of this activity greater than 60 days was calculated according to formula [1]

$$Q = 3515at, \qquad (1)$$

where a is the activity of the fragments (decays/min) which have fallen out on 1 cm^2 of the soil; t is the age of the fragments which have fallen out (days).

The number of future decays for an age of the activity less than 60 days was found according to the formula

$$Q = a\varphi(t), \qquad (2)$$

where $\varphi(t)$ was found by use of a curve given in [1]. The measurement of the activity of the fallout of fission products per 1 cm^2 of soil was made daily from the 6th of March, 1954, according to the method described in [2]. Activity of an unknown age was conditionally related to the middle of the series of tests just prior to the fallout of the activity. The results of the calculation of the numbers of future decays are given in Table 1.

Considering the relatively small amount of testing which was carried out up to 1954, one can assume that

TABLE 1

Number of Future Decays on 1 cm² of Soil

Year of fallout	Number of future decays on 1 cm² of soil
1954	$8{,}88 \cdot 10^6$
1955	$14{,}7 \cdot 10^6$
1956	$10{,}9 \cdot 10^6$
1954–1956	$34{,}5 \cdot 10^6$

the activity of all the fragments which had fallen prior to 1954 did not exceed the activity of the fragments during 1954. So the number of future decays per cm² of soil from all the testing is estimated as $Q = 4.3 \cdot 10^7$ decays/cm².

The calculation of the coefficient k was carried out in three steps: 1) the calculation of the number of γ quanta per one future β decay of the mixture of fission fragments; 2) the calculation of the flux of γ quanta from an infinite plane which passes through a 1 cm² area located at a height of 100 cm above the earth; 3) calculation of the γ radiation dosage in roentgens.

The number of γ quanta per future β decay depends on the age of the fragments at the time of fallout, which for the sake of simplicity in the calculation was taken as 75 days.

Those beta-active fragments whose proportion of a 75 day-old mixture of fragments was greater than 0.2% of the total are given in Table 2.

It is taken into account in Table 2 that in the Ru^{106}–Rh^{106} equilibrium chain there is one β decay which is recorded, since the energy of the β particles of Ru^{106} is so small that in a measurement with a thick source the they are not recorded. For this reason Pm^{147} and Sm^{151} are missing from the table.

The average number of γ quanta per decay is found according to the formula

$$\nu = \frac{\sum_{i=1}^{11} a_i b_i}{\sum_{i=1}^{11} a_i}. \qquad (3)$$

The average energy of the γ quanta emitted is found according to the formula

$$E_{av} = \frac{\sum_{i=1}^{11} a_i b_i c_i}{\sum_{i=1}^{11} a_i b_i}. \qquad (4)$$

At an age of 75 days, the mixture of fragments has $\nu = 0.45$ quanta per 1 future β decay; $E_{av} = 0.60$ Mev.

The flux of γ quanta emitted by an infinite plane contaminated with fission fragments (passing through a 1 cm² area 100 cm above the plane) is given by (neglecting secondary radiation) formula (5) of [3].

$$N = -\frac{Q\nu}{2} Ei(-100\mu), \qquad (5)$$

where N is the γ-quantum flux; Q is the number of β decays per 1 cm² of soil; ν is the number of γ quanta per 1 β decay; Ei (-100μ) is the function Ei of the argument (-100μ); μ is the attenuation coefficient of the rays in atmosphere in 1 cm^{-1} (for $E_{av} = 0.60$ Mev), equal to $10.8 \cdot 10^{-5}$ cm^{-1}.

The γ-ray energy loss in air for a small coefficient of true absorption $\tau + \sigma\beta$ amounts to

$$\Delta I = I_0 - I = I_0 \left\{1 - e^{-(\tau+\sigma_\beta)x}\right\} = I_0(\tau + \sigma_\beta)x, \qquad (6)$$

TABLE 2

Relative Number of Future Decays of Fragments in a 75 Day-Old Mixture

Isotope	Period	Yield at time of formation, %	Portion of the total number of future decays, a	Number of γ quanta per 1 β decay, b	Average γ-quantum energy, c
Sr^{89}	54 days	5	0,058	0	0
Sr^{90}	27 years	5	0,150	0	0
Y^{91}	61 days	5	0,060	0	0
Zr^{95}–Nb^{95}	65 days	6	0,160	1	0,72
Nb^{95}	35 days	0	0,054	1	0,75
Ru^{103}	42 days	3	0,032	1	0,5
Ru^{106}–Rh^{106}	1 year	2,5	0,066	0,2	0,8
Cs^{137}	33 years	5	0,150	0,92	0,66
Ce^{141}	33 days	6	0,044	0,7	0,15
Ce^{144}	290 days	5	0,113	0,5	0,08
Pr^{144}	—	5	0,113	0,01	—

where $I_0 = NE_{av}$; x is the path length of the γ rays in air (in cm); $(\tau + \sigma_\beta)$ is the coefficient of true absorption in the Compton effect and photoeffect; $\tau + \sigma_\beta = 3.8 \cdot 10^{-5}$ cm^{-1}.

The energy yield of the γ radiation in penetrating 1 cm of air is

$$\Delta W = I(\tau + \sigma_\beta) = NE_{av}(\tau + \sigma_\beta) \text{ Mev}, \quad (7)$$

while the dose in roentgens [3] is

$$D = 1{,}45 \cdot 10^{-5} NE_{av}(\tau + \sigma_\beta). \quad (8)$$

On substituting expression (5) for N into (8), we obtain

$$D = -1{,}45 \cdot 10^{-5} \frac{Q\nu(\tau + \sigma_\beta) E_{av}}{2} Ei(-100\mu) \text{ r}. \quad (9)$$

Putting in the numerical values for ν, $\tau + \sigma_\beta$, E_{av}, and $Ei(-100\mu)$, we get

$$D = 3{,}7 \cdot 10^{-10} Q \text{ r}. \quad (10)$$

The value $3.7 \cdot 10^{-10}$ is the dose rate at a point 100 cm above the earth corresponding to 1 decay per cm^2 on the earth's surface. Estimation of this quantity based on data in the literature yields the following values (r/decay): $8.2 \cdot 10^{-10}$ [4]; $4.6 \cdot 10^{-10}$ [5]; $16 \cdot 10^{-10}$ [6]; $3.4 \cdot 10^{-10}$ [7].

One should regard the first of the values just given as too high, since it was assumed in calculating that for each β decay 1 γ quantum is radiated. If one used the value of 0.45 γ quanta radiated for each decay, the value $3.7 \cdot 10^{-10}$ r/decay is obtained instead in the first case.

The authors of [6] note that they give only the order of magnitude of the quantity. Taking these limitations into account, the various estimates of the value of the dosage rate per decay agree well with the values found in this article. On substituting the previously calculated value $Q = 4.3 \cdot 10^7$ decay/cm^2 into expression (10) for D, one obtains

D = 0.016 r for a 30-year period.

The dosage value for England is estimated [8] at 0.055 r. For the USA, the value of the dosage calculated using the assumptions of the present paper fluctuates in the range 0.006-0.160 r [9], depending on the distance from the firing ground. The value of the dosage received by humans over a period of 30 years from cosmic rays and the natural radioactivity of the soil is between 4.3 and 5.5 r [10, 11].

By comparing the data adduced, it is clear that the γ-radiation dosages obtained for several countries are approximately the same in value, and much less than the natural γ-ray dosage. Although, as is shown by these data, the external γ radiation of radioactive fragments does not present an immediate danger, nevertheless the presence of additional radiation can become a cause of undesirable genetic consequences. In addition, a considerable part of the fallout activity belongs to Sr^{90}, whose capture inside an organism is dangerous.

The authors express their gratitude to Prof. K. K. Aglintsev for his valuable guidance and advice in the completion of the present undertaking.

LITERATURE CITED

1. V. A. Blinov and L. I. Gedeonov, Reactor Physics and Heat Engineering [in Russian] Atomnaya Énergiya (1958) Supplement No. 1, p. 96.
2. V. P. Shvedov, V. A. Blimov, L. I. Gedeonov, and E. P. Ankudinov, Atomnaya Énergiya 5, 577 (1958)*
3. G. V. Gorshkov, Gamma Radiation of Radioactive Substances [in Russian] (LGU, Leningrad, 1956).
4. The Effects of Atomic Weapons (US Gov. Print. Office, Washington, 1950).
5. R. Lapp, Bull. Atomic Scientists 11, 45 (1955).
6. M. Eisenbud and J. Harley, Science 121, 677 (1955).
7. I. Blifford and H. Rosenstock, Science 123, 619 (1955).
8. J. Cockroft, Nature 175, 873 (1955).
9. M. Eisenbud and J. Harley, Science 124, 251 (1956).
10. R. Lapp, Bull. Atomic Scientists 11, 216 (1955).
11. Science 123, 1157 (1956).

* Original Russian Pagination. See C. B. translation.

* * *

THE NEW ISOTOPES Sb^{112} AND Sb^{114} AND THE IDENTIFICATION OF Sb^{113} AND Sb^{115}

I. B. Selinov, Ya. A. Grits, Yu. P. Kushakevich,
Yu. A. Bliodze, S. S. Vasil'ev, and T. N. Mikhaleva

Translated from Atomnaya Énergiya, Vol. 7, No. 6, pp. 547-549
December, 1959
Original article submitted February 7, 1959

In searching for new isotopes of antimony, and with the aim of identifying the antimony isotopes whose half lives are 7 and 31 min [1], a study was undertaken of the activities formed in sufficiently thick targets enriched with tin isotopes (of mass numbers 112, 114-118) upon irradiation of the targets in the 120-centimeter phasotron at the MGU Scientific Research Institute of Nuclear Physics. In order to isolate the isotopes obtained in the (p, n) and (p, 2n) reactions, the irradiation was carried out at several proton energies of 7 to 30 Mev.

A comparison of the activities formed in various enriched isotopes of tin as a result of bombardment by protons of various energies showed that the 7-minute and 31-minute activities belonged to Sb^{113} and Sb^{115} respectively, these having been obtained in the Sn^{114} (p, 2n) Sb^{113} and Sn^{116} (p, 2n) Sb^{115} reactions.

We did not observe in the case of Sb^{115} an activity with a half-life $T_{\frac{1}{2}}$ = 60 min (which was ascribed to the latter isotope in [2]); one can assume that the γ lines which were related to Sb^{115} do not in fact belong to Sb^{115}, but to Sb^{116}, which has $T_{\frac{1}{2}}$ = 60 min. In addition, we discovered two new isotopes: Sb^{112}, with $T_{\frac{1}{2}} = 0.9 \pm 0.1$ min, and Sb^{114}, with $T_{\frac{1}{2}} = 3.3 \pm 0.3$ min (Figs. 1 and 2). These isotopes were obtained in the Sn^{112} (p, n) Sb^{112} and Sn^{114} (p, n) Sb^{114} reactions.

The chemical separation of the antimony was done just as in [1]. In studying the short-lived isotope Sb^{112}, it became necessary to use an incomplete separation

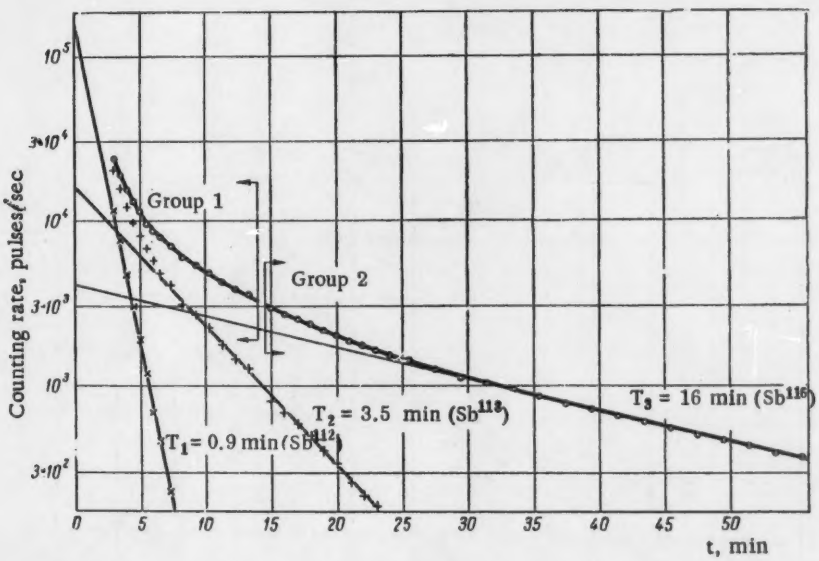

Fig. 1. Half-lives of radioactive isotopes of antimony chemically separated from tin enriched with Sn^{112}, after irradiation of the tin by protons.
Isotopic composition of the target (in percent): Sn^{112} – 52.3; Sn^{114} – 1.5; Sn^{115} – 1.5; Sn^{116} – 11.2; Sn^{117} – 4.2; Sn^{118} – 11.2; Sn^{119} – 4; Sn^{120} – 10.7; Sn^{122} – 1.4; Sn^{124} – 0.2.
Proton energy 15 Mev; exposure 1 min. The activity with a half-life of T = 3.5 min is determined for the most part by the isotope Sb^{113} (T = 3.5 min), and partially by the isotope Sb^{114} (T = 3.4 min), since the Sn^{113} content in the target is 7.5 times as large as that of Sn^{114}.

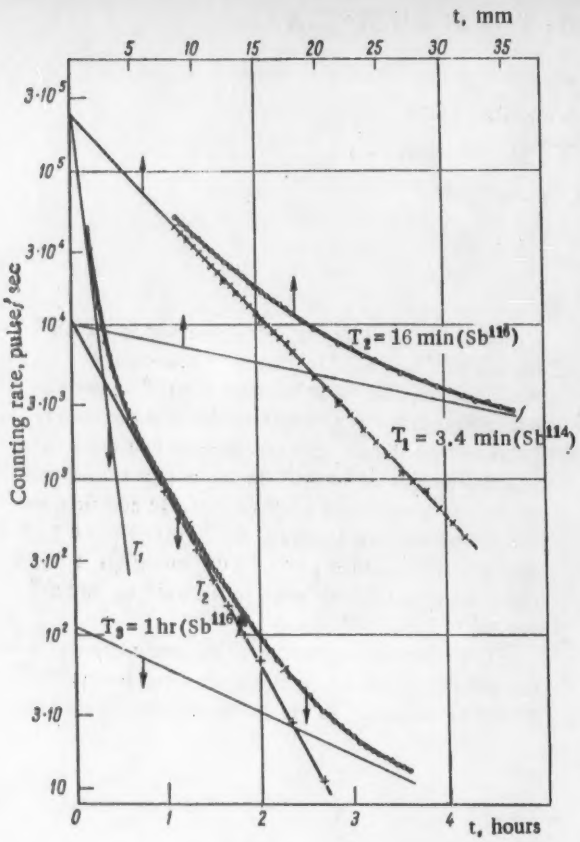

Fig. 2. Half-lives of radioactive isotopes of antimony chemically separated from tin enriched with Sn^{114}, after irradiation of the tin by protons.
Isotopic composition of target (in percent): Sn^{112} – 0.6; Sn^{114} – 57.2; Sn^{115} – 3.3; Sn^{116} – 19.6; Sn^{117} – 10.8; Sn^{118} – 6.8; Sn^{119} – 0.4; Sn^{120} – 1.3; Sn^{122} – 0.1; Sn^{124} – 0.1. Proton energy 15 Mev; exposure 1 min.

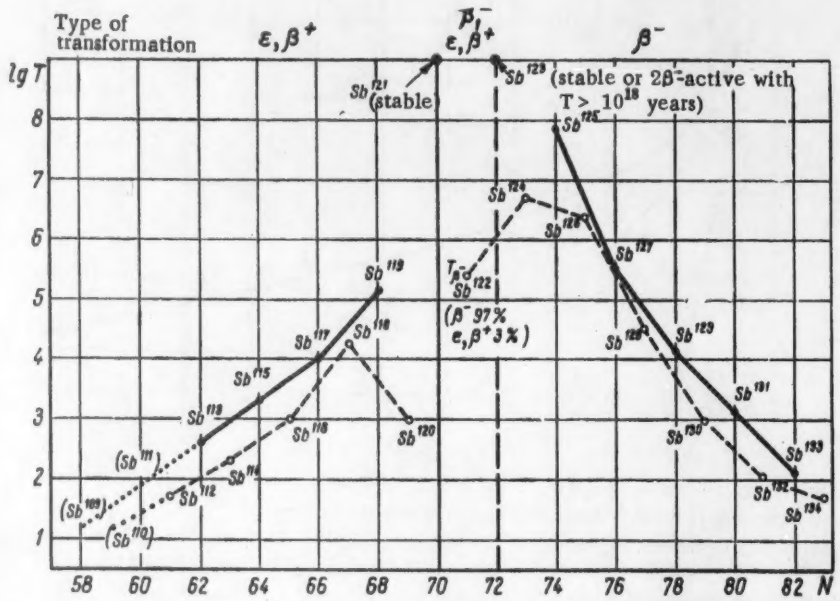

Fig. 3. Half-lives of radioactive isotopes of antimony. Neutron number N is plotted on on the abscissa. The left branch of the curve corresponds to ε- and β^+-active isotopes, and the right branch corresponds to β^--active isotopes. As yet undiscovered isotopes are indicated in parentheses.

of the antimony (about 1%), in order to start the measurement of the activity within 3 min after terminating the bombardment. The initial intensity of the antimony with $T_{\frac{1}{2}}$ = 0.9 min which was separated from the target which had been enriched with Sn^{112} and bombarded by 15 Mev protons was 15 times as high as the initial intensity from a mixture of other isotopes of antimony. The analogous ratio for Sb^{114} was equal to 30.

The maximum energy of the β^+ emission as determined by the absorption method amounted to 2.7±0.2 Mev in the case of Sb^{114}. The gamma spectrum, which was measured with a scintillation spectrometer using a 100-channel pulse-height analyzer, consists of three lines: the γ line of the annihilation radiation, the 1300±30 kev line, and the less intense 900±60 kev line. The gamma spectrum of Sb^{112} has, besides the annihilation line, only one γ line, whose energy is 1270±30 kev. As is evident in Fig. 3, the isotopes of antimony with even neutron numbers (Sb^{113}, Sb^{115}, Sb^{117}) have a greater $T_{\frac{1}{2}}$ than the isotopes next to them with odd neutron numbers(Sb^{112}, Sb^{114}, Sb^{116}). It is to be anticipated that the still undiscovered isotope Sb^{111} has a value $T_{\frac{1}{2}} \simeq$ ≃ 1.1 - 1.5 min; i.e., somewhat larger than the $T_{\frac{1}{2}}$ of Sb^{112}. A more detailed description of work on the new isotopes of antimony will be given later.

The authors express their gratitude to V. S. Zolotarev for making enriched isotopes of tin available, to Yu. A. Vorob'ev and the members of the phasotron staff, and also to L. Ya. Shavtvalov for his work on the spectrometer.

LITERATURE CITED

1. I. P. Selinov, Yu. A. Grits, D. E. Khulelidze, E. E. Baroni, Yu. A. Bliodze, A. G. Demin, and Yu. P. Kushakevich, Atomnaya Énergiya 5, 660 (1958).*
2. D. Strominger, J. Hollander, and G. Seaborg, Rev. Mod. Phys. 30, 585 (1958).

*Original Russian pagination. See C. B. translation.

* * *

STABILITY OF A CHARGED BEAM IN STORAGE SYSTEMS

A. A. Kolomenskii and A. N. Lebedev

Translated from Atomnaya Énergiya, Vol. 7, No. 6, pp. 549-550
December, 1959
Original article submitted June 8, 1959

In connection with the proposal on the feasibility of reactions with intersecting beams of relativistic particles [1], there has been increased discussion recently concerning methods of storage [2] of high current in annular magnetic systems. Of particular interest for such systems is the study of the interaction of the large number of particles in a storage orbit. Besides the lateral repulsion of the beam, which mainly affects the betatron oscillations, there are also interesting effects connected with the azimuthal inhomogeneities of the density and the resulting redistribution in energy of the particles.

It follows from quite simple physical considerations that under certain conditions, a distribution of the beam which is homogeneous with respect to the azimuthal direction is unstable. For simplicity, let us consider a monoenergetic beam. The field due to a positive density fluctuation which is formed accelerates particles moving in front of the fluctuation and decelerates particles moving behind it. If at the same time the rotation frequency decreases with a rise in energy $\frac{d\omega}{dE} < 0$, a further increase in the fluctuation will be brought about; for $\frac{d\omega}{dE} > 0$, the fluctuation tends to be resolved. The condition $\frac{d\omega}{dE} < 0$ is obtained in weak-focusing and strong-focusing systems above the critical energy. In view of the practical importance of the question, and the physical interest which plasma effects exhibit in storage systems, it is therefore appropriate to examine such instability in greater detail.*

The change in energy of a particle in the presence of an azimuthal electric field is described by the Hamiltonian [2]

$$H = -e \int \mathcal{E}(\varphi, t)\, d\varphi + \left(v \frac{d\omega}{dE}\right)_S \frac{W^2}{2}, \qquad (1)$$

*After this note was written to the press, another study [3] was published, in which the beam stability was also examined in the region above the critical energy.

in which the canonic momentum W is connected with the energy E by the relation

$$W=\int_{E_S}^{E}\frac{dE}{v(E)}, \tag{2}$$

where v is the velocity of the particle. (The index S indicates quantities evaluated at the average energy of the stored beam.) The canonical coordinate φ which is conjugated to W is connected with the azimuthal angle θ by the relation $\varphi = \theta - \omega_S t$; in the general case of arbitrary periodic systems, θ is the so-called generalized azimuth [4]. The quantity $\mathcal{E}(\varphi, t)$ is the azimuthal component of the electric field of the beam.

We will describe the state of the beam by the distribution function F(W, φ, t), which can be represented in the form of a sum

$$F(W,\varphi,t)=F_0(W)+f(W,\varphi,t);\quad f\ll F_0, \tag{3}$$

i.e., we shall examine small deviations from an equilibrium state which is homogeneous with respect to the azimuthal direction. It is clear from physical considerations that $\mathcal{E} = 0$ in the equilibrium state, since the linearized kinetic equation has the form

$$\frac{\partial f}{\partial t}+\frac{\partial f}{\partial\varphi}\left(v\frac{d\omega}{dE}\right)_S W=-\frac{\partial F_0}{\partial W}e\mathcal{E}(\varphi,t) \tag{4}$$

or, if we take the Fourier transform on the azimuthal angle and a Laplace transform on time;

$$f_p\left[p+ikW\left(v\frac{d\omega}{dE}\right)_S\right]=f(k,0)-\frac{\partial F_0}{\partial W}e\mathcal{E}_p(k). \tag{5}$$

In order to connect $\mathcal{E}(k)$ with the Fourier component of the charge density, we make use of the fact that the electric field of the beam is well shielded by the horizontal covers of the vacuum chamber and is practically the same as the field of a rectilinear beam which is located between two conducting planes. Whence

$$\mathcal{E}(k,t)=-\frac{i\Lambda ke}{R^2\gamma^2}\int_{-\infty}^{+\infty}f(W,k,t)\,dW;\quad \gamma=\left(1-\frac{v^2}{c^2}\right)^{-1/2}, \tag{6}$$

where R is the average radius of the orbit.

This same expression can be obtained rigorously, if we use for the field of the shielded circular current the expressions given, for example, in [5]. The exact result of expression (6) will be given in a more detailed study; we will note here only that the quantity Λ, which depends on the ratio of the transverse dimensions of the beam to the gap width d, has a value in the range 2-3 in cases of practical interest. Expression (6) was obtained by using the assumption that the dimensions of the inhomogeneity are large in comparison with the aperture of the chamber; i.e., $k \ll \frac{R}{d}$.

By using the usual method of solution of equations (5) and (6), it is easy to arrive at the conclusion that the asymptotic behavior of the perturbation is determined by the root of the equation

$$\frac{\Lambda e^2ki}{R^2\gamma^2}\int_{-\infty}^{+\infty}\frac{\partial F_0/\partial W\,dW}{\left[p+ikW\left(v\frac{d\omega}{dE}\right)_S\right]}=1, \tag{7}$$

which has the largest real part. Since we are interested in the existence of an unstable solution (i.e., roots for which Rep > 0), the integration in expression (7) is carried out just along the real axis.

Let us consider now two concrete distributions for $F_0(W)$.

1. The homogeneous distribution

$$F_0=\begin{cases}\dfrac{N}{4\pi W_0} & \text{for } |W|\leq W_0.\\ 0\end{cases} \tag{8}$$

After simple calculations we obtain from (7)

$$\frac{p}{kW_0\left|v\frac{d\omega}{dE}\right|_S}=[\xi-1]^{1/2}, \tag{9}$$

where

$$\xi=\frac{2N\Lambda r_0}{\pi R\delta^2\gamma^3}\frac{\gamma^2-1}{\alpha\gamma^2-1};\quad r_0=\frac{e^2}{mc^2} \tag{10}$$

(δ is the relative spread in energy of the beam, and α is the coefficient of expansion of the orbit).

It is clear from relation (9) that the instability (Rep > 0) can occur, first of all, only in the region above the critical point ($\alpha\gamma^2 > 1$), and secondly, for a sufficiently narrow distribution:

$$\delta^2<\frac{2N\Lambda r_0}{\pi R\gamma^3}\frac{\gamma^2-1}{\alpha\gamma^2-1}. \tag{11}$$

2. Now we let

$$F_0=\frac{NW_0}{2\pi^2}\frac{1}{W^2+W_0^2}, \tag{12}$$

whence

$$\frac{p}{kW_0\left|v\frac{d\omega}{dE}\right|_S}=\sqrt{\xi}-1. \tag{13}$$

The same conclusions follow from this equality as from expression (9); the instability can occur only for the case in which $\frac{d\omega}{dE} < 0$ ($\xi > 0$) and condition (11) is satisfied. For $\xi < 0$, the density of the beam undergoes in both cases small unstable oscillations, with a frequency determined by Imp. The question of the possible damping of such oscillations must be examined separately.

In order to illustrate the formulas obtained, we may point out that for an electron storage system whose parameters are $\gamma = 60$, $\alpha = 5\ 10^{-2}$, $R = 1.5 \cdot 10^2$ cm, $\Lambda = 3$, $N = 10^{14}$, the growth time of the instability

$T \simeq \frac{1}{p} = 4 \cdot 10^{-5}$ sec for $\delta = 5 \cdot 10^{-3}$. It should be noted, however, that the development of the disturbance increases the non-monoenergetic character of the beam, which can ultimately limit the development of the fluctuation.

We may remark in conclusion that these effects disappear for the case of a small region of increased density which is bounded in the azimuthal direction accompanied by the presence of a high frequency accelerating field, provided that the growth time of the instability is much larger than the period of the synchrotron oscillations. This is connected with the fact that the effect on the particle of the field due to the fluctuation is zero, when averaged over the period of the oscillations.

LITERATURE CITED

1. D. Kerst, CERN Symposium (1956).
2. K. Symon, and A. Sessler, CERN Symposium (1956).
3. C. Nielsen and A. Sessler, Rev. Scient. Instrum. 30, 80 (1959).
4. A. A. Kolomenskii, Dissertation [in Russian] (FIAN, 1957).
5. M. L. Levin, Zhur. Tekh. Fiz. 17, 1159 (1957).

* * *

THE ALBEDO OF γ-RAYS AND THE REFLECTION BUILD-UP FACTOR

B. P. Bulatov and O. I. Leipunskii

Translated from Atomnaya Énergiya, Vol. 7, No. 6, pp. 551-553, December, 1959
Original article submitted March 19, 1959

In considering problems connected with the reflection of γ rays, we may distinguish two cases.

First case (Fig. 1a). A narrow beam of monoenergetic γ quanta is incident on a broad scatterer. The ratio of the total back-scattered energy (or number of quanta) J_p to the energy (or number of quanta) J_0 (incident on the scatterer) is called the energy albedo η_E (or number of quanta η_n) for γ-rays, $\eta = J_p/J_0$,

$$\eta_n = 2\pi \int_0^{\pi/2} \int_0^{E_{max}} N(\varphi, E) \cos\varphi \, dE \, d\varphi, \qquad (1)$$

$$\eta_E = \frac{2\pi}{E_0} \int_0^{\pi/2} \int_0^{E_{max}} N(\varphi, E) \, E \cos\varphi \, dE \, d\varphi, \qquad (2)$$

where $N(\varphi, E)$ is the distribution function of the scattered γ quanta, E is the energy, φ is the angle of emergence of the scattered γ quanta, and E_0 is the photon energy of the primary radiation.

Second case (Fig. 1b). An infinitely broad uniform flux of monoenergetic γ quanta is incident on an infinitely broad scatterer.

An isotropic detector measures the energy (or quanta) flux density of the γ rays with the scatterer $I = I_0 + I_p$ and without it $I = I_0$. The ratio of these quantities is called the energy reflection build-up factor B_{re} or (quantum) number reflection build-up factor B_{rn}, and is equal to

$$B_r = \frac{I_0 + I_p}{I_0} = 1 + \frac{I_p}{I_0}; \qquad (3)$$

$$B_{rn} = 1 + 2\pi \int_0^{\pi/2} \int_0^{E_{max}} N(\varphi, E) \frac{\cos\varphi}{\sin\varphi} \, dE \, d\varphi;$$

$$B_{re} = 1 + \frac{2\pi}{E_0} \int_0^{\pi/2} \int_0^{E_{max}} N(\varphi, E) \, E \frac{\cos\varphi}{\sin\varphi} \, dE \, d\varphi. \qquad (4)$$

From expressions (1)-(4) it follows that $B_{re} - 1 > \eta_E$, and $B_{rn} - 1 > \eta_n$.

In the present work the quantitative relations between the energy albedo and the build-up factor for γ rays on reflection from light materials with $Z \leq 26$ were determined experimentally. The method for determining experimentally the distribution function $N(\varphi, E)$ is described in [1]. The scheme for the experiments is shown in Fig. 1a, b, c. The counter STS-5 [1] and the ionization chamber KID-1 were used as γ-ray detectors. The error in the measurements was ±15%.

The measured dependence of the energy flux density of the Au^{198} γ rays scattered by iron on the angle of emergence φ of the quanta (distribution function) is accurately expressed by the formula.

$$J_p(\varphi) = 3 \cdot 10^2 \cdot \sin^{0,7}\varphi \text{ Mev/cm}^2 \cdot \text{sec}. \quad (5)$$

The total energy of γ-rays back-scattered from iron is

$$J_p = 2{,}94 \cdot 10^5 \int_0^{\pi/2} \sin^{0,7}\varphi \, d(\sin\varphi) = 1{,}73 \cdot 10^5 \text{ Mev/sec}. \quad (6)$$

Dividing the expression (6) by the total energy flux of the incident radiation, which is equal to $2.01 \cdot 10^6$ Mev/sec, we get the value of the energy albedo of Au^{198} γ rays from iron $\eta_e = 0.086$.

It is possible to calculate the reflection build-up factor using the distribution function (5). The density of the energy flux of the γ rays scattered from a ring $2\pi r dr$ and falling on to the receiver is expressed by the formula

$$I_p(\varphi) = 300 \frac{2\pi r \, dr \, I_0}{I_0 \Delta S} \frac{R_0^2}{R^2} \sin^{0,7}\varphi. \quad (7)$$

Since $r = h \operatorname{ctg}\varphi$ and $R = \frac{h}{\sin\varphi}$, the energy flux density of the γ radiation scattered from the infinite surface of the scatterer in the direction of the detector can be wittten in the form

$$I_p = 0{,}14 I_0 \int_0^{\pi/2} \operatorname{ctg}\varphi \sin^{0,7}\varphi d\varphi = 0{,}20 I_0. \quad (8)$$

Hence $$B_{re} = 1 + \frac{I_p}{I_0} = 1{,}20.$$

For the Co^{60} γ rays back-scattered from iron the distribution function has the form

$$J_p(\varphi) = 7{,}7 \cdot 10^2 \sqrt{\sin\varphi} \text{ Mev/cm}^2 \cdot \text{sec}. \quad (9)$$

The values of the albedo and build-up energy factor calculated using this function are equal to 0.025 and 1.075, respectively. The results obtained agree well with the data in [1-3].

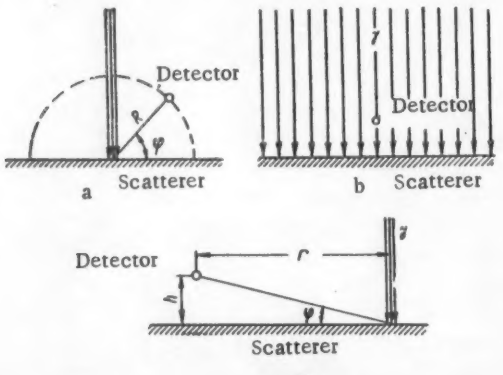

Fig. 1. Scheme for experiments.

Graphs of the dependence of the reflection build-up factors of Au^{198} γ rays on the dimensions of the scatterer (carbon) surface are shown in Fig. 2.

The dependence of the energy flux density of the scattered radiation I (Mev/cm² · sec) on the energy flux density of the primary radiation I_0 (Mev/cm² · sec), the energy of the primary photons E_γ (Mev) (0.4 Mev ≤ E_γ ≤ ≤ 1.25 Mev) and the quantities h and r [r is the distance between the detector and the point of intersection be-

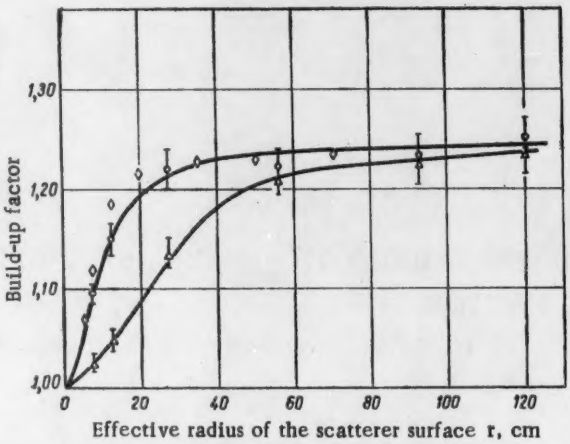

Fig. 2. The dependence of the value of the reflection energy build-up factor for Au^{198} γ rays on the size of the scattering surface: ○, △) experimental points (h is 1.1 and 12.5 cm, respectively); ◇) calculated points [h = 1.1 cm (11)].

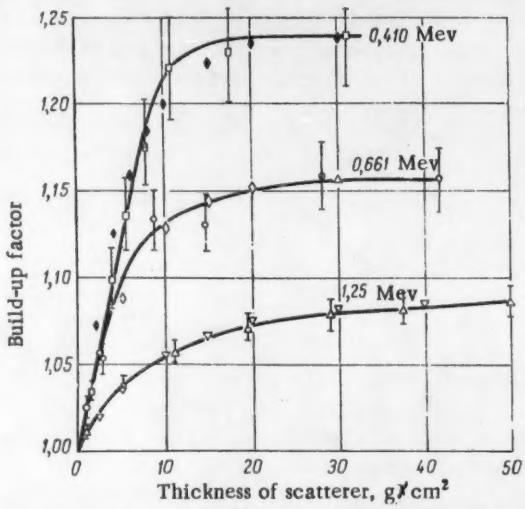

Fig. 3. Dependence of the value of the energy build-up factor on the thickness of the scattering material: □, ○, △) experimental points; ◆, ◇, ▽) calculated points (12).

tween the surface of the scatterer and a narrow beam diameter 3.8 cm of primary γ quanta (see Fig. 1c)] is satisfactorily expressed by the empirical relation

$$I = 1 \cdot 10^{-2} \frac{I_0}{hE_\gamma} e^{-\frac{0,23}{\sqrt{h}} r} \qquad (10)$$

Using expression (10), the energy build-up factor of γ rays reflected from light materials can be calculated:

$$B_{re} = 1 + \frac{5,5 \cdot 10^{-3}}{E_\gamma h} \int_0^\infty e^{-\frac{0,23}{\sqrt{h}} r} r dr. \qquad (11)$$

The values of B_{re} when γ quanta from Co^{60} and Au^{198} are scattered from carbon were obtained empirically, from experiments with a wide beam (1.26 and 1.088, respectively), and those calculated using (11) agree with those calculated by the Monte Carlo method [3] (1.24 and 1.084).

The results of measuring the dependence of the value of the energy build-up factor on the thickness of the scatterers (aluminum) are shown in Fig. 3. This dependence is satisfactorily described by the empirical formula

$$[B_{re}(d) - 1] = [B_{re}(\infty) - 1](1 - e^{-d/a}), \qquad (12)$$

where $B_{re}(\infty)$ is the limiting value of the build-up factor for an infinitely thick scatterer; d is the thickness of the scatterer (g/cm²); and a is a constant, equal to approximately half the free path of the primary radiation in the material of the scatterer.

In agreement with the data given in [1] for a given energy of the primary radiation, the constant a is the same for all substances with $Z \leq 26$. The points calculated from (12) are shown in Fig. 3.

It follows from the diagrams that the limiting value of the reflection build-up factors in scattering by light elements is reached when the thickness of the scatterer is equal to 1.5-2 times the γ-quantum free path of the primary radiation in the scatterer.

The results obtained correspond to those in [3-5].

In conclusion, the authors express their gratitude to B. V. Novozhilov and V. N. Zakharov for their interest in the work and discussion of the results.

LITERATURE CITED

1. B. P. Bulatov and E. A. Garusov, Atomnaya Énergiya, 5, 631 (1958).*
2. E. Hayward and I. Hubbell, Phys. Rev. 93, 955 (1954).
3. M. Berger and I. Doddett, J. Res. Nat. Bur. Standards, 56, 89 (1956).
4. M. Berger, J. Res. Nat. Bur. Standards, 55, 343 (1955).
5. J. Perkins, J. Appl. Phys. 26, 1372 (1955).

*Original Russian pagination. See C. B. translation.

* * *

APPLICATION OF MASS-PRODUCED SCINTILLATION EQUIPMENT IN RADIOMETRIC CONTROL OF THE BOUNDARIES OF PETROLEUM PRODUCT MIXTURES IN PIPING

L. N. Posik

Translated from Atomnaya Énergiya, Vol. 7, No. 6, pp. 553-554
December, 1959
Original article submitted January 8, 1959

In the paper by B. Z. Votlokhin et al.*, the radiometric control method is recommended for determining the dividing boundary between two petroleum products. An Sb^{124} source with an activity of 10-12 μC (in the form of a solution in 4 ml of triphenylstilbene) was used for this purpose. The activity of petroleum products was measured by means of special equipment consisting of a data transmitter, a PS-64 scaling device, a four-range integrator, and an ÉPD-17 electronic potentiometer with a contactor device. A bank of VS-9

*B. Z. Votlokhin, A. V. Dorogochinskii, and N. B. Mel'nikov, Atomnaya Énergiya 4, 475 (1958)[Original Russian pagination. See C. B. translation].

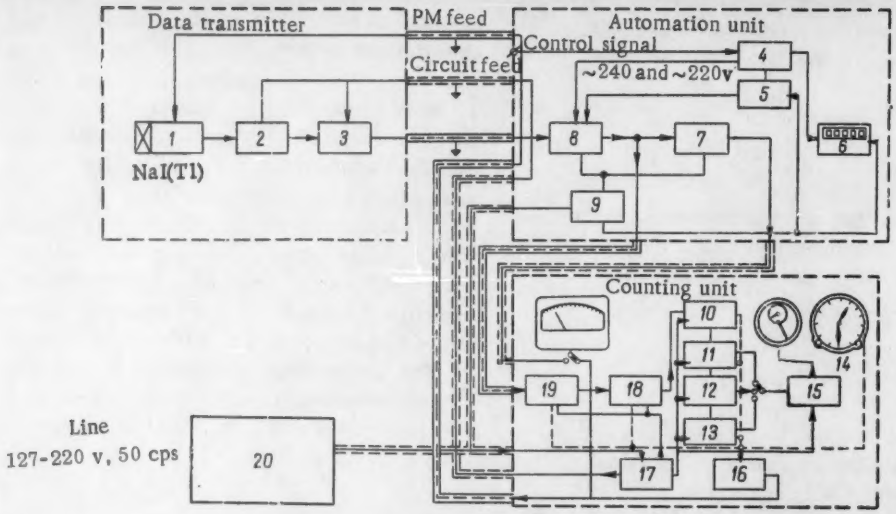

Fig. 1. Schematic diagram of the RSU device. 1) Photomultiplier; 2) multivibrator; 3) cathode follower; 4) automatic control circuit; 5) time relay; 6) electric clock; 7) intensity meter; 8) input stage; 9) feed unit; 10-13) scaling circuits; 14) clock; 15) EMS stage; 16) high-voltage feed units; 17) feed units; 18) scaling circuit; 19) input stage; 20) SNÉ-220-05 stabilizer.

Fig. 2. External view of the RSU device.

counters was used in the annular data transmitter, while suitably sized data transmitters were required for different pipe diameters. It follows from the above brief description of the equipment that, regardless of its considerable practical value, it is very cumbersome; this hinders a speedy introduction of the described method into the rapidly expanding network of petroleum pipelines in our country.

Since the publication of the above paper, it became possible to use scintillation equipment of a new type for controlling the boundaries of petroleum products mixtures. Best results can be achieved by using a mass-produced RSU device.

The schematic diagram and the external view of the device are shown in Figs. 1 and 2. The efficiency of the data transmitter with an FÉU-29 photomultiplier and an NaI(Tl) crystal is 5-8 $\frac{\text{pulse/sec}}{\mu\text{r/hr}}$, which is equivalent to the efficiency of 40 to 65 STS-8 gas-discharge counters. The data transmitter is designed for use at temperatures from −20 to +40°C and for a relative air humidity of up to 95%. The connecting

cable, which is 100 to 150 m long, and the data transmitter design make it possible to mount it at the most convenient point in piping of any diameter. The intensity meter of the device has three ranges – 500, 200, and 50 thousand pulses/min with RC = 1 sec, a needle indicator, and a jack for a self-recorder with a current of up to 3 ma. The entire device is fed from a 127-220-v line, and the over-all power consumption is ~ 200 va. For line voltage fluctuations from −20 to +15% of the nominal value, the ferromagnetic stabilizer secures a reading stability of ± 5%. The device is designed for continuous measurement over a period of 8-16 hr, and with interruptions lasting from 1 to 2 hr. the device can operate 24 hr a day.

* * *

IMPROVED DEPOSITION OF URANIUM AND THORIUM LAYERS BY THE METHOD OF ATOMIZATION IN AN ELECTRIC FIELD

Yu. A. Selitskii

Translated from Atomnaya Énergiya, Vol. 7, No. 6, pp. 554-555, December, 1959
Original article submitted June 4, 1959

From among the different methods of depositing thin layers on metallic foils and organic films [1 and 2], the method of atomizing a solution of the substance from a capillary under the action of an electric field [3], which had been applied not so long ago, deserves attention. The basic advantage of this method consists in the fact that the substance can be dissolved in a small volume, and the atomization can be performed with a relatively small loss of the substance, which is uniformly distributed on the target surface. Moreover, as is shown in the present paper, this method is entirely suitable for the production of layers on thin organic films.

It is mentioned in paper [2] that only very thin layers are of a good quality, and that, if the amount of the substance is increased, the surface becomes uneven. Experiments show that surface nonuniformity in the case where thorium nitrate or uranyl nitrate solutions in alcohol are atomized is the consequence of their hygroscopic nature. The developed nonuniformity rapidly increases with an increase in the thickness of the substance layer. In storage, a layer ~ 100 $\mu g/cm^2$ thick continues to deteriorate due to the fact that the substance crystallizes in the form of small separate stars as the layer absorbs moisture from air.

In the present work, nitrates were converted into nonhygroscopic compounds in order to eliminate the surface unevenness. If a base-layer which can withstand calcination is used, a uniform thin nitrate layer 40-50 $\mu g/cm^2$ thick can be readily oxidized. A consecutive alternation of nitrate atomization and calcination makes it possible to obtain uniform layers with the required thickness (~ 1 mg/cm^2). If aluminum disks are used, it is convenient to convert thorium nitrate to thorium hydroxide, and uranyl nitrate to ammonium diuranate by exposure in the vapor of an 8% solution of ammonia for 10-15 min. In the first case, the developed NH_4NO_3 quickly dissolves when the disk is rinsed in water. The dried layer is then again spray-coated with the nitrate. Thorium hydroxide is nonhygroscopic and is more convenient in work, since the useful substance weight represents a larger percentage of the total weight. Control weighing showed that not more than two water molecules per one hydroxide molecule are present; heating to 100°C removes the water completely [4]. The amount of uranium in ammonium diuranate, determined by weighing, is 71%.

In certain cases, for instance, in the simultaneous recording of even fission fragments, the fissionable material must be deposited on a very thin, usually organic, film. The electrolytic deposition method requires the use of metallic base film, which is connected with an undesirable increase in the base-layer weight.

The atomization of a solution from a capillary in an electric field is accompanied by very small currents (~2 μa); this makes it possible to use the following method of layer deposition. A collodion or celluloid film, which was pasted on a light aluminum ring with an inside diameter of 40 mm, was placed on a cylindrical

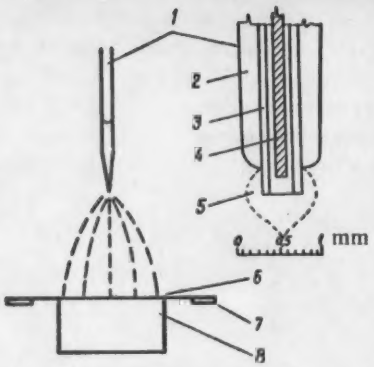

Method of layer deposition: 1) Glass capillary 0.4 to 0.5 mm in diameter; 2) paraffin; 3) capillary; 4) tungsten; 5) conical solution drop; 6) organic film; 7) aluminum ring; 8) aluminum support.

aluminum support with a polished end-face (height: 20 mm; diameter: 26 mm), which, as can be seen from the figure, served as one of the electrodes in the substance atomization.

In order to secure the necessary conductivity between the film and the aluminum support, they must be brought into intimate contact over the entire surface, which can be readily achieved by one of the following methods:

1. A water drop, which is placed on the support end-face, is evenly forced out and the air is expelled when the ring with the film is placed on the support. After drying, the film is in intimate contact with the support polished surface.

2. The ring with the film is put on the support and placed under a hood. After evacuation to $\sim 10^{-1}$ mm Hg, the glowing discharge from a lead-in which is at a negative voltage of ~ 1000 v charges the film surface, which leads to an intimate contact between the film and the support.

After this preliminary operation, the atomized substance uniformly settles on the film portion which adheres to the support, while the formed surface charge prevents deposition on the remaining film surface, which remains clean. Thus, the diameter of the covered area is determined by the support diameter.

The film with the nitrate is treated with ammonia vapors and is rinsed in slowly running water. All the subsequent operations, until a layer of sufficient thickness is formed, are performed before the film is taken off the support. Then, the film is gently taken off under water and then dried, after which it is fixed in a holder of a design suitable for the work on hand. By careful handling, even a "black" collodion film with a thickness of $\sim 15\ \mu g/cm^2$ can be readily taken off.

The solution can be atomized by using either polarity. Best quality layers were obtained for a positive capillary voltage of ~7 kv, a distance to the film equal to 50 mm, and a nitrate concentration of 50-200 mg/cm^3 in the alcohol solution (for the prevention of hydrolysis in depositing thorium, a nitrate solution with a 0.14 N acidity was used).

Observations by means of an M-24 long-focus binocular microscope revealed that the solution concentration in the drop at the capillary end increases during the atomization process, which can cause the disruption of small crystals and a deterioration of the layer quality. In order to prevent a quick drying of the solution on the external, well-wetted wall, the capillary was coated with a thin paraffin layer, which was removed with ether at the capillary end.

For a suitable electric field strength, a periodically pulsating cone-shaped drop with a constantly mixing solution is formed at the end of such a capillary, which secures a good, uniform quality of the layer.

The author is deeply grateful to A. N. Protopopov, S. M. Solov'ev, M. I. Kuznetsov, and G. P. Lepnev for their advice and help in the work.

LITERATURE CITED

1. R. Blanchard, B. Kahn, and R. Birkhoff, Chem. Abstrs. 52, 4343 (1958).
2. J. Povelites, Paper No. 604 presented by the USA at the Second International Conference on the Peaceful Uses of Atomic Energy (Geneva, 1958).
3. D. Casswell and J. Milsted, J. Nucl. Energy 4, 51 (1957).
4. G. Seaborg and J. Katz, Actinides [Russian translation] (IL, Moscow, 1955) p. 70.

* * *

ABOUT THE SINGLE-STAGE SEPARATION COEFFICIENT OF LITHIUM ISOTOPES BY THE ION-EXCHANGE METHOD

G. M. Panchenkov, E. M. Kuznetsova, O. N. Kaznadzei

Translated from Atomnaya Énergiya, Vol. 7, No. 6, pp. 556-557
December, 1959
Original article submitted November 5, 1958

The idea of a difference between isotopes in ion-exchange reactions was suggested and confirmed in 1936 in [1, 2]. In 1940 a patent was published [3]; in [4] it was found that when lithium carbonate and lithium phosphate are precipitated the solution is enriched in the light isotope. The same result is given in [5]. Our calculations according to a formula given in [6] showed that the coefficient of single-stage distribution in precipitation processes, according to the data of the various authors, oscillates from 1.016 to 1.021, and the solution is always enriched in the light isotope.

In our work, we have considered the problem of determining the coefficient of single-stage separation of lithium isotopes for the ion-exchange reaction on domestic cationite, and also of clarifying the dependence of this coefficient upon the nature of the salts and of the cationites, and upon the concentration of the solution. We carried out our work in regard to the determination of the coefficient of single-stage separation by using the half-absorption method, since in this case after a small number of stages a sufficiently good degree of enrichment was achieved. The analysis of the isotope ratio was carried out on the domestic mass-spectrometer MS-3 with the help of an aluminum silicate ion emitter [7].

In order to clarify the influence of the anion of the initial salt on the coefficient of single-stage separation, we chose carbonate, benzoate, chloride and hydroxide solutions.. As an ion-exchanger we used sulfonated coal in hydrogenated form, previously washed from impurity cations and iron, and also from traces of hydrochloric acid until it gave a negative methyl orange test. The data relating to the experiments about the influence of the anions of the initial lithium salts on the coefficient of single-stage separation (the initial salt concentration being 0.1 N) are given below:

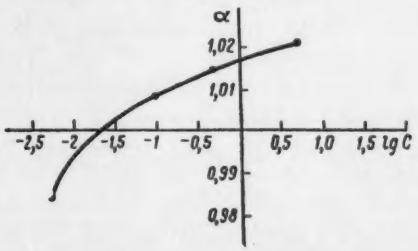

Fig. 1. Dependence of the single-stage separation coefficient upon the concentration of the solution.

Anion	OH^-	$CO_3^{=}$	$C_6H_5COO^-$	Cl^-
Separation coefficient . . .	1.009	1.003	1.003	0.996

It is interesting to note that in all experiments the solution was enriched in the light isotope, except in those with lithium chloride. Besides, it was evident that in continuing the experiments the most appropriate salt would be lithium hydroxide.

In order to determine the dependence of the single-stage separation coefficient upon the concentrations, experiments were made with lithium hydroxide at different initial concentrations. The data are reported below and in Fig. 1.

Initial concentration, N	5	0.5	0.1	0.005
Separation coefficient	1.021	1.015	1.009	0.985

As can be seen, for lithium hydroxide solution an inverse behavior of the single-stage separation coefficient and of the solution concentration is observed: for concentrations 0.005 N the solution is enriched in the lithium isotope of mass 7, and for concentrations of 0.1 N and above it is enriched in the light isotope of mass 6.

Also experiments with a 0.5 N solution of lithium hydroxide on synthetic aluminum silicates having the compositions 13% Al_2O_3, 87% SiO_2 and 14% Al_2O_3, 86% SiO_2 and prepared in different ways were carried out. The results of the experiments for the determination of single-stage separation coefficients with different cationites are reported below:

Cationite	Sulfonated coal	Aluminum silicates of composition, %	
		13 – Al_2O_3 87 – SiO_2	14 – Al_2O_3 86 – SiO_2
Separation coefficient	1.015	1.009	1.017

It is evident that the single-stage separation coefficients of lithium isotopes on aluminum silicates are approximately the same as on sulfonated coal.

It would be interesting to find a general approach to the interpretation of the influence of the various factors on the separation process. The separation of

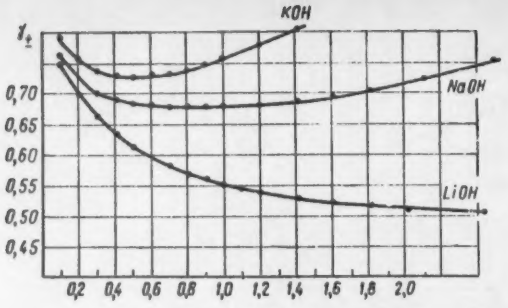

Fig. 2. Dependence of the activity coefficients of the hydroxides of alkali metals upon the concentrations of their solutions.

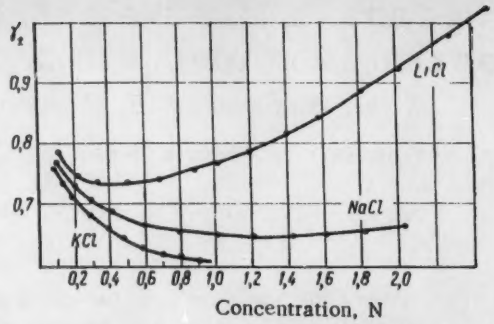

Fig. 3. Dependence of the activity coefficients of alkali metal chlorides upon the concentrations of their solutions.

isotopes in multi-stage experiments was carried out in equilibrium conditions, under which Li^6 and Li^7 were distributed among the phases according to the reaction

$$Li^6R + (Li^7)^+ \rightleftarrows Li^7R + (Li^6)^+. \quad (1)$$

The equilibrium constant of this process is expressed by means of the activities of the reacting species:

$$K = \frac{(Li^7R)\,\gamma_{Li^7R}\,(Li^6)^+\,\gamma_{(Li^6)^+}}{(Li^6R)\,\gamma_{Li^6R}\,(Li^7)^+\,\gamma_{(Li^7)^+}}. \quad (2)$$

If one assumes that

$$\frac{\gamma_{Li^7R}}{\gamma_{Li^6R}} \simeq 1, \quad (3)$$

expression (2) leads to the conclusion that the single-stage separation coefficient is

$$\alpha = \frac{\gamma_{(Li^7)^+}}{\gamma_{(Li^6)^+}} K. \quad (4)$$

From this expression it is evident that the conditions affecting the activity coefficients of the ions (concentration, nature of the anion, nature of the medium) should also affect the value of the single-stage separation coefficient.

If one assumes that, in the case of a 0.005 N solution of lithium hydroxide, the activity coefficients are equal to one, expression (4) gives that

$$\alpha = K.$$

According to the above data the value of the single-stage separation coefficient is in this case 0.985, i.e., less than unity. However, when the concentration is increased the single-stage separation coefficient increases and becomes larger than one, and this can only be interpreted as implying that for a lithium hydroxide solution $\frac{\gamma(Li^7)^+}{\gamma(Li^6)^+} > 1$ and increases when the concentration increases.

No direct experimental data about the activity coefficients of lithium isotopes are available; however, if one considers the activity coefficients of the hydroxides of alkali metals (Fig. 2), one can see that the activity coefficients for heavy elements of the alkali-metal group are higher than those of lighter elements of the same group [8]. Therefore, the assumption that $\frac{\gamma(Li^7)^+}{\gamma(Li^6)^+} > 1$ seems to be entirely reasonable. Starting with these considerations, it becomes easy to understand the dependence of the single-stage separation coefficient upon the concentration of a water solution of lithium hydroxide (Fig. 1). A similar assumption could be made also as regards the experiments with lithium carbonate and lithium benzoate.

As has been shown above, the single-stage separation coefficient for lithium chloride was lower than unity. This can obviously be explained by assuming that in this case $\frac{\gamma(Li^7)^+}{\gamma(Li^6)^+} < 1$. In fact, if one considers the dependence of the activity coefficients of alkali metal chlorides (Fig. 3), one can see that the activity coefficients of chlorides decrease when the cation mass increases.

LITERATURE CITED

1. T. Taylor and H. Urey, J. Chem. Phys. 5, 597 (1937).
2. T. Taylor and H. Urey, J. Chem. Phys. 6, 429 (1938).
3. G. Dean, US Patent 2204072 (June, 1940).
4. A. Cameron, J. Amer. Chem. Soc. 77, 2731 (1955).
5. G. Wagner and A. Pelz, Monatsh. Chem. 86, 414 (1955).
6. E. M. Kuznetsova, A. V. Makarov, G. M. Panchenkov, Zhur. Fiz. Khim. 32, 2641 (1958).
7. G. M. Panchenkov, P. A. Akishin, and N. N. Vasil'ev, Zhur. Fiz. Khim. 30, 1380 (1957).
8. B. Conway, Electrochemical Data (Elsevier Publishing Co., 1952).

CREEP IN HOT ROLLED URANIUM

G. Ya. Sergeev and A. M. Kaptel'tsev

Translated from Atomnaya Énergiya, Vol. 7, No. 6, pp. 558-560
December, 1959
Original article submitted June 8, 1959

Uranium is a readily oxidizable metal; extensive tests of uranium specimens at high temperatures are therefore only possible in specially equipped machines, in a vacuum or an atmosphere of inert gases (such as argon or helium), freed from chemically active impurities.

The rate of creep in uranium depends strongly on the size of the grain and the texture, and the grain size can vary during the tests. When testing uranium for creep, it is essential to keep the temperature of the specimen strictly constant and, if possible, to avoid switching off the machines during the tests, since otherwise the rate of creep accelerates considerably due to the expansion of uranium under the action of thermal cycles [1, 2, 3].

If these facts are not allowed for during prolonged tests, variations can be caused in the creep resistance of the uranium, about which very little data has been published [2, 3, 4]. These papers do not give information on the chemical composition, structure and machining processes for the tested specimens and do not describe methods for testing creep.

The authors studied uranium which had been rolled at temperatures in the γ region with a total degree of deformation of the order of 85-90% and slowly cooled in air. The content of basic impurities in the uranium varied in different melts within the limits shown in Table 1. Specimens of one melt were used to study the change in the creep rate in relation to the stress and temperature.

TABLE 1 Content of Basic Impurities in the Studied Uranium Melts, %

Fe	Si	Al	Ni	Mn	Co	Cu	B	N	C
$5\cdot10^{-3}$—$14\cdot10^{-3}$	$1\cdot10^{-3}$—$7\cdot10^{-3}$	About $1\cdot10^{-2}$	$2\cdot10^{-4}$—$2\cdot10^{-3}$	$1\cdot10^{-3}$—$2\cdot10^{-3}$	$9\cdot10^{-5}$—$3\cdot10^{-4}$	$4\cdot10^{-4}$—$2\cdot10^{-3}$	$1\cdot10^{-5}$—$2\cdot10^{-5}$	$5\cdot10^{-3}$—$7\cdot10^{-3}$	0,01—0,12.

TABLE 2 Resistance of Hot Rolled Uranium to Creep, in Relation to Temperature and Stresses (Fe = $5\cdot10^{-3}$%; Si = $1.4\cdot10^{-3}$%; C = 0.01 %)

Temperature of tests, °C	Stress kg/mm²	Stress at instant of loading, %	Rate of creep, %/hr	Range for measuring creep rate, hr	Total creep stress		Remarks
					hr	%	
20	25	0,70	$2,3\cdot10^{-5}$	1100—3300	3300	1,12	Specimen did not tear
	30	2,00	$4,8\cdot10^{-5}$	1000—3300	3300	3,47	The same
200	15	0,20	$1,7\cdot10^{-5}$	360—820	820	0,31	" "
	18	0,49	$2,7\cdot10^{-5}$	360—820	820	0,63	" "
300	15	0,22	$6,6\cdot10^{-5}$	200—785	785	0,36	" "
	18	0,58	$1,0\cdot10^{-4}$	200—815	815	0,81	" "
400	8	0,12	$2,2\cdot10^{-4}$	275—735	735	0,42	" "
	10	0,15	$6,1\cdot10^{-4}$	300—735	735	0,70	" "
500	3	0,05	$1,1\cdot10^{-3}$	275—750	800	1,05	" "
	4	0,05	$3,6\cdot10^{-3}$	75—750	750	2,80	" "
600	1	0,02	$2,2\cdot10^{-3}$	25—150	850	3,15	" "

The uranium studied had a coarse-grained dendritic macrostructure with an average grain size of 8-12 mm. Some of the macrograins were as large as 10 x 20 mm.

The microstructure of the uranium consisted of large grains (1.0-1.5 mm) formed by subgrains (mosaic) which were close in orientation, the size of which varied from 200 to 500 μ and averaged about 300-400 μ.

The resistance of uranium to creep was determined on TsKTI-3 machines, specially equipped for testing readily oxidizable metals in an atmosphere of purified helium. The tests were carried out on standard specimens of 10 mm diameter and length of the working part 100 mm. The temperature of the specimen was maintained with an accuracy of $\pm 2°C$ and was measured with chromel-alumel thermocouples at three points along the height of the specimen. The drop in temperatures along the height of the specimen was about 2-4°C. The strain was measured by clock-type indicators with divisions of 0.01 or 0.002 mm depending on the load on the specimen and the rate of creep.

The rate of creep was determined from primary curves plotted with extension – time as the coordinates. The relative creep rate (at the second section) was determined from the formula

$$v = \frac{\Delta l}{l_0 \Delta \tau} 100\ \%/\text{hr}$$

where l_0 is the initial working length of the specimen; Δl is the extension of the specimen during time $\Delta \tau$.

The tests were conducted at stresses between 0.5 and 38 kg/mm^2 and lasted up to 6000 hr.

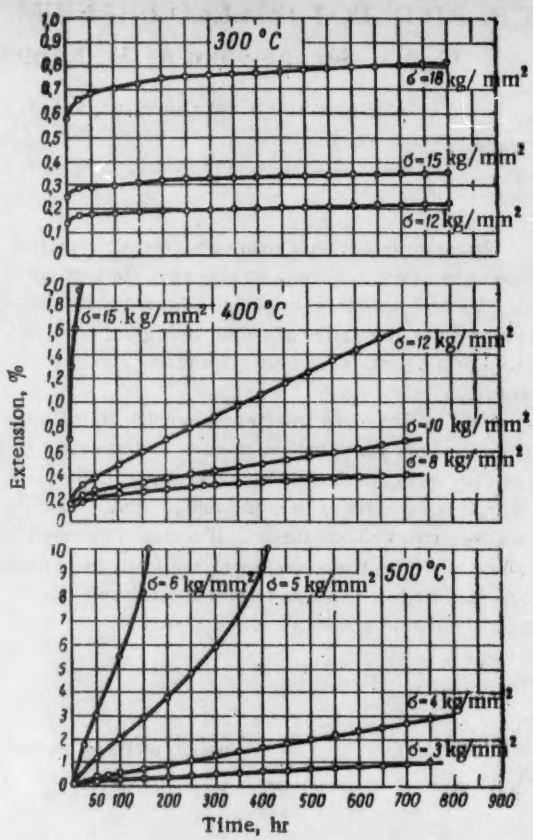

Fig. 1. Primary curves for creep in hot rolled uranium at temperatures of 300, 400, and 500°C and stresses between 3 and 18 kg/mm^2.

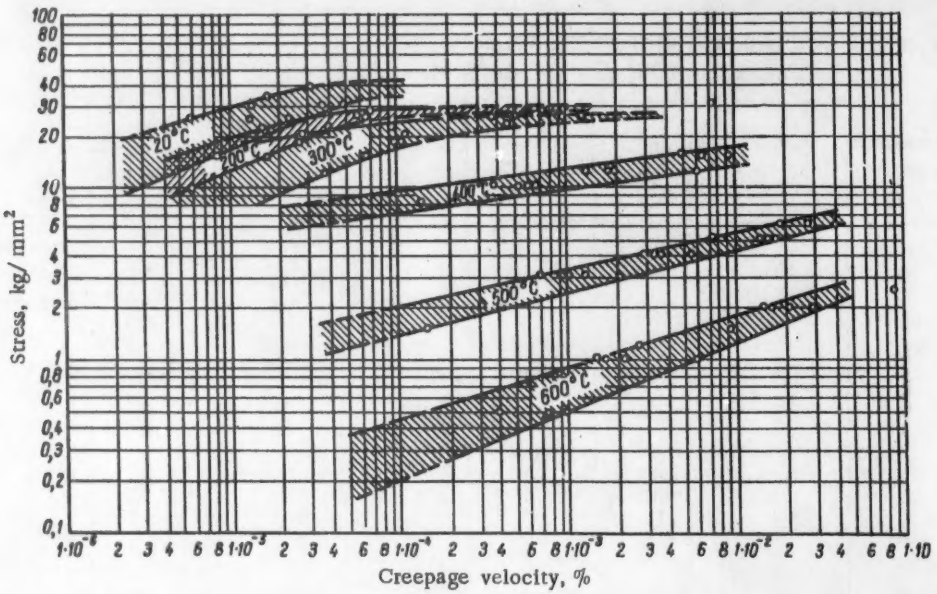

Fig. 2. Change in the creep rate of hot rolled uranium in relation to the temperature and stress.

Table 2 gives the results of some tests for creep, and Fig. 1 gives a number of primary curves for creep in hot rolled uranium at temperatures of 300, 400 and 500°C.

Using the obtained results, logarithmic coordinates were used to plot the relationship between the creep rate (at a section of uniform creep) and the stress (Fig. 2) from which it is possible to determine the limits of creep for various temperatures. The wide range of the change in creep rate at constant temperature and stress is mainly due to fluctuations in the content of impurities of the melts studied and partially due to the small difference in the grain size.

It can be seen from these data that in the lower temperature range of the α-phase, the hot rolled uranium has a noticeable creep rate which starts to increase sharply at 400°C and above. At 400°C the creep of uranium is about 10 times, and at 500°C it is 100-400 times larger than for carbon steel, which is not known for its high resistance to creep.

LITERATURE CITED

1. A. A. Bochvar, G. Ya. Sergeev, A. A. Zhul'kova, and G. I. Tomson, Report No. 2190 presented at the Second International Conference on the Peaceful Uses of Atomic Energy (Geneva, 1958).
2. R. Nichols, Nucl. Engng. 2, 355 (1957).
3. A. McIntosh and T. Heal, Report No. 49 presented by Great Britain at the Second International Conference on the Peaceful Uses of Atomic Energy (Geneva, 1958).
4. G. Ya. Sergeev, V. V. Titova, Z. P. Nikolaeva, A. M. Kaptel'tsev and L.I. Kolobneva, Report No. 2307 presented at the Second International Conference on the Peaceful Uses of Atomic Energy (Geneva, 1958).

* * *

ON THE PARAMETERS OF A REACTOR WITH MINIMUM CRITICAL LOADING

V. Ya. Pupko and L. I. Ermakova

Translated from Atomnaya Énergiya, Vol. 7, No. 6, pp. 560-561
December, 1959
Original article submitted August 3, 1959

It was shown in paper [1] that the parameters of a bare reactor of given construction with minimum possible loading of the fissionable substance could be found from the simultaneous solution of two transcendental equations

$$\varkappa^2 L^2 = -\frac{1}{2}\left(1-\frac{L^2}{2\tau}\right)\left[1 \mp \sqrt{1+12\,\frac{L^2}{2\tau}\,\frac{1-\theta}{(1-L^2/2\tau)^2}}\right], \quad (1)$$

$$1 = \frac{k_\infty e^{-\varkappa^2\tau}}{1+\varkappa^2 L^2}, \quad (2)$$

where κ^2 is the parameter associated with the materials of the reactor, L^2 is the square of the diffusion length of the thermal neutrons in the reactor, τ is the age of the thermal neutrons, θ is the coefficient of utilization of the thermal neutrons, and k_∞ is the coefficient of neutron multiplication in an infinite medium. The equations were derived under the assumption that a reactor with a minimum critical mass is purely a heat reactor and that in such a reactor the neutron flow may be expressed by the diffusion-age approximation. Formula (1) is the consequence of the equality of neutron leakage from the reactor α, and η is the index of efficiency of the fissionable substance (it was proved in paper [1] that

$$\left(\frac{\partial G}{\partial V}\right)_{k\,\mathrm{eff}} = \frac{G}{V}\left(1-\frac{\alpha}{\eta}\right),$$

where G denotes the loading of the reactor and V denotes its volume). Equation (2) is well known.

Having determined the parameters κ^2 and θ (L^2 and k_∞ depend upon the latter) from the indicated system of equations we find the critical dimensions and mass of the desired reactor.

Therefore we can find directly by means of this method a minimally loaded reactor for a given quantity of construction material without carrying out multiple iterated computations for reactors with varying concentrations of fissionable material in the moderator. Even though the computations are carried out for

TABLE 1 Moderator Constants Used in the Computations

Moderator	Specific gravity γ, g/cm^3	Macroscopic absorption cross section Σ_a^{mod}, cm^{-1}	Age of thermal neutrons τ, cm^2	Length of the diffusion of thermal neutrons in moderator L_{mod}, cm
D_2O	1,1	$8,6\cdot10^{-5}$	120	100
Be	1,85	$1,1\cdot10^{-3}$	97	21
BeO	3	$6,10^{-4}$	130	30
C	1,67	$3,7\cdot10^{-4}$	344	50,5
50% Be+50% C	1,76	$7,35\cdot10^{-4}$	145	34

TABLE 2 Results of Computations of Critical Mass on Reactor Dimensions

Moderator	$\varkappa$, cm^{-1}	θ	R, cm	G_5, kg	ρ_{mod}/ρ_5	Date of paper [2]		
						R, cm	G_5, kg	ρ_{mod}/ρ_5
D_2O	0,046	0,963	67	1,8	10^4	~70	~1,9	$1,1\cdot10^4$
Be	0,0563	0,823	54	2,16	$1,5\cdot10^4$	~53	~2,1	$1,4\cdot10^4$
BeO	0,0521	0,859	59,1	2,02	$1,2\cdot10^4$	~59	~2	$1,2\cdot10^4$
C	0,0295	0,85	104	6,32	$2,44\cdot10^4$	~100	~6	$2,3\cdot10^4$
50% Be+50% C	0,045	0,84	68,5	3,59	$1,52\cdot10^4$	~70	~3,5	$1,6\cdot10^4$

a bare reactor, the method described above permits us to determine rapidly the parameters for a reactor with a reflector if in the latter case we make use of the known value of the effective supplements (additions).

As an illustration of the method of determining the minimum loading parameters of the reactor, we present the results of calculations made for the following nonporous systems: pure U^{235} with heavy water, beryllium oxide and a 50% mixture of beryllium and graphite. The computed data are compared with the parameters of reactors of the same composition with minimum critical mass which were obtained using curves presented in the book [2]. This book contains the data obtained by Safonova who computed the critical radii and loading of bare spherical reactors with various moderators for a wide range of relative concentrations of U^{235} and moderators. For purposes of comparison in our computations we made use of the same physical constants for the moderators that were indicated in paper [2]. These constants, together with the computed constants for the graphite-beryllium mixture, are given in Table 1.

For U^{235} the following constants were used: capture cross section of thermal neutrons $\sigma_c^{(5)} = 610$ barns effective number of secondary neutrons during the capture of a thermal neutron $\nu_{eff} = 2.08$. In all the cases that were examined it was obvious that $L^2 = L^2_{mod}(1-\theta)$ and $k_\infty = \nu_{eff}\theta$ where $\theta = \frac{1}{1+\frac{\Sigma_a^{mod}}{\rho_5\sigma_c^{(5)}}}$ (ρ_5 is the nuclear concentration of U^{235}). Thus the system of equations (1) and (2) permits us to find, simultaneously, ρ_5 and the material parameter κ^2, which are connected with the reactor radius by the relationship

$$R = \frac{\pi}{\varkappa} - \frac{0,71}{\Sigma_{tn}},$$

where Σ_{tn}, the mean value of the transport cross section of the active zone for the neutrons leaving the reactor [3].

The U^{235} loading of the reactor is determined from the formula:

$$G_{(kg)} = \frac{4}{3}\pi R^3 \rho_5 \frac{0,235}{0,6023\cdot10^{24}}.$$

The simplest possible method of solving the system of equations (1) and (2) is by the graphical method; the functions $\kappa^2 = \kappa^2(\theta)$ of equation (1) and

$\theta = \theta(\kappa^2)$ of equation (2) are plotted and the point of intersection of both curves then yields the desired κ^2 and θ. Newton's method [4] may be used to obtain a more accurate determination of the roots of these equations. For all the cases which have been studied, except the case where heavy water is used as the moderator, a minus sign must be used in front of the root of equation (1) to obtain the actual value of the parameter.

The results of the computations are given in Table 2 (ρ_{mod} = nuclear concentration of the moderator).

The data obtained from paper [2] are inexact since they were obtained from curves plotted on a logarithmic scale.

It can be seen from Table 2 that the agreement between this data and computations is entirely satisfactory.

LITERATURE CITED

1. V. Ya. Pupko, The Physics and Heat Engineering of Reactors Supplement No. 1 to "Atomnaya Énergiya" (1958) p. 44.
2. R. Bussard and R. DeLauer, Nuclear Rocket Propulsion (New York, 1958) p. 208.
3. Materials of the Atomic Energy Commission of the USA, Nuclear Reactors [Russian translation] (IL, 1956). Vol. II.
4. V. E. Milne, Numerical Analysis [Russian translation] (IL, Moscow, 1951).

* * *

FOURTH INTERNATIONAL CONFERENCE ON IONIZATION PHENOMENA IN GASES*

L. Kovrizhnykh and N. Sobolev

The Fourth International Conference on Ionization Phenomena in Gases was held in Uppsala, Sweden, August 17-21, 1959. Over 600 delegates from 26 countries attended, presenting over 250 papers. The 25-man USSR delegation presented 25 papers.

Eight review papers were presented at the plenary sessions: W. Fite's "Progress in the study of collisional processes in gases," G. Weissler's "Radiation processes in gases," "Contemporary work on testing and development of discharges" by G. Ruther, "Progress in the study of arc discharges" by W. Lochte Holtgreven, "Plasma instabilities and magnetohydrodynamic waves" by W. Thompson, "Progress in the study of shock waves" by A. C. Kolb, "High-frequency waves in ionized gases" by W. Braun, "Structure of spectral lines observed in plasma" by H. Margenau.

The findings of original research were presented in papers delivered at four panels meeting simultaneously.

The first panel dealt with investigations of the basic processes taking place in gaseous discharges.

The second panel considered various types of gas discharges and their uses in physics and engineering.

The third panel took up theoretical and experimental research on plasma physics. Papers presented at this panel may be broken down into three groups according to subject matter: a) transport phenomena and plasma dynamics in electric and magnetic fields; b) microwave research techniques; c) spectroscopic study of plasmas.

The overwhelming bulk of the papers in the first category were theoretical in nature.

M. N. Rosenbluth and N. Rostoker (USA) discussed the question of energy losses of a charged particle moving in a plasma immersed in a magnetic field.

G. Keppler (West Germany) reported on the derivation of Liouville macroscopic equations for a fully ionized gas taking interactions between radiation and matter into account.

The problem of the effect of collective oscillations on transport phenomena was taken up in a report by K. Champion and S. Zimmerman (USA).

R. M. Kulsrud (USA) and B. Kadomtsev (USSR) applied the energy method in investigating the stability of a low-pressure plasma in a strong magnetic field. The necessary stability criteria were derived.

Within the framework of magnetohydrodynamics, and assuming ideal conductivity, J. Butler (USA) solved the problem of the stability of a conducting sphere placed in a spherical resonator with a rotating field, and in a constant magnetic field directed parallel to the axis of rotation.

Employing the technique evolved by Chandrasekhar and others in solving the Boltzmann equation with no collisional terms, which involves expansion of the solution in reciprocal powers of the magnetic field, W. Thompson (UK) derived transport equations and studied their discontinuous solutions. He demonstrated in particular that the solution of equations of this type is not an analytic function of a certain parameter (equal to the ratio of the Larmor radius of the ion to the characteristic dimensions of the system), although the initial equations were obtained by expanding the Boltzmann equation in powers of that parameter.

A new mechanism for magnetohydrodynamic shock waves was considered in a paper by R. Sagdeev (USSR).

G. Roser (West Germany) made an attempt to find a nonlinear solution to the problem of the excitation of plasma waves by an electron beam. However, the transient response was not examined, and the author limited his investigation to the stationary case. In this area, we may note two other interesting points, by Ya. Fainberg et al. and by R. Demirkhanov et al. (USSR), on experimental research on the excitation of longitudinal waves and instability of electron beams in a plasma.

A theoretical study of longitudinal waves in a cold plasma and interactions between the waves and electromagnetic waves was presented in several papers by O. Rydbäck (Sweden).

The problem of electron distribution according to velocities in a fully ionized plasma placed in an external electric field, and the study of the effect of "runaway" particles were discussed in reports by I. B. Bernstein (USA), L. Kovrizhnykh (USSR), C. LeCouteur (Australia), G. Wesson (UK), and H. Baglin et al. (France).

* The proceedings of the Conference are to be published by the North Holland Publishing Company in Amsterdam, sometime during February-March, 1960.

D. Reagan (UK) showed in his report that electrons in high-current pinch discharges with an axially stabilized magnetic field may under certain conditions lose their energy in exciting H-waves, and the related possibility of reducing thermal losses of ions by heating them with H-waves was discussed.

The results of experimental research on ion cyclotron resonance, of special interest from the standpoint of utilizing high-frequency fields for plasma heating, were outlined in a report by K. Sinel'nikov et al. (USSR).

An appreciable number of the reports were devoted to studies of microwave radiation of plasmas, and of ways of utilizing microwave techniques in plasma diagnoses.

C. B. Wharton (USA) presented the results of a study of microwave radiation of a high-temperature plasma, and its absorptivity, in an attempt to shed some light on the question of the existence of thermal equilibrium. Electron temperatures found by microwave radiometry agree with data obtained by other techniques, to within 50% accuracy.

A paper by N. George (USA) was devoted to a study of noise radiation from the plasma in a gas discharge.

D. Formato and A. Gilardini (Italy) reported on the results of measurements of electron temperature and high-frequency conductivity in a plasma. Reliable measurements of collisional frequency were successfully obtained only at electron energies above 0.3 ev. The results show excellent agreement with data obtained by beam scattering methods.

T. Dutt and A. Stainsby (UK) reported on measurements of particle density and collisional frequency in a decaying plasma. The presence of mutiple resonances observed when signals at a frequency of 10^2 - 10^5 Mc were passed between pickup probes placed outside the glass tube were noted, and an explanation was offered for the phenomena.

Over 10 reports were devoted to spectroscopic plasma measurements.

H. Griem and A. C. Kolb (USA) developed a theory of Stark broadening of spectral lines in their paper. The authors, steering clear of the adiabatic treatment of broadening of spectral lines in response to electrons, generalized shock theory and used exact integration of Schrödinger's equation to calculate the profiles of the spectral lines, with the effects of ions and electrons taken into account.

L. Gold (USA) calculated the profiles of spectral lines, radiated by gaseous volumes, taking into account distribution of velocities and density of spectral-line broadening due to the Doppler effect.

The development of a technique for measuring the temperature of a homogeneous plasma, based on measurements of the intensity of two waves of different length, was presented in a paper by A. Bauer (West Germany).

R. Williams and S. Kaufman (UK) explained a technique for measuring the electron temperature of a high-temperature plasma, based on measurements of the absolute intensity of the $2^3S - 2^3P_2$ emission line. Measurements performed on the "Sceptre-III" facility showed that the temperature of the electrons on the axis of the torus in the typical mode of operation is approximately $2 \cdot 10^5$ °K.

In his report, A. Gabriel (UK) presented the results of spectroscopic investigations of a straight deuterium discharge. The intensity of impurity lines increases after the first pinch; the Balmer series is not observed until a very advanced stage of the discharge.

D. Dimoc (USA) reported on experiments on spectroscopic studies of plasma contamination in the stellarator machine. It was found by the intensity of the CII and CIII lines that there was 0.02-0.1 carbon atom to each hydrogen atom at the moment of peak CIII intensity.

C. Breton and L. Hermann (France) studied the glow of a discharge in the TA-2000 facility. The temperature of the ions, determined from the width of CIII 2296.9 lines, proved to be of the order of $45 \cdot 10^4$ °K; the electron temperature varied during the time of the discharge from $4 \cdot 10^4$ to $9 \cdot 10^4$ °K.

R. W. McWhirter et al. (UK) reported on results of spectroscopic research on the ZETA facility.

At the fourth panel, the questions discussed centered on the generation, confinement, and heating of a highly ionized plasma. The papers presented were devoted to a theoretical and experimental investigation of a longitudinal pinch discharge, "mirror machines," and azimuthal pinch discharge, shock waves, and several other methods for generating and confining a plasma, as well as plasma acceleration methods.

Of the theoretical papers on longitudinal discharge, the only ones to be noted are those of M. Haynes and N. Phillips (UK). The first paper by M. Haynes was devoted to a study of the so-called inverse skin effect in pinch discharges. Within the framework of magnetohydrodynamics, an analytic solution was found for the problem, and an expression was derived for the current density as a function of radius and time.

In a second paper, M. Haynes found the temperature distribution in a straight discharge of finite length for the stationary case, taking into account heat losses across the electrodes, and showed that the peak temperature prevalent at the center of the discharge is directly proportional to the applied voltage. For reasonable values of the machine parameters, the peak temperature value ranged from 10^6 to 10^7 °K.

N. Phillips' paper dealt with calculations of the trapping of a neutral gas in a pinch discharge, assuming the principal role to be played by collision events leading to ionization.

Of the experimental papers, we may mention in the first instance some interesting papers presented

by D. Bodsall et al. (USA) on a straight and a toroidal "rigid pinch discharge," and also a report by B. Etkin et al. (UK) on a "reflex pinch discharge."

In their first paper, D. Bodsall and associates outlined the findings of a study of instabilities in a straight discharge in the presence of a longitudinal magnetic field and an isolated central conductor in which the current may be arbitrarily varied. The results of their measurements demonstrate that protracted stabilization (~50 μsec) of the discharge may be had with success in correspondence with a certain assignment of values to the axial field, gas and reflex currents. The high-frequency instabilities on the other hand have a non-hydromagnetic nature, in the authors' view, and might possibly owe their origin to the presence of electrodes, in particular. Similar findings are reported by B. Etkin and associates, who also investigated a straight discharge with an isolated central conductor through which the gas current was shorted.

In their second paper, D. Bodsall and associates presented the results of preliminary experiments on generating a "rigid" discharge in a toroidal chamber, at the center of which a low-frequency magnetic field of relatively low field strength was used to support a metal conductor. A system of this type must result in increased hydromagnetic stability on the part of the discharge, while the absence of electrodes must lead to elimination of high-frequency instability, making possible fairly good thermal insulation.

Several papers were devoted to measurements of the magnetic field distribution in toroidal high-current discharges. On the basis of these measurements, data were obtained on the current distribution over the cross section, and estimates were made of the conductivity, electron temperature, and several other plasma constants.

D. Asby (UK) reported results of an investigation using a toroidal chamber (small diameter 10 cm, large diameter 64 cm, peak current value ~10^5 amp) on magnetohydrodynamic instabilities and the effect of an axial magnetic field on such instabilities. The report of Dolgov-Savel'ev and co-workers (USSR) was also devoted to a toroidal high-current ring discharge.

Of the papers dealing with an azimuthal pinch and a discharge in magnetic fields with mirrors, we might make particular mention of one by A. C. Kolb and H. Griem (USA), who obtained a high-temperature plasma of high density (~10^{17} particles/cm^3) in a chamber 35 cm in length and 2.5 cm in diameter, by using preionization and heating the plasma with a rapidly increasing axial field with mirrors. X radiation and bremsstrahlung were observed along with neutron production, which the authors ascribed to a thermonuclear origin. The neutron burst lasted a fraction of a microsecond, and the temperature found on the basis of these data was $2 \cdot 10^7$ °K. Some data on the building of a similar facility of large size were also reported.

H. Bodin et al. (UK) reported results of an experimental study on rapid constriction of a deuterium plasma, using an axial magnetic field (thetatron). The discharge chamber involved was a cylinder 20 cm long and 5 cm in diameter. Fields varying in intensity up to $1.1 \cdot 10^5$ gauss were used, with a voltage of 30 kv across the condensers and a discharge period of 8 μsec. X radiation and neutron production were observed. The neutron yield reached its peak value at a pressure of 10^{-2} mm Hg and was 10^5 particles/sec; the duration of the neutron burst was of the order of 2-3 μsec.

F. Ribe (USA) reported on experiments dealing with the constriction and heating of a plasma in magnetic fields with a mirror configuration (Scylla) and investigations of a rotating plasma (Ixion). Measurements of x radiation and spatial distribution of d– d-protons were performed on the Scylla, enabling the authors to determine the range of penetration of the particles. The temperature of the plasma electrons, estimated on the basis of the radiation, was of the order of 220 ev. Rotation of the plasma was observed on the Ixion, and the diamagnetic properties of the plasma were investigated. It was shown that a system of this type has a very high equivalent capacity, which may vary as a function of the magnitude of the applied magnetic field.

The study of fast induction discharges in mirror-configuration magnetic fields and instabilities resulting in magnetic fields were discussed in a paper presented by M. Alidier and co-workers (France).

Also worthy of mention is an interesting paper by J. Lewis (USA) on the results of a study of the properties of a hollow cylindrical arc and the possibility of using it to trap high-energy ions in the DCX machine. The experiments were performed on an arc 100 cm long and 17.5 cm in diameter. The total current of the arc was 3600 amp, while the pumping speed was calculated from the arc to be above 100,000 liters/sec.

The theoretical and experimental study of shock waves received a good deal of attention.

A paper presented by A. Kantrowitz and colleagues (USA) dealt with a theoretical and experimental investigation of shocks propagated in a strong magnetic field (mean free path length much shorter than the Larmor radius of the ion). The mechanism of energy transfer to the ions, associated with the excitation of magnetohydrodynamic waves, was examined. A facility was set up to generate shocks. Data on the speed of shock waves and plasma density data were obtained from the findings of measurements of bremsstrahlung intensity. The speed of the shock wave reached $4.5 \cdot 10^7$ cm/sec, the plasma temperature aft of the shock wave was $1.2 \cdot 10^6$ °K, and the plasma density was $5 \cdot 10^{15}$ particles/cm^3. For a mean free path of 20 cm and a Larmor ion radius of 0.2 cm, the

thickness of the leading edge of the shock wave was 2 cm.

J. Wright (UK) developed a simple apparatus for generating intense plane shock waves. The shock waves were established in deuterium at an initial pressure of 1 mm Hg. When two shocks collided, the temperature (found from the Rankine-Hugoniot equation) reached 10^6 °K for a deuteron density of the order of 10^{18} particles/cm^3.

The paper by O. Greenberg and colleagues (USA) gave a theoretical treatment of the effect of charge separation on the structure of a shock wave propagating through a plasma. A qualitative investigation of the equations obtained demonstrates that the proton and electron densities in the electric field vary, and that these fluctuations have a delicate structure, the amplitude values appreciably exceeding the values found from the Rankine-Hugoniot condition.

C. C. Payne and P. Smith (UK) reported results of research on the interaction between a magnetic field and an argon plasma advancing at a speed of $5 \cdot 10^5$ cm/sec.

R. Allis et al. (USA) reported on research work probing into particle losses in ohmic heating in the stellarator. The measurements done show in particular that the lifetime of particles in the stellarator is inversely proportional to the square root, rather than the square, of the magnetic field intensity, as predicted theoretically. It was found that the superposition of an additional magnetic field of special configuration for eliminating magnetohydrodynamic instabilities had no effect on particle lifetime; this fact favors the assertion that the losses taking place are not linked to magnetohydrodynamic stability, and may possibly be due to instabilities of an electrostatic nature.

G. Chino et al. (USA) reported on attempts to confine a plasma by applying high-frequency fields. The results obtained indicate the possibility of high-frequency containment of a plasma with an electron temperature of $2 \cdot 10^4$ to $4 \cdot 10^4$ °K and a density of the order of 10^{14} particles/cm^3. Several variants of high-frequency systems are considered in the paper.

A report by O. Anderson et al. (USA) was devoted to experimental research on a highly ionized rotating plasma in a magnetic field. These workers detected a substantially inhomogeneous current distribution, and are probing for the possible reasons underlying this phenomenon.

M. Ioffe and co-workers (USSR) reported on the results of measurements of the decay time of a plasma in systems with magnetic bottles.

At the closing plenary session of the Conference, review papers read dealt with the status of experiments on setting up a controlled fusion reaction in several laboratories in the USA (Los Alamos, J. Tuck; Livermore, R. Post; Oak Ridge, A. Snell) and in Britain (Harwell, W. Thompson; Aldermaston, Niblett).

THE IX INTERNATIONAL RADIOLOGICAL CONGRESS

K. K. Aglintsev

The IX Radiological Congress was held at Munich (West Germany) on July 23-30, 1959. About 5,000 delegates from 63 countries were in attendance at the Congress; symposia were organized on several topics and an exposition of radiological equipment and instruments was opened up at the Congress.

Seven panel sessions were organized: diagnostics; therapy; nuclear medicine and radiation therapy; radiobiology and biophysics; radiation injuries and radiological shielding; health physics and dosimetry; juridical problems, economics, teaching, and history of radiology.

From 14 countries, 124 firms displayed their products at the exposition, these including: x-ray equipment, tubes, kenotrons, screens, photographic materials; contract materials; shielding materials; betatrons and other types of accelerators; dosimetry hardware; equipment for gamma-radiation, and medical-electrical and electronic instrumentation.

The 27-man Soviet delegation was headed by Prof. M. N. Pobedinskii, Doctor Med. Sci.; three health physicists, four engineers, and twenty radiologist-physicians and radiobiologists made up the group.

A considerable portion of the papers presented dealt with special problems in medicine and radiobiology which were of interest only to a comparatively narrow circle of specialists. However, some of the papers reflected substantial progress in the area of the

use of radiations, and are therefore deserving of detailed examination at this time.

Serious steps forward were made in the field of x-ray diagnostics. X-ray television techniques and improvements in the quality of images on x-ray screens, as well as automation of x-ray diagnostic operations, are more and more commonly encountered. A special branch of pharmacology dealing with the preparation of contrast materials is developing. Serious attention is being given to reduction of the radiation load on patients. Interesting data were forthcoming on the power levels of up-to-date x-ray equipment: current of 1000 ma can be handled with a voltage of 100 kv.

In the field of radiation therapy and nuclear medicine, we might mention progress in designs of γ-irradiating facilities, and a trend toward wider utilization of high-energy radiations.

The most advanced γ facilities use Co^{60} or Cs^{137} of up to 3-5,000 curies activity; their design makes it possible to irradiate the patient with a sweep-scan beam or rotating beam of γ rays. The use of linear accelerators in radiation therapy is on the increase. 4 Mev linear accelerators enable a dose rate of bremsstrahlung of the order of 500-900 r/min to be obtained at a distance of one meter from the anode. The dose rate of the electrons at the window exit is about 3,000 rep/min.

Problems of radiology per se are not considered in this review; we shall restrict our remarks on this point to the fact that the authors of several papers paid much attention to the role of chemical factors in the biological effects of radiation.

At the panel session on radiation injuries and radiological shielding, statistical data on the radiation exposure of a population in x-ray diagnostic procedures and possible ways of reducing x-ray exposure were examined in detail. In addition, problems arising in the organization of individual dosimetric monitoring and the investigation of shielding facilities for various types of setups were discussed.

About 60 papers were devoted to dosimetry. In several papers, there was an analysis of the nature of dosimetric quantities and their units. Detailed discussion was given to the possibility and need of using physical units in radiobiology. Two trends are apparently to be noted in this area: one of them calls for improvement in the concept of relative biological effectiveness and in the relationship between the RBE and rad, the basic contention being that the proportionality factor between them should be assigned for each biological test; while the second approach calls for improvements in the techniques of determining the linear ionization density along the tracks of particles moving through tissue, as well as improvements in the relationship between linear ionization density and biological effects of radiation.

It is probable that any refinements in the physical nature of the dosimetry units will be inevitably followed by a need to improve the correlation between the physical units and biological effects.

Considerable attention was devoted to the problem of correlating the national standards of dosimetric units used in different countries.

In papers dealing with the use of high-energy electron beams in radiation therapy, data were provided on the depth doses of electron beams found by using ionization chambers and chemical dosimeters, as well as data originating in studies of measurements techniques. In this field, as in others, a tendency was noted to measure the dose in rads.

A portion of the papers was related to theoretical and experimental research on the spectral makeup of x rays and γ rays. Data were also reported on the intensity of scattered radiation and the distribution of radiation obtained by collimating a beam. This showed that there has been an intensification in recent years of work aimed at disclosing the nature of the "dose field" surrounding a radiation source in a medium.

Results of measurements of β spectra in the "dose field" of a β emitter were made available only in one report presented by the USSR delegation.* This paper pointed out the importance of studies of β spectra in the fields of β emitters for dosimetry.

Several papers reflected the continuous advances registered in scintillation techniques. We may mention papers on dose measurement in the case of intratissue introduction of radioactive preparations, on the use of hollow scintillation spheres for determining radium content in the human body by the radon exhaled, on designing tissue-equivalent dosimeters with a scintillator volume of 0.1 cm^3. A method based on the use of thermoluminescence was proposed for neutron dosimetry. This method is similar to one developed in the USSR involving scintillation phosphors.

Several papers were devoted to chemical and calorimetric dosimetry techniques, with the use of calorimeters with tissue-equivalent absorbers suggested in the latter case.

Some firms put samples of dosimetric equipment on display. The general tendency seems to be to develop instruments with improved parameters, of more sophisticated appearance, greater convenience in operation, and with reduced weight and size.

Other exhibit items included several types of counter devices and arrangements using dekatrons and adapted for automatic sample changing; a large quantity of scintillation counters adapted for measurements of α-,

*K. K. Aglintsev, V. P. Kasatkin. Atomnaya Énergiya 7, No. 2, 138 (1959) [Original Russian pagination. See C. B. translation].

β-, γ-rays, and neutrons; samples for measuring the activity of radioactive substances placed inside the human body; a liquid scintillator counter (put out by the British firm EKCO Electronics Ltd.) devised to measure tritium and C^{14} content; crystals, scintillating plastics, and liquid scintillators.

Meriting special mention are arrangements for monitoring the activity of water, sensitivity 10^{-10} curie / m^3 for beta radiation and 10^{-11} curie / m^3 for alpha radiation, with continuous monitoring of sensitivity 10^{-8} curie / m^3, as well as some assembly-line counters using a methane flow. An interesting piece of accessory equipment displayed was a dynamic-condenser electrometer put out by Frieseck Hopfner, with a sensitivity of $5 \cdot 10^{-16}$ coulomb with respect to charge and 10^{-17} amp with respect to current.

THE LINDE APPROACH TO THE PRODUCTION OF HEAVY WATER BY LOW-TEMPERATURE DISTILLATION OF HYDROGEN

K. Sakodynskii

India adopted a decision in 1955 to organize heavy water production at the fertilizer plant at Nangal [1]. After looking over several variants of production process schemes, the method of fractional distillation of hydrogen with pre-enrichment of the water by electrolysis [2] was selected. Bids for building the plant were offered by a number of companies, and the contract was awarded to the well-known West German Linde firm [3]. A brief description of the proposed process flow scheme, similar to the one set up by Linde at the Farbwerke Höchst plant, has since appeared in print [4].

Hydrogen containing up to 0.045% deuterium, obtained by electrolysis of water in a three-stage cascade, is compressed by a compressor 1 to a pressure of 5 atmos. The hydrogen passes to a purifying stage 2 to remove oxygen, the content O_2 being lowered from 0.2% to 0.0001%. Water is frozen out in a regenerative heat exchanger 3, and carbon dioxide is likewise frozen out in the regenerative heat exchanger 4. The temperature of the stream of hydrogen feed is reduced to 65°K in the hydrogen-cooled heat exchangers 3 and 4, and in the heat exchanger 5, cooled by liquid nitrogen. Traces of impurities are trapped in heat exchanger 6, and the hydrogen is further cooled to 26°K. Hydrogen cooled under a pressure of 3 atmos is then admitted to the midpoint of the lower section of the first fractionat-

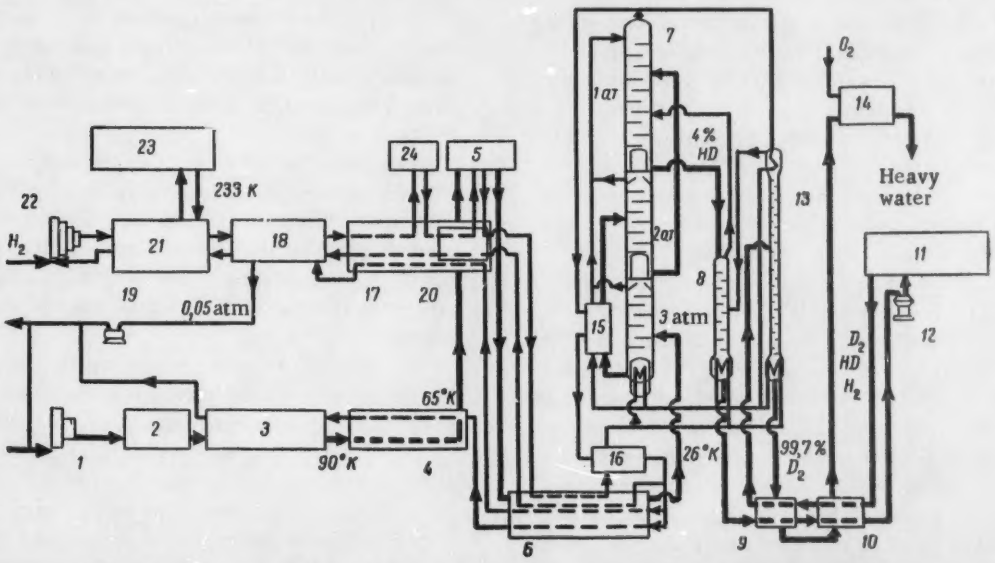

Flowscheme of production of heavy water by the low-temperature distillation method.

ing tower 7. The midsection of tower 7 operates under a pressure of 2 atmos, while the top is under 1 atmos. Hydrogen enriched to 4% HD is then admitted to the second tower 8, in which enrichment is carried further to 90% HD. The hydrogen is fed from the still of the second tower by a diaphragm condenser 12 through heat exchangers 9 and 10 to a reactor 11, charged with a catalyst. HD molecules are converted to H_2 and D_2 molecules in the reactor. The mixture so formed is cooled in heat exchangers 9 and 10 and fed into the midpoint of the third tower 13, in which enrichment is brought to 99.8% D_2. The outgoing deuterium stream injects heat to heat exchangers 9 and 10 and passes to a burner 14, in which the heavy water is produced.

Stripped hydrogen with 0.002% HD content issues from the top of fractionating tower 7, gives up its cold in heat exchangers 15 and 16, and then divides into two streams. One stream leads out of the system, giving up its cold in series heat exchangers 6, 4, 3; the other stream is recycled through the system as reflux, while its vapor moiety functions as a heat-transfer medium to heat up the stills of all three fractionating columns. Compression of the hydrogen reflux takes place in compressor 22, with precooling and drying in heat exchanger 21 by the cold established by an ammonia machine 23; heat exchanger 24 is cooled by nitrogen. The hydrogen stream used to cool heat exchangers 20, 17, and 18, is drawn off with the aid of a vacuum pump 19.

A complicated system of cold regeneration allows maximum exploitation to be made of the cold attained, while nesting of the entire system into two boxes, one inner and one outer, provides excellent thermal insulation. Based on tentative calaculations [2, 5], the cost of 1 kg of heavy water produced at the plant will be 61.5 dollars.

LITERATURE CITED

1. Atomwirtschaft 1 H. 3, 110 (1956).
2. D. C. Gami et al., Geneva 1958, Paper 1649.
3. Chemische Industrie 10 H. 10, 712 (1958); Atomwirtschaft 3 H. 12, 522 (1958); 4, H. 1, 42 (1959).
4. Chem. Engng 66, No. 4, 68 (1959).
5. Nucleonics 16, No. 9, 109 (1958).

* * *

THE ATOMIC ENERGY SECTION OF POLAND'S INDUSTRIAL EXHIBIT IN MOSCOW

Yu. Koryakin

The achievements of the Polish People's Republic in the area of the uses of atomic energy were widely displayed at the Polish Industrial Exhibit held in Moscow during September 1959. The atomic energy section was represented by three departments: the scientific research conducted by nuclear research institutions in Warsaw and Cracow, radiochemical equipment, electronic and measuring instrumentation.

The first section reflected the following basic trends in the work of the institutions:

1) Research in the field of the physics of the atomic nucleus, elementary particles, and high-energy physics (cosmic rays). This research is served by a 25-Mev cyclotron accelerating α particles, built by the Soviet Union for the University of Cracow, and a 10-Mev linear proton accelerator now under construction at the Institute of Warsaw (a model of which was on exhibit), which may possibly be adjusted to accelerate protons to higher energies, as well as a 4-Mev Van de Graaff accelerator. These accelerators will be in service within one to two years.

2) Design and manufacture of electronic equipment. The electronics department of the Institute of Nuclear Research in Warsaw is the source of electronic hardware for the Institute's laboratory; it has also devised instruments for the Joint Institute for Nuclear Research at Dubna.

3) Chemical research. This research has as its aim development of process technology for reactor materials. There are uranium ore deposits in Poland, and specialists are tackling the problems involved in working them. In particular, a scaled-up pilot plant for processing these ores has been assembled at the Warsaw Institute.

4) Research in analytical chemistry. This research is geared toward microdeterminations of trace impurities in reactor materials.

5) Research in radiation chemistry, chemistry, and uses of isotopes. The technology involved in the use of isotopes in extraction and adsorption processes is undergoing development. Polish scientists feel that the best usage for atomic energy in their country is in the

use of radiations in polymerization processes, treatment of foodstuffs, etc.

6) Research in radiobiology and radiation shielding. The problems concerned with radiation effects on organisms are being studied, and methods for manufacturing the most highly effective shielding materials are being worked out. Research in this area also envisages measuring radioactive fallout on Polish territory.

Fig. 1. Charge-discharge machine for the Polish research reactor.

7) Isotope production. With the startup of Poland's first research reactor, a 2000 kw swimming pool type reactor (built with the aid of the Soviet Union), Poland has begun to produce radioactive isotopes, e.g., I^{131}, S^{35}, P^{32}, Co^{60}, Tm^{169}, Ir^{191} (albeit still in small quantities, and only for local needs). A laboratory for producing isotopes is being built. Polish specialists have devised a charge-discharge electromagnetically actuated machine for the first operating reactor, at Warsaw Institute (Fig. 1). The machine is capable of loading and unloading reactor fuel assemblies rapidly and automatically, is convenient for carrying out a variety of operations in the reactor channels and placing and removing isotope capsules, is reliable in operation, and provides maximum safety to personnel.

A large selection of instruments and equipment used in research in the atomic energy field was displayed in the remaining two departments. The overwhelming bulk of the instruments and other hardware was not experimental or developmental in character. They are being manufactured on an assembly-line basis and shipped to East Germany, Czechoslovakia, and Yugoslavia. Poland is also willing to sell this equipment to any other countries desiring to acquire it.

The radiochemical equipment section exhibited a variety of containers for radioactive isotopes, boxes, and special tables (equipped with master-slave mani-

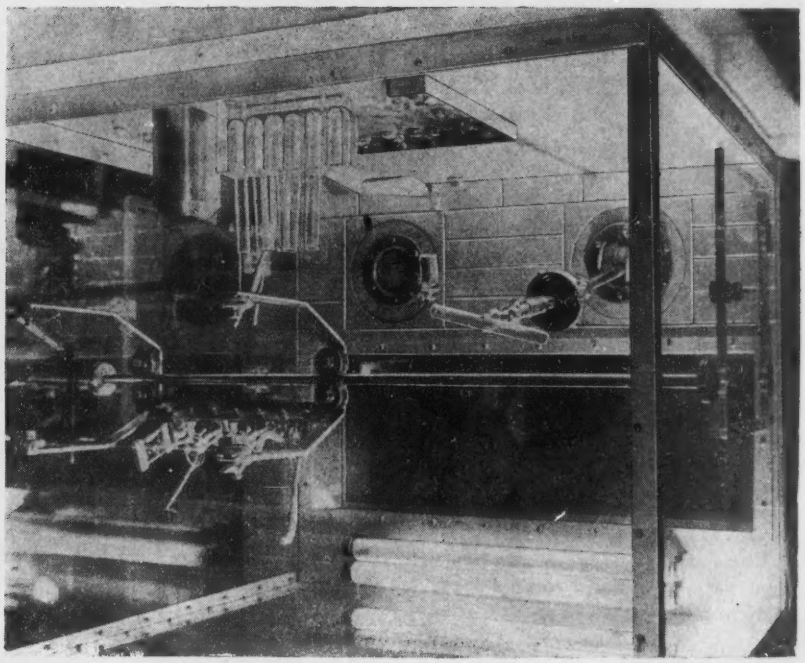

Fig. 2. Hot cell with manipulator.

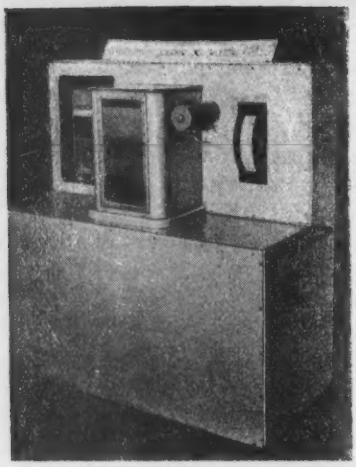

Fig. 3. Liquid level measuring facility.

pulators) for handling isotopes. A mockup of a hot cell with manipulators of original design was found interesting (Fig. 2).

The department displaying electronic and measuring instruments had instruments for measuring the radiation intensity of sources or samples, dosimeters, power supplies for instruments, scalers (with scale-often circuitry and resolving time of 1.40 and 50 μsec), and a wideband amplifier. Also interesting were two devices operating reliably: one for maintaining a constant liquid level, another for measuring liquid level (Fig. 3). Both devices are being used at the chemical plant at Ketrzyn.

Polish scientists are participating actively in international "atomic society." An International Conference on Radiation Chemistry organized by the IAEA met in Warsaw in early September, with several hundred delegates representing many countries in attendance. Polish scientists delivered a number of papers at this gathering. Poland was the initiator of the appeal for a conference of socialistic countries on nuclear engineering equipment. This conference is slated to be held in Warsaw in early 1960. The purpose of the conference will be to coordinate work on the design and manufacture of instruments, and on the exchange of experience in that area.

The prominent Polish scientists L. Jurkiewicz and M. Mensowicz participated in the Geneva meeting of experts on detection of atomic explosions.

Special departments in several Polish institutions of advanced training are engaged in a program of training personnel to staff the growing atomic energy industry in Poland.

Polish students are matriculated in many Soviet technical schools, and Polish specialists are currently working at the Dubna Joint Institute for Nuclear Research.

Reflecting the progress achieved by the country in the field of atomic energy, the Polish scientific periodical "Nukleonika" is presently engaged in publishing many original articles and review articles by Polish scientists. In addition, the "Bulletin of the Polish Academy of Sciences" is being published in Poland, with a good deal of space given to work in atomic energy. Special monographs and a large selection of popular science literature is also being published on this topic.

On the whole, the atomic section of the Polish industrial exhibit in Moscow attests to the significant successes registered by Poland in the field of the peaceful uses of atomic energy.

* * *

A TRADE ENTERPRISE UNIQUE IN ITS WAY

Yu. Koryakin

The use of radioactive and stable isotopes in the national economy of the USSR, constantly on the increase and widening out into new areas, has called forth new forms for supplying the broad range of interested institutions with needed isotopes. The "Isotopes" demonstration hall and center has been opened up on Lenin Prospect in the heart of Moscow, to serve those ends more efficiently.

The name chosen for the center is well advised: it is a qualitative characterization of a completely new form making its appearance in trade enterprising. One of the primary tasks of the center will be the exhibition

and advertising of radioactive products and equipment and stable isotopes manufactured in the Soviet Union, by means of exhibits, stands, and other media. A section devoted to periodic exhibits will be functioning at the center, and the various scientific research institutes and organizations will use it to demonstrate their work in the field of utilization of isotopes. Highly qualified consultants will be on hand to service visitors with extensive information on any problem of interest. The center will make available, to any one requesting it, typical designs of laboratories for using radioactive isotopes in metallurgy, flaw detection, for studies of wear on machine parts and tools, uses of radioactive isotopes in agriculture, etc. A variety of handbooks, catalogs, etc., dealing with the production and use of isotopes, shielding practice, associated equipment, etc., will be available. A lecture program is given top billing. Lectures and scientific and popular science films will be open to the public in a special auditorium.

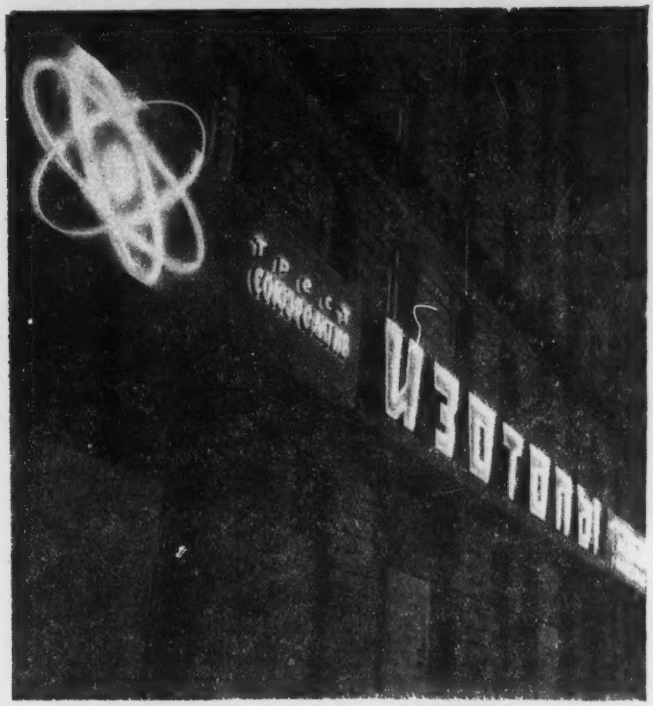

Department of stable isotopes. This section will sell and demonstrate isotopes and their samples.

Five trade departments will be set up in the demonstration center:

Department of radioactive isotopes and labeled compounds used in science, medicine, industry, and agriculture.

Department of sources of radiation. This section will deal with sources for γ facilities used in nondestructive flaw testing and in medical therapy, sources for process quality control in industry and for facilities designed to remove static charges; in addition, standard sources and targets for elementary-particle accelerators will be on sale. It stands to reason that any radioactive sources which might present a hazard to health and therefore require special and expert handling will not be available at the demonstration center, but will be stored in a special warehouse. The sale of such sources will be facilitated by simulators which fully reproduce the external appearance of the sources in question.

Instruments, equipment, and units based on the use of hot sources for various purposes will be demonstrated in this department, as well as medical plaster-of-paris models depicting treatment of patients by radiation therapy techniques and source containers.

The department for irradiation of parts and materials, and associated equipment. In this section, containers and cases for irradiation operations will be demonstrated.

Department of stable isotopes. This section will sell and demonstrate isotopes and their samples.

Department of shielding techniques. This section will demonstrate units, stands, and drawings explaining the principles underlying shielding against radiations,

and the nature of the interaction between radiations and matter; cabinets and cells for work with weakly radioactive materials and specimens, carriers and safes for γ and neutron emitters.

This section will embrace two subsections: one for remote-controlled instruments, another for special-purpose clothing: remote-controlled equipment, master-slave manipulators, lead-lined junior caves, screens, shielding brickwork, pallets for hauling containers, lab tables and chairs, wetting baths, stalls for experimental animals and small-animal hotels, etc. The second subsection will feature special overalls, boots, aprons, respirators, special-purpose gloves, and various plastic items needed for handling radioactive isotopes.

The sale of isotopes and labeled compounds (B^{10}, Ne^{20}, Ne^{22}, $C^{13}H_4$, $B^{10}F_3$, D_2O, etc.) and equipment will be made only with organizations on the basis of special prior orders upon presentation of signed approval from the Gossaninspektsiya [State Public Health Inspection Agency] authorizing the use of isotopes and labeled compounds in the organization concerned. In addition, the center will keep on hand a reserve supply of materials in demand, for speedy fulfillment of incoming orders.

In view of the fact that the Soviet Union is currently exporting isotopes to many countries, foreign organizations have been offered the opportunity of placing orders for desired isotopes and equipment.

Sales promotion and marketing of such a highly specific product require correspondingly specialized knowledge and training. It is therefore hardly surprising that the majority of the workers staffing the center possess technical and advanced technical backgrounds. The scientific management of the center will be chosen on the Candidate of Science [MS] level.

Workers at the center and interior decorating and display personnel have expended considerable effort in making the center a comfortable place for visitors. Good lighting, bright window displays with mechanized equipment, original signs, large bright neon panels on the roof of the building announcing "Atoms For Peace" in three languages (Russian, English, French) render the center conspicuous and attractive.

The inauguration of this unique "Isotopes" demonstration center is a testimony to the far-reaching successes achieved in the peaceful uses of atomic energy in the Soviet Union.

NEW LITERATURE

Yu. V. Novozhilov, Elementary Particles (Fizmatgiz, Moscow, 1959) 184 pp. 2 rubles, 75 kopeks.

This book is devoted to one of the most interesting and rapidly expanding topics in physics, the physics of elementary particles. In a simple form accessible to the reader, the author outlines the basic information accumulated on elementary particles, their interactions with each other and their transformations. Without resorting to the mathematical tools of modern physics, the author tells of the latest achievements in the study of elementary particles, and shows the enormous importance which this branch of physics has in unlocking the secrets of nature.

The book will be found interesting by a wide audience of readers interested in the accomplishments of modern physics.

Kerntechnik. Physik. Technologie. Reaktoren. [Nuclear Physics Engineering, Reactor Technology] Publishers: W. Riezler, W. Walcher, Stuttgart, B. G. Teubner, 1958. 1002 pages [in German].

This encyclopedia of "Nuclear Engineering" has been published in six volumes. They deal with the four fundamental topics covering the subject matter: fundamentals of nuclear physics; technological problems in nuclear engineering; reactors; economic and juridical problems.

Much of the information made available in the encyclopedia was secured from experiments and research on the uses of atomic energy in various countries. The large quantity of practical data and an extensive bibliography following each chapter render this publication highly useful for a broad selection of specialists working in the field of atomic energy.

MISSING PAGES ARE INDEX PAGES
WHICH HAVE BEEN PHOTOGRAPHED
AT THE BEGINNING OF THE VOLUME(S)